EEG-Based Control of Working Memory Maintenance Using Closed-Loop Binaural Stimulation

Christine E. Beauchene

Dissertation submitted to the Faculty of the

Virginia Polytechnic Institute and State University

in partial fulfillment of the requirements for the degree of

Doctor of Philosophy

in

Mechanical Engineering

Alexander Leonessa, Co-chair

Nicole T. Abaid, Co-chair

Rachel A. Diana

Rosalyn J. Moran

Steve C. Southward

April 17, 2018

Blacksburg, Virginia

EEG-Based Control of Working Memory Maintenance Using Closed-Loop Binaural Stimulation

Christine E. Beauchene

(ABSTRACT)

The brain is a highly complex network of nonlinear systems with internal dynamic states that are not easily quantified. As a result, it is essential to understand the properties of the connectivity network linking disparate parts of the brain used in complex cognitive processes, such as working memory. Working memory is the system in control of temporary retention and online organization of thoughts for successful goal directed behavior. Individuals exhibit a typically small capacity limit on the number of items that can be simultaneously retained in working memory. To modify network connections and thereby augment working memory capacity, researchers have targeted brain areas using a variety of noninvasive stimulation interventions. However, few existing methods take advantage of the brain's own structure to actively generate and entrain internal oscillatory modulations in locations deep within the auditory pathways. One technique is known as binaural beats, which arises from the brain's interpretation of two pure tones, with a small frequency mismatch, delivered independently to each ear. The mismatch between these tones is perceived as a so-called beat frequency which can be used to modulate behavioral performance and cortical connectivity. Currently, all binaural stimulation therapeutic systems are open-loop "one-size-fits-all" approaches. However, these methods can prove not as effective because each person's brain responds slightly differently to exogenous stimuli. Therefore, the driving motivation for developing a closed-loop stimulation system is to help populations with large individual variability. One such example is persons with mild cognitive impairment (MCI), which causes cognitive impairments beyond those expected based on age. Therefore, applying a closed-loop binaural beat control system to increase the cognitive load level to people with MCI could potentially maintain their quality of life.In this dissertation, I will present a comparison of algorithms to determine brain connectivity, results of open-loop based binaural stimulation, the development of a closed-loop brain network simulation platform, and finally an experimental study to determine the effectiveness of closed-loop control to modulate brain networks hence influencing cognitive abilities.

EEG-Based Control of Working Memory Maintenance Using Closed-Loop Binaural Stimulation

Christine E. Beauchene

(GENERAL AUDIENCE ABSTRACT)

In order to do complex tasks, such as creating a memory, multiple regions of the brain must interact to become a network. Specifically for this work, we are looking at working memory which is the system that allows us to remember and manipulate information in the presence of additional incoming information. Working memory capacity, which is the number of items we can remember, is dependent upon synchronization between particular regions of the brain, particularly the frontal and parietal lobes. Higher synchronization means that people will, on average, respond with higher accuracy during a working memory task. To modify the connections in the network and thereby augment working memory capacity, a non-invasive brain stimulation technique called binaural beats can be used. Binaural beats take advantage of the brain's response to two pure tones, delivered independently to each ear, when those tones have a small frequency mismatch. The mismatch between the tones is interpreted as a beat frequency, which may act to synchronize brain waves. This research seeks to answer the question of whether binaural beats can be used to identify and control working memory. Currently, nearly all therapeutic stimulation systems are open-loop "one-size-fits-all" approaches. However, these methods can prove not as effective because each person's brain responds slightly differently to external stimuli. Therefore, the driving motivation for developing a closed-loop stimulation system is to help populations with large individual variability. One such example is persons with mild cognitive impairment (MCI) which is considered a precursor to Alzheimer's. Therefore, applying a closed-loop binaural beat control system to increase the cognitive load level to people with MCI could potentially maintain their quality of life. In this dissertation, we have showed that we can successfully increase the connectivity in the brain using binaural beats in a closed-loop system.

Dedication

I would like to dedicate this dissertation to my family. Thank you for your support and encouragement in all my educational endeavors.

Acknowledgments

First and foremost, I would like to thank my advisors Dr. Alexander Leonessa and Dr. Nicole Abaid. I am very thankful for all the support and encouragement I have received while completing my doctoral studies. I also would like to thank all the committee members, who were also instrumental to finishing this research. I am also very thankful to my friends and lab-mates for the coffee runs, lunches, and spontaneous hallway conversations about current research challenges and anything else. I would especially like to thank Paola Jaramillo, Garret Burks, and Amanda Hashimoto for their friendship, wisdom, and encouragement. I am also very grateful to my three undergraduate students: Mr. James Simon, Ms. Juliette Parks, and Mr. Michael Harring, who dedicated so much of their work to develop the experimental setups and computer models. I am also enormously thankful to my family who has been always there for me in the journey of life. Their love and support has empowered me through the ups and downs of my studies and my life.

Contents

List of Figures

xviii

List of Tables

Chapter 1

Introduction

The frequency response of the brain has been associated with a wide range of brain states and abilities, including concentration, mood, attention, and memory. To access particular neural responses, a variety of interventions target stimulating areas of the brain at certain frequencies; methods of stimulation include electrical signals, magnetic fields, and ultrasounds. However, few existing techniques take advantage of the brain's structure to actively generate and entrain internal oscillatory modulations in locations deep within the auditory pathways. One technique that does exploit existing brain structure is known as binaural beats, which arises from the brain's interpretation of two pure tones, with a small frequency mismatch, delivered independently to each ear. The mismatch between these tones is perceived as a so-called beat frequency. The use of binaural beats to entrain certain brain structures has been preliminarily explored, and results suggest that this safe and accessible stimulation method can be used to modulate behavioral performance.

This dissertation seeks to answer the question of whether binaural beats can be used to identify and control working memory. Working memory is the system in control of temporary retention and online organization of thoughts for successful goal-directed behavior. Remarkably, individuals exhibit a typically small capacity limit or 'maximum load' on the number of items that can be simultaneously retained in working memory.

Before binaural beats can be used within a closed-loop system to augment working memory, the open-loop brain and behavioral responses to binaural beats must be assessed. Therefore,

two experiments are completed to assess the effects of constant binaural beats on working memory performance. The results of the studies show that binaural beats can produce a more connected network and the more accurate responses during the tasks. Based on these outcomes, a closed-loop system can be developed to control the binaural beat frequency using measured brain signals.

Currently, nearly all therapeutic stimulation systems are open-loop 'one-size-fits-all' approaches. However, these methods can prove not as effective because each person's brain responds slightly differently to exogenous stimuli. Therefore, the driving motivation for developing a closed-loop stimulation system is to help populations with large individual variability. One such example is persons with mild cognitive impairment (MCI). MCI causes cognitive impairments beyond those expected based on age, but which are not significant enough to interfere with their daily life or independent function [2]. However, MCI is considered to be an early symptom of Alzheimer's disease. Previous studies have found that, overall, approximately 1 in 10 people with MCI progress to probable Alzheimer's disease per year [3]. In MCI, working memory capacity and the ability to maintain complex task subgoals are impaired. Therefore, applying a closed-loop binaural beat control system to increase the cognitive load level to people with MCI could potentially reduce their rate of cognitive decline and maintain their quality of life.

1.1 Cortical Structure and Functionality

1.1.1 Overview

The cerebral cortex is an incredibly complex brain structure capable of acquiring, analyzing, and inducing action based on data from different sources. At the cellular level, the cerebral

cortex is primarily composed of neurons and synapses, which transmit information through electrical signals. When a large number of neurons synchronize their firing patterns, macroscopic oscillations can be recorded using electroencephalography (EEG). The frequencies of these oscillations are characterized as gamma (25-40Hz), beta (12-25Hz), alpha (8-12Hz), theta (4-8Hz), and delta waves (0-4Hz), and these ranges are associated with higher mental activity, alertness, relaxation, drowsiness, and deep sleep, respectively [4, 5].

At the macroscopic level, the cerebral cortex can be divided into different regions of functionality, as shown in Figure 1.1. The frontal, parietal, occipital, and temporal lobes are primarily associated with high-level decision making, the perception of sensory information, visual processing, and auditory processing, respectively [6].
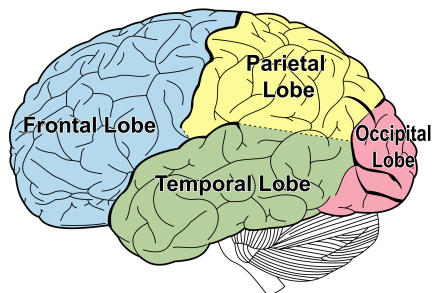
Figure 1.1: The brain, divided into the frontal, temporal, parietal, and occipital lobes.

The brain is a highly complex network of nonlinear systems with internal dynamic states that are not easily quantified. Understanding how the brain is connected is of utmost importance for understanding its functionality. Findings from the cognitive neuroimaging literature show that the large-scale brain networks are required for complex cognitive processing (e.g., some memory tasks involve prefrontal, temporal, and parietal cortical processes). In memory tasks, these interactions are reflected in multiple EEG oscillatory bands, particularly at theta and gamma frequencies [7, 8, 9, 10]. Networks describing the interconnections between these regions exhibit a high degree of randomness, high modularity, and relatively low heterogene-

ity. The network properties, which are conserved over all scales, include small world degree distributions, short path lengths, modularity, hierarchy, hub nodes, and robustness [11]. To understand the complex cortical networks, three main types of connectivity (Structural, Functional, and Effective) have been defined to provide an operational framework.

1.1.2   Structural Connectivity

Structural connectivity refers to the anatomical connections between neural elements and scales from single cell circuits to networks connecting different cortical regions. On a short time scale (seconds to minutes), these networks are considered to be static. Nevertheless, on a larger time scale (hours to days), the networks are considered to be plastic and modify, for example, during learning or aging [11]. Neuroimaging techniques, such as magnetic resonance imaging (MRI), can identify neuronal connections to quantify the structural connectivity [12].

1.1.3   Functional Connectivity

Functional connectivity refers to the statistical dependencies between observed neuronal population responses. Functional connectivity may be inferred from EEG, magnetoencephalography (MEG), functional MRI (fMRI), or other time series data. Dynamic coupling is assumed in cases when two regions are no longer statistically independent [12]. Functional connectivity does not depend on a given model, but rather it is simply a measure of the multivariate responses probability distributions. Therefore, no inference can be made about the causal interactions between nodes [13].

Typical statistical methods for measuring of the dependencies include coherence [14] and synchronization measures [15, 16]. The coherence of two signals measures the phase consistency between them in each frequency band [14].

Since EEG is noisy, non-linear, and non-stationary, phase synchronization is well suited for cortical network determination. Short-range, or local, phase synchronization can be interpreted as creating regional "perceptual binding" [17]. Long-range phase synchronization, between brain regions, is thought to sub-serve motor planning [18, 19], emotion [20, 21], and memory [22, 23, 24, 25].

One measure of synchronization is Phase Locking Value (PLV) which has been applied in the fields of nonlinear dynamics and chaotic systems [26, 27, 28]. The PLV is a measure of the phase coherence between two signals [29]. For example, the PLV of two oscillators with the same frequency equals one, regardless of the phase shift, $\Delta\phi$, between them, as shown in Figure 1.2. PLV is different from coherence because only the phase information from the two signals are used determine the coupling strength.
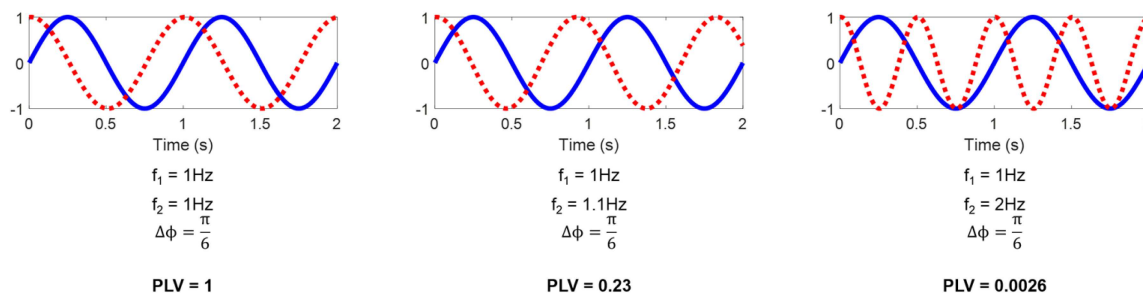
Figure 1.2: PLV values for three examples of coupled oscillators.

1.1.4 Effective Connectivity

Effective connectivity refers to the causal effect one neuronal population (brain region) exerts over another. The connectivity can be inferred through model-based or model-free time series analysis. Model-based techniques include Structural Equation Modeling [30] and Dynamic Causal Modeling [31]. Conversely, information theory concepts, which are model-free, namely Transfer Entropy (TE) [32] and Granger Causality (GC) [33], have been used to define effective connectivity networks based on patterns in data alone [11]. A newly developed

method of assessing causation between time series, Convergent Cross-Mapping (CCM) [34], has been shown to identify predefined causal relationships in manufactured datasets that GC may miss due to the time series inherent nonlinearity or deterministic nature. CCM has been applied in a limited number of studies using different neuroimaging modalities including EEG [35], lead field potentials [36], and fMRI [37].

1.2   Working Memory

The four-part working memory model developed by Baddeley and Hitch in [38] proposed that a central executive system is necessary for reasoning, comprehension, and successful goal-directed behavior. It is responsible for the online organization and processing of information by controlling the flow of information to its subsystems, the phonological loop, visual-spatial sketchpad, and episodic buffer. The phonological loop stores spoken and written information. The visual-spatial sketchpad stores information about what the objects look like and where they are. The episodic buffer is responsible for connecting the visual, spatial, and verbal information to form integrated memories with time [38, 39].

Humans exhibit a capacity limit on the 'load', or number of items, that can be actively maintained. Capacity is defined as $K_C = C(H - F)$, where C is the load, H is the hit rate, and F is the false alarm rate. The hit rate is the percentage of correctly identified matches, and the false alarm rate is the percentage of non-matches identified as matches [40]. Thus, capacity measures how well the participants can identify correct matches scaled by the number of targets in the task.

A popular working memory test is the visuospatial delayed match-to-sample task, as shown in Figure 1.3a. After encoding an initial image, the subject must retain the image in the absence of continuing input during working memory maintenance. During the retrieval

process, the subject must compare the retained and current image to indicate if the images match or not. Another test is an N-back task, where the subject is presented with a sequence of letters, one at a time, and must indicate when the current letter on the screen matches the letter "N" steps before, as shown in Figure 1.3b.
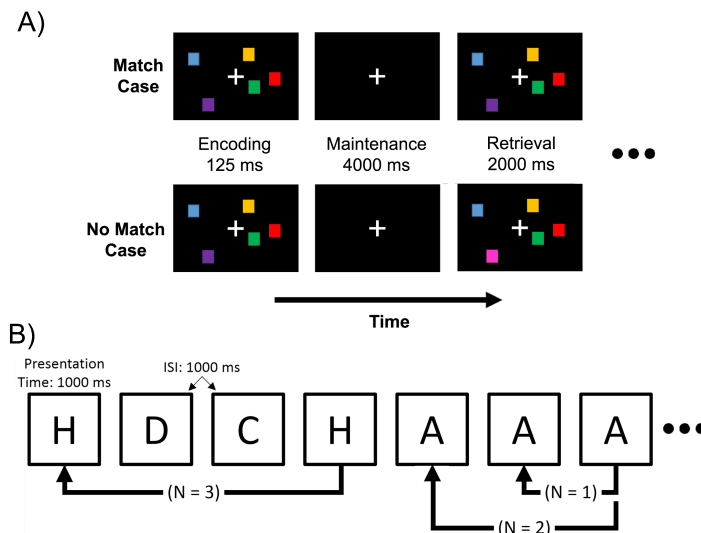
Figure 1.3: a) Match and no-match trials of a visuospatial delayed match-to-sample working memory task. b) Examples of a 1-, 2-, and 3-back task.

From a neurophysiological point of view, the network governing working memory is distributed over a large part of the brain. Previous neuroimaging data suggests that hemispheric specialization varies with the working memory domain (verbal or visuospatial) [41]. Verbal working memory tasks tend to be left lateralized and recruit more regions in the left hemisphere. Visuospatial working memory tasks tend to be right lateralized and recruit more regions from the right hemisphere. Alternatively, it has been proposed that verbal working memory performance rely on the successful encoding of a stimulus as both a spatial object in the right hemisphere and a verbal construct in the left hemisphere [42]. Also, throughout working memory maintenance, the prefrontal and parietal neuronal ensembles are activated simultaneously, as shown in Figure 1.4 [43, 44]. A positive correlation exists between the degree of connectivity and the difficulty of the working memory tasks [45].
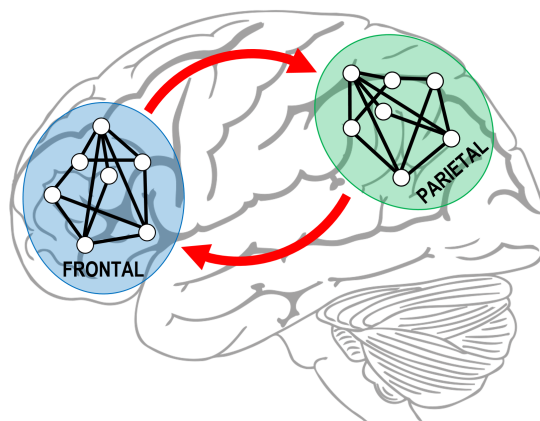
Figure 1.4: The fronto-parietal Working Memory Network

1.2.1 Cortical Synchronization and Working Memory

Since working memory relies upon communication between brain regions and plasticity, it is benefited by phase synchronization of theta, beta, and gamma waves [25], as demonstrated by the literature below. Previous research has shown that an increase in electrocortical phase synchronization across the cortex facilitates neural communication, promotes neural plasticity, and supports working memory [25]. Increased neural communication is facilitated when several synaptic inputs arrive simultaneously at a postsynaptic neuron resulting in higher firing rate output than usual [46]. Synchronous gamma oscillations are confined to local neuronal areas, whereas theta synchronization is effective across long distances (i.e., disparate regions of the brain) [47, 48, 49]. Studies have shown that successful encoding of information during a working memory task requires increased phase synchronization [22, 50, 51, 52, 53, 54, 55]. Theta phase synchronization during a working memory task is sustained during encoding, maintenance, and retrieval between the prefrontal and parietal regions and increases with memory load (difficulty of the task) [48, 56]. Induced beta and gamma synchronization produce increased coherence between frontal and parietal areas during working memory maintenance [57, 58].

1.2.2 Mild Cognitive Impairment and Working Memory

During various working memory tasks, people with MCI show impaired performance and decreased working memory capacity [59, 60, 61]. Most importantly, MCI is associated with a loss of synchronization among neural networks. Both Pijnenburg and Koenig reported that synchronization in the alpha and beta bands is significantly decreased [62, 63]. Also, reduced beta band synchronization is correlated with cognitive impairment [64]. This suggests that, if phase synchronization is increased in people with MCI, then their working memory abilities could be persistently augmented.

1.3 Common Noninvasive Brain Stimulation Methods

Over the past two decades, noninvasive brain stimulation (NIBS) has been a beneficial tool for probing the dynamics of the brain. NIBS provides a safe way to investigate causal links between brain structures involved with cognition, sensory and motor functions. Also, local and regional brain network organization can be determined [65]. The two most common methods of noninvasive brain stimulation are transcranial magnetic stimulation (TMS) and transcranial direct current stimulation (tDCS).

TMS uses a coil connected to a magnetic stimulator to induce current flow and neural activation in the targeted area, as shown in Figure 1.5a. The coil is placed over the desired stimulation region. When the TMS is pulsed repetitively, known as rTMS, inhibitory or excitatory neurons can be activated [66]. TMS is considered to be safe, but some adverse effects include pain and temporary impaired cognition.

tDCS uses a stimulator which delivers weak (<1 mA) currents between two saline-soaked surface sponge electrodes, with one placed on the scalp over the desired area of stimulation

and the other over a reference location, as shown in Figure 1.5b. Anodal and cathodal stimulation produce inhibition and excitation, respectively [67]. A few potential minor side effects to tDCS include skin irritation, nausea, and headaches.
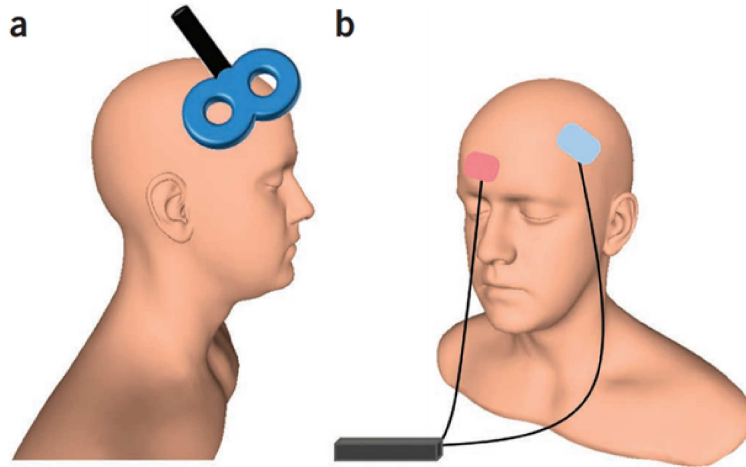
Figure 1.5: a) Standard figure-eight TMS coil placed on the scalp. b) Bipolar tDCS electrode configuration [67].

1.3.1   rTMS and tDCS Effects on Working Memory

Some studies using rTMS and tDCS have explored the influence of the dorsolateral prefrontal cortex (DLPFC) on working memory. A meta-analysis completed by [68] compared 33 N-back studies (19 tDCS and 14 rTMS) who stimulated the DLPFC. The primary results from the analysis showed that, overall, participants who received the NIBS had significantly faster and accurate responses than those who received the sham, or control condition. In addition, stimulating the parietal cortex [69], the cerebellum[70], and the temporal cortex[71] also produced increases in working memory performance. Therefore, noninvasive brain stimulation approaches can induce working memory improvement.

1.4   Binaural Beats

Binaural beats utilize a phenomenon that occurs within the cortex when two different tones are presented separately to each ear [72]. A simplification of the auditory pathway, as shown in Figure 1.6a, begins with the cochlea which converts sound waves entering the ears into electrical impulses which travel up the vestibulocochlear nerve. A third phantom binaural beat, whose frequency is equal to the difference of the two presented tones, is produced within the inferior colliculus (IC). The IC compares the minute differences in timing and timbre from each ear to determine the direction of the sound. The interaural phase difference (IPD) is computed in the IC. The binaural beat is projected up the auditory pathway to primary auditory cortex (A1) [73]. A1 contains a tonotopic map, a representative structure of the cochlea, to map the decomposed frequencies of the acoustic input from high to low. The afferent nerves from the tonotopic map continue to other cortical processing areas [74]. Figure 1.6b shows an example of a 15Hz binaural beat.
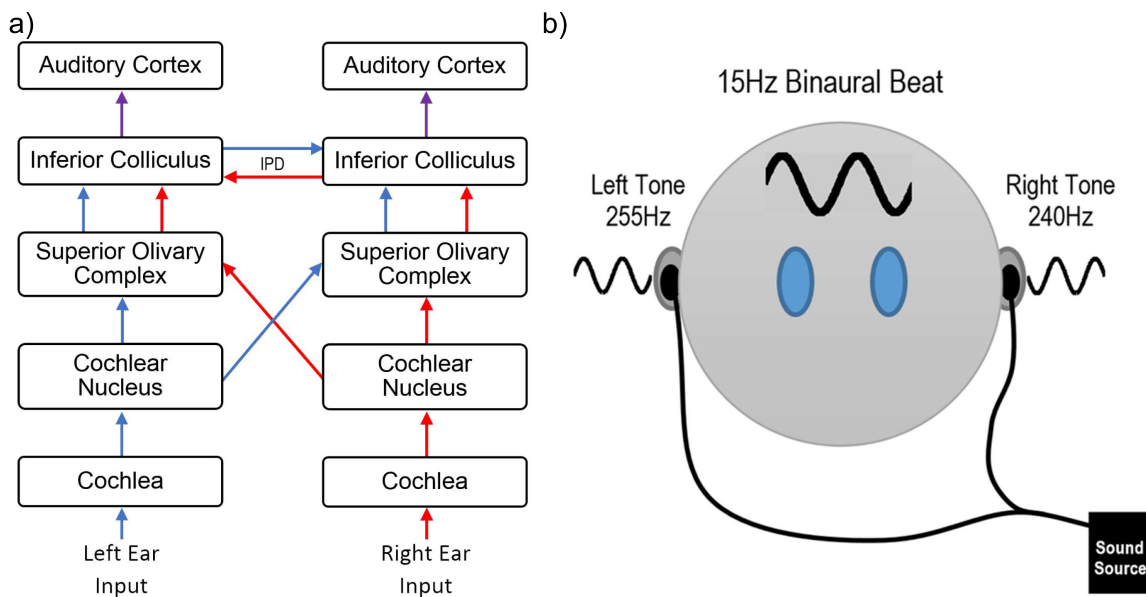
Figure 1.6: a) Auditory pathway which transmits sounds from the cochlea to the auditory cortex. b) Example of 15Hz binaural beats.

Based on the results of Fitzpatrick *et al.*, the auditory cortex experiences the highest amount of synchronization due to binaural beats in the beta band around 16Hz [75]. By selecting appropriate frequencies, auditory entrainment occurs which is characterized by the amplification and transmission of the binaural beat to other areas of the cerebral cortex. Previous research has shown that binaural beats can affect the frequency-specific EEG responses and cortical phase synchronization.

1.4.1 Frequency-Specific Effects

The majority of the studies investigating binaural beat effects on the frequency response are in the gamma range at 40Hz. Ross *et al.* found that binaural beats using a base frequency less that 3kHz is necessary to produce entrainment. He reported that 40Hz binaural beats produced the largest gamma response [76]. Draganova *et al.* determined that the sources creating the auditory steady state responses to 40Hz binaural beats are found in the frontal and medial areas of the cortex [77]. Schwarz and Taylor presented a binaural beat of 40Hz to evoke a steady response. The results of the study indicate that a higher frequency binaural beat exhibited less power but the entrainment is evident in the measured responses over the frontal and parietal lobes [78]. Pastor *et al.* used positron emission topography (PET) and regional cerebral blood flow (rCBF) to find that an increase in rCBF corresponded with oscillatory responses at 40Hz when the subject with presented with a 40Hz binaural beat. The increase in steady state amplitude peak is associated with increased cortical synaptic activity [79]. Some additional studies have investigated lower binaural beat frequencies. Frederick *et al.* reported results that a binaural stimulation at 18.5Hz increased EEG amplitude by 21% at the vertex (top of the head) [80]. Kennerly reported evidence of auditory entrainment after five minutes of binaural stimulation. The binaural stimuli are designed to target the theta or delta ranges. When listening to the presented stimuli, the participants exhibited increased

theta or delta EEG activity during the theta or delta stimulation, respectively [81]. Karino *et al.* published evidence of entrainment within the theta range with the presentation of a binaural beat in the theta frequency range. Also, source analysis showed that the primary activation sites are found in the parietal, frontal cortices, and temporal areas including the auditory cortex [82]. Pratt *et al.* stated that theta binaural beat stimuli evoked typical event related potential (ERP) components followed by oscillations at the binaural beat frequency. Source analysis determined that binaural beats activate the frontal and temporoparietal areas [83]. Gao *et al.* investigated the how binaural beats of differing frequencies affect the EEG activity. They conclude that the various frequency bands influence each other. During delta and alpha binaural beat stimulations, the relative power increased in theta and alpha frequency band response [84].

1.4.2 Phase Synchronization

Becher *et al.* investigated how binaural beats change cortical phase synchronization. They found that EEG power and phase synchronization is significantly modulated at the intracranial EEG temporal-basal, temporal-lateral, mediotemporal sites, and surface EEG sites. Phase synchronization increased at the temporal-lateral site during a 5Hz binaural beat. In addition, EEG power at the mediotemporal, temporal-basal anterior, and temporal-lateral sites increased during a 10Hz binaural beat [85]. Ioannou *et al.* determined that musical expertise does not affect electrocortical activity in response to binaural beats. However, EEG analysis indicates that listening to alpha binaural beats produces the most significance steady state response. Also, cortical network analysis based on phase synchronization shows that listening to theta and alpha binaural beats had a significant impact on the structure of the cortical connectivity network [86].

1.4.3   Cognitive Effect on Memory

Kennerly investigated the effect of beta frequency binaural beat on different measures of human memory. Participants performed tests while binaural beats are played with instrumental music and just during instrumental music. He concluded that the binaural beat group performed significantly better during the word list recall test, the digit symbol test, and the digit span test [87]. Lane *et al.* tested participant performance during a 1-back working memory test while listening to either theta or beta range binaural beats. EEG analysis showed improvement in target deduction and decreased false alarm rate while listening to binaural beats in the beta frequency range compared to theta range. Furthermore, beta binaural beats caused lower task-related confusion and fatigue when compared to theta binaural beats [88]. Fernandez *et al.* tested the effects of theta binaural beat on verbal memory. Participants performed significantly better at the word recall task when listening to 5Hz binaural beat compared to 13Hz [89].

1.5   Noninvasive Brain Stimulation Controllers

In the majority of clinical trials and therapy sessions, NIBS is applied in an open-loop stimulation setting. However, recently, TMS stimulation protocols have been developed which are controlled by the EEG to close the loop. Specific brain state markers, such as a certain phase or power of cortical oscillatory activity, are continuously monitored and used to trigger the NIBS in a feed-forward manner [90]. This paradigm is used to modulate brain activity during non-REM sleep by pulsing the TMS in phase and out of phase of the slow-wave oscillations detected by EEG [91]. Alternatively, similar experiments used visual flashes [92] or auditory stimulation [93], in the form of short bursts of noise, to drive the cortical oscillations at the desired low frequency.

Brittain *et al.* demonstrated that NIBS could be used in conjunction with a closed-loop controller to suppress tremor amplitude in people with Parkinson's disease [94]. The phase of the tremor, as measured by an accelerometer, is used as the feedback signal to the controller. The proportional controller generated transcranial alternating current (tACS) oscillations to phase-cancel the endogenous tremor rhythm. The stimulation is applied to the motor cortex. Overall, the tremor amplitudes could be suppressed up to 50% by using the closed-loop control method.

To the best of our knowledge, only once before have binaural beats been utilized within a closed-loop control system for neural stimulation. In [95], Settapat *et al.* developed a binaural beat control system to entrain the user to a meditative state in real-time. An autoregressive forecasting model is implemented to predict the user's arousal state from the frequency response of the EEG within the alpha band. A fuzzy logic controller is used to modulate the presented binaural beat based on the EEG power and forecasting error signal. The results of the experiment showed that the arousal state of the participant could be altered to be maintained within the meditative state. If the arousal state is too high, then a lower frequency binaural beat is played bringing the arousal state down, or inversely if the arousal state is too low [95]. While this work promises the ability to drive EEG with binaural beats, the controller is unable to dynamically adapt to subjects' states and furthermore does not demonstrate behavioral outcomes that may be associated with such controlled signals.

Up to this point, no closed-loop controllers and noninvasive brain stimulation methods have been coupled to modulate working memory.

1.6   Summary of Work

The research presented in this dissertation includes a comparison of techniques to build networks, open-loop binaural beat stimulation studies, development of a closed-loop control brain network simulation environment, and an experimental closed-loop EEG-based binaural beat study.

The second chapter compares the results of using PLV and CCM to develop resting state brain connectivity networks. The resting state network is primarily activated when the person allows their mind to wander and the brain is resting, but awake. When the person is not purposefully engaging in a task, this network activates "by default". The results suggest that the network characteristics follow the same trends and the similarity between the computed networks, for both algorithms, is highly significant. However, CCM is able to identify low or one-way connection strengths better than PLV but takes exponentially longer to compute.

The third chapter through the fifth chapter details the results of the use of open-loop binaural beats used to entrain certain brain structures utilized during working memory via existing neural pathways. The brain signals are recorded using EEG. In these two studies, we determined the effects of different acoustic stimulation conditions on participant response accuracy and cortical network topology, as measured by EEG recordings, during visuospatial (Chapter 3) and verbal (Chapter 4) working memory tasks. Three acoustic stimulation control conditions and three binaural beat stimulation conditions are used: None, Pure Tone, Classical Music, 5Hz binaural beats, 10Hz binaural beats, and 15Hz binaural beats. Chapter 5 shows additional analysis which compares the networks developed for each task. Overall, these results suggest that this safe and accessible stimulation method can be used to modulate behavioral performance and cortical connectivity.

Chapter 6 describes the large scale brain network model used to assess closed-loop controller performance. Using a computational model of the brain (The Virtual Brain), we studied, in simulation, the effect of a binaural beat stimulus on key brain regions associated with auditory processing. The simulations are used to test both a linear and adaptive controller's ability to change cortical responses using the controlled binaural beat stimulus.

Chapter 7 details the development and testing of an experimental closed-loop EEG-based controller used to modulate the binaural beat stimulus that the person hears during a working memory task. Each person's brain functions in slightly different ways, so an open-loop control system for brain stimulation is impractical from a control engineering perspective. The input of the system will be binaural beats delivered through headphones. Entrainment of the beat frequency throughout the brain will be recorded using EEG.

1.6.1 Significance of Work

Only a limited number of studies have investigated the effects of binaural beats on working memory, which controls the temporary retention and online processing of information. Furthermore, no studies have evaluated the effects of binaural beats on brain connectivity during working memory tasks.

Connectivity Metric Comparison. We found that PLV is a fast metric to compute functional connectivity which makes it ideal for on-line network identification and as a feedback signal within a closed-loop control system since it is an excellent approximation of the network computed with CCM.

Visuospatial Working Memory Task. We found that listening to 15Hz binaural beats during the delayed match-to-sample visuospatial working memory task not only increased the response accuracy but also modified the strengths of key connections in the cortical

networks during the task. The three auditory control conditions and the 5Hz and 10Hz binaural beats all decreased accuracy. Based on graphical network analyses, the cortical activity during 15Hz binaural beats produced networks characteristic of high information transfer with consistent connection strengths throughout the visuospatial task.

Verbal Working Memory Task. We determined that listening to 15Hz BB during an N-Back working memory task increased the individual participant's accuracy, and changed the connection strengths of the cortical networks during the task. Only the 15Hz BB produced a significant change in relative accuracy compared to the None condition. Based on graphical network analyses, listening to 15Hz BB produced networks characterized by higher information transfer during the N-back task than other auditory stimulation conditions.

Closed-Loop Simulation Platform. We developed the first simulation environment for an EEG-based closed-loop control of TVB using binaural beats. Results suggest that the connectivity networks, constructed from simulated EEG, may change with certain binaural beats stimulation frequency. In this work, we demonstrated that a linear controller and an adaptive controller can successfully modulate TVB connectivity.

EEG-based closed-loop control of working memory. The developed system provides the first experimental assessment of cortical connectivity using closed-loop binaural beats. Compared to current methods of brain stimulation both for system identification or therapeutic interventions (i.e., transcranial alternating/direct current, transcranial magnetic stimulation, and ultrasound), binaural beats capitalize on existing brain structures to entrain higher-level areas of the cortex. In addition, binaural stimulation does not require extensive equipment or a clinical setting to be used safely. As a result, this system has the potential to be further developed into a medical device to identify and control working memory disorders indicative of cognitive impairment even outside clinical settings. Thus, any associated therapies developed in the future have a strong potential for broad application and usability.

Chapter 2

Comparison of Phase Locking Value and Convergent Cross Mapping

Quantifying the resting state connectivity of the brain–which is a complex network of neural circuits–is a nontrivial task. The resting state network is primarily activated when the person allows their mind to wander and the brain is resting, but awake. When the person is not purposefully engaging in a task, this network activates "by default". The primary regions activated in the network are the posterior cingulate cortex and medial prefrontal cortex [96, 97, 98]. The purpose of this chapter is to compare the resulting connectivity networks using both the PLV and CCM algorithms. PLV is a model-based metric since the data is assumed to be oscillatory. PLV is typically a better choice than correlation for EEG data, since it is more robust to amplitude fluctuations [99, 100]. Networks defined using PLV are undirected weighted graphs since PLV is a functional connectivity metric, and therefore pairwise comparisons between nodes are symmetric. On the other hand, CCM is a model-free method, since it detects causal influences based on the ability to estimate one time series with another. Networks developed using CCM are directed weighted graphs since CCM is an effective connectivity metric, which is generally not symmetric. In terms of computation

time, PLV is significantly faster than CCM. However, CCM is able to identify and quantify more nuanced pairwise interactions than PLV. To investigate the two methods, we apply both PLV and CCM algorithms to simulation and resting-state fMRI and EEG datasets. The connectivity networks they generate are analyzed using network characteristic metrics and a similarity metric.

2.1   Methods

Three different datasets are used in this analysis. The first is a toy dataset made up of simulations to test the PLV and CCM algorithms under different known synchronization conditions. The second and third datasets contain experimental resting state EEG and fMRI data, respectively.

2.1.1   Toy Synchronization Dataset

To understand the output of the two analytical methods on a known system, we created a toy synchronization dataset from a two degree of freedom mass-spring-damper system illustrated in Figure 2.1 and with governing equations

$$m_1\ddot{x}_1 = -c\dot{x}_1 - kx_1 + a_1(x_2 - x_1) + F_1, \tag{2.1}$$

$$m_2\ddot{x}_2 = -c\dot{x}_2 - kx_2 + a_2(x_1 - x_2) + F_2, \tag{2.2}$$

where the masses (m) are $m_1 = m_2 = 1$ kg, the spring constant is $k = 5000 \text{ kg} \cdot \text{s}^{-2}$, and the damping coefficient is $c = 2\zeta\sqrt{mk} = 70.71 \text{ kg} \cdot \text{s}^{-1}$ using a damping ratio $\zeta = 0.5$. The initial starting conditions are $\dot{x}_1 = 0.01$, $x_1 = 1$, $\dot{x}_2 = 0.01$, and $x_2 = 1$. The coupling strengths, a_1 and a_2, are equal to ak where $a \in \{0\%, 25\%, 50\%\}$. Each mass is displaced by

its respective forcing function F_1 or F_2. Each forcing function is a linear combination of five different sine waves with an amplitude of 1 N and frequencies selected between 4Hz and 8Hz using a uniformly distributed random variable. The simulated inputs are designed to mimic endogenous theta/alpha oscillatory inputs with random power and frequencies (within this range) and thus demonstrate the robustness of each method to variations in endogenous dynamics. As a_1 increases, x_1 converges to the x_2 response since the coupling between the system dominates the individual forcing. Alternatively, as a_2 increases, x_2 converges to the x_1 response similarly. The governing equations are numerically solved in Matlab using ode45 with a fixed time step of 0.01 seconds for a total of 21 seconds. The first second of data is chopped to remove the transient.

Figure 2.2 illustrates the structure of the toy synchronization dataset generated from the numerical solver. A simulation is defined as the set all of the trials using the same forcing functions F_1 and F_2. A trial is defined as the resulting time series for a specific combination of a_1 and a_2. Every combination of a_1 and a_2 is used, which results in a total of nine different trials per simulation. In total, we ran 1000 simulations to understand the distribution of responses resulting from the random forcing functions.
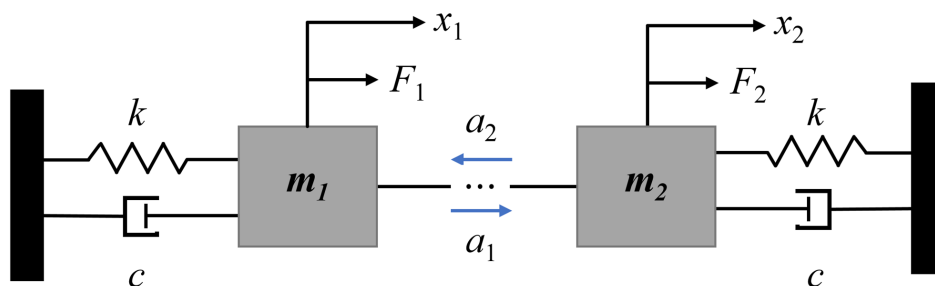
Figure 2.1: Illustration of the coupled mass-spring-damper dynamical system used to create the toy dataset.
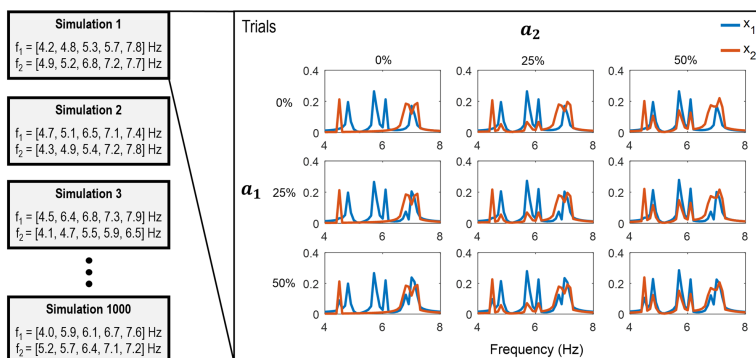
Figure 2.2: The structure of the toy synchronization dataset. In each simulation box, the five frequencies used in the forcing functions are listed. The breakout box shows all of the trials within Simulation 1 for different a_1 and a_2 combinations. The 9 graphs show the frequency responses of x_1 and x_2.

2.1.2 Resting State Datasets

For this paper, we tested an EEG dataset and a fMRI dataset, from participants at rest, to compute the resting state networks. The resting state EEG dataset is obtained from [101], which is the data presented in [102]. In total, they comprise recorded 64 channels of data from 12 participants (6 females, aged 26.6 ± 2.1 years) for 5 minutes [102]. The channels are placed according to the 10-20 system. The resting state fMRI data set, called Beijing_Zang [103], is obtained from the 1000 Functional Connectomes Project database. For acquisition, the researchers use a 3T scanner with a repetition time (TR) value of 2 seconds, 33 slices, and a total of 225 time points. Of the total 198 healthy adult subjects in the dataset (122 female, aged $18 - 26$), 50 participants are randomly selected for this analysis.

EEG Data Processing

The EEGlab toolbox in Matlab is used to preprocess the raw EEG data [104] (Table S1). First, the EOG, ECG, TP9, and TP10 channels are removed. Next, the EEG data is

downsampled to 500Hz from 5000Hz. Then, the data is bandpass filtered (0.5Hz – 50Hz) to remove drift and the 60Hz power line noise. Next, the filtered EEG is re-referenced to the average. Subsequently, the artifacts are removed using automatic continuous rejection in EEGlab. Independent component analysis is used to remove the eye blink components [105]. Next, the clean EEG is bandpass filtered (8Hz – 12Hz) to focus on the alpha band which has previously been associated with resting state [106, 107, 108]. Finally, the network computation is only performed on the last minute of clean EEG data to ensure the participant had achieved resting state.

fMRI Data Processing

The SPM12 [109] and CONN toolboxes [110, 111] in Matlab are used to extract the regional activity. First, the images are preprocessed using SPM12, where slice-timing correction, realignment, normalization, and segmentation are performed. Then, in CONN, the functional data is smoothed, the voxel-to-voxel covariance is computed, and the regional activity is extracted. By default, CONN uses a combination of the Harvard-Oxford atlas and the AAL atlas to define 136 regions of interest (ROI). For this paper, the 91 ROIs from the Harvard-Oxford atlas are used.

2.1.3 Connectivity Networks

Using the time series data from each of the datasets, we develop networks that are comprised of nodes and edge weights. The toy data network is made up of two nodes which represent the responses x_1 and x_2, for each simulation. For the EEG and fMRI datasets, the electrode channels and the ROIs are set as the nodes, respectively. In this paper, we assume all networks are all-to-all and we apply two different measures to define the edge weights, namely

Phase Locking Value and Convergent Cross-Mapping.

Phase Locking Value

PLV measures the phase coherence between two signals. For example, the PLV of two identical oscillators is 1 if the phase difference is continually fixed, and is 0 if constantly changing [29]. We compute the PLV by first converting the time series into analytic signals using a Hilbert transform [112]. The phase, in radians, of channel h is denoted $\phi_h(t)$. The phase difference between channels h and i is given by

$$\theta_{hi}(t) = (\phi_h(t) - \phi_i(t)) \mod 2\pi. \tag{2.3}$$

All pairs of channels are compared against each other via the PLV defined as

$$\text{PLV}_{hi} = \frac{1}{N} \left| \sum_{k=1}^{N} \exp\left(j\theta_{hi}(k\Delta t) \right) \right|, \tag{2.4}$$

where $j = \sqrt{-1}$ is the imaginary unit, and $\Delta t = \frac{T}{N}$ where T is the time series duration and N is total number of discrete time steps. The implemented PLV algorithm uses the entire length of the time series for the phase difference computation. However, before the computation of the PLV value, the initial 10% and final 10% of the data is removed to account for the edge effect from the Hilbert transform.

Convergent Cross-Mapping

As opposed to the functional connectivity measured by PLV, we seek a method to quantify causal relationships, and thus effective connections, in imaging data at different brain regions. However, the lack of universal definition of causality has attracted researchers from various disciplines, and a variety of methods have been proposed. The earliest method developed

is Granger causality [33], which relies on the idea of separability. Separability indicates separating the influence of causative factors from the effects [34, 113]. GC is a model-dependent method as it assumes a linear vector-autoregressive model to fit the dataset [114], and hence reliably captures a linear relationship. Since most real-world systems are non-linear, research has turned toward the discovery of model-free methods that do not assume a background model, namely transfer entropy [32] and convergent cross-mapping [34]. Transfer entropy and Granger causality both have the underlying assumption that cause precedes the effect, and hence can better predict the future of the effect. In addition, TE and GC are equivalent measures for Gaussian-distributed random variables [115]. The idea of separability in GC has been identified to be problematic as the causal variables can be falsely removed from the set of causes without deteriorating the predictability of the effect (see an example in the supplementary information of [34]). Recently, a multivariate extension of GC has been developed and applied to neuroscience applications [115, 116]. CCM is relatively recent and introduces a new definition of causality based on the hypothesis that the cause is better estimated by the effect, thus the definition differs fundamentally from GC and TE. Furthermore, CCM has the potential to capture non-linear relationships and may be better at correctly identifying the causal variable in comparison to both TE and GC, particularly for systems with strong deterministic components [34]. CCM has only been explored in the context of neuroscience in a couple of journal publications [35, 36, 37]. This study seeks to test the usability of CCM for effective connectivity brain networks from both EEG and fMRI data, and to compare these results to PLV.

CCM is an algorithm to detect and quantify causal influence between two time series variables, and is first introduced in [34]. Given two causally related time series variables, $X(t)$ and $Y(t)$ where t denotes the time index and in the case of unidirectional causality (X drives Y), the causal variable (X) is assumed to imprint evidence of causation on the af-

fected variable (Y). CCM exploits this idea by testing whether past values of Y can be used to better estimate the values of X. In particular, the algorithm compares the ability of lagged components of one time series variable to estimate the dynamics of another, and the relative skill of estimation is defined as the strength causal influence. A detailed description of the algorithm can be found in the supplementary materials of [34] which is summarized as follows. The first step of the algorithm is to create a shadow manifold from time-delayed projections of each time series independently. We compute the shadow manifold for X by embedding the time series on an E-dimensional manifold as points of the form $(X(t), X(t - \tau), X(t - 2\tau), \cdots, X(t - (E - 1)\tau))$, where τ is a constant time delay. These data points are defined for $t \in \{1 + (E - 1)\tau, 2 + (E - 1)\tau, \cdots, L\}$, where L, also called the library size, is the length of the time series used for the embedding. The E-dimensional manifold containing these points is called the shadow manifold of X, denoted by M_X. Similarly, we construct a shadow manifold of Y, called M_Y. Next, cross-mapped estimates of $Y(t)$ (and $X(t)$) are computed by locating the nearest neighbors on M_X (and M_Y). Finally, cross-mapped estimation skill is evaluated using Pearson's correlation coefficient between Y and estimated Y, where correlation coefficient values close to one indicate better estimation skill. The negative correlation values are replaced by zeros in line with the method in [34], and the CCM values range in between 0 and 1 and are unitless. As the library size is increased, the cross-mapped estimation improves and converges to a constant value, and thus the causal variable is identified by the asymptotic value of cross-mapped estimation. In real-world datasets, the convergence value is dictated by the presence of measurement error, process noise, and the length of the dataset [34]. CCM in the present study is implemented using rEDM package [117] in R, where the optimal embedding dimension E is evaluated following Simplex Projection method [118], and the lag τ used for the construction of the shadow manifold is set to 1 by default. Note that the computation of E follows an existing method that may yield the same result as other methods seeking optimal embedding dimen-

sions, but the use of the E-dimensional time-delayed shadow manifold to estimate causality through nearest-neighbor relationships is unique to CCM.

Network Construction and Computation Time

The graphical network is constructed using the index of a set of time series as the nodes ($\mathcal{V} = \{1, ..., n\}$), where $n = 2$ (Toy data), $n = 60$ (EEG data), and $n = 91$ (fMRI data). The connectivity network is assumed to be all-to-all, meaning there is an edge between every pair of nodes. The weights associated with these edges are computed using both PLV and CCM, and they are represented in weighted adjacency matrices whose ijth entry captures the weight of connection from node i to node j. Using PLV, we define the weighted adjacency matrix W_{PLV} with elements $w_{ij} = \mathrm{PLV}_{ij}$, $i, j = 1, 2, ..., n$. Due to the properties of PLV, w_{ij} is in $[0, 1]$ and W_{PLV} is symmetric since PLV (and hence the network) is undirected. Using CCM, we define the weighted adjacency matrix W_{CCM} with elements w_{ij} as the cross-mapped skill from node i to node j. The network is directed since W_{CCM} is not symmetric in general.

The computation time for the PLV algorithm is much faster than the CCM algorithm. As the number of nodes and length of the time series increases, the computation time for CCM increases exponentially while the increase for PLV is linear. The results presented in this paper are run on a Windows 8 64-bit computer with an Intel i7-2600 CPU at 3.40GHz using 16GB of RAM. Table 2.1 lists the mean and standard deviation of the computation time, over 5 runs, for the toy, EEG, and fMRI datasets.

Table 2.1: Computation time statistics, over 5 runs, for each of the datasets.

	Toy Data Set		EEG Dataset		fMRI Dataset	
	PLV	CCM	PLV	CCM	PLV	CCM
Mean	5.51 E-3 s	4.02 s	2.57 s	4.14 E+4 s	1.91 s	105.12 s
SD	2.93 E-3 s	0.06 s	0.07 s	9.65 s	0.01 s	0.12 s

Network Similarity Statistic

A general similarity metric between two networks, W_{PLV} and W_{CCM}, is defined as

$$S(k) = 1 - \frac{||W_{\mathrm{PLV}}(k) - W_{\mathrm{CCM}}(k)||_2}{||W_{\mathrm{PLV}}(k)||_2}, \tag{2.5}$$

where k is the index of networks in the dataset, and $||\cdot||_2$ is the Euclidean norm. The range of the similarity metric is between 0 and 1, where 1 indicates perfect similarity or that the matrices are equal. The second term in the equation is roughly equivalent to percent difference. Therefore, as the difference between the two matrices increases, the second term becomes larger, which causes the similarity metric to decrease. For the toy dataset, the similarity metric is notated with subscripts S_{a_1, a_2} since it is also a function of the coupling strengths a_1 and a_2. For the neuroimaging datasets, the diagonal values of W_{PLV} and W_{CCM} are 1 and 0, respectively. Therefore, in order to not consider the diagonal values in the similarity metric, they are all set to zero before computation.

In order to assess the significance of the similarity between the CCM and PLV networks from the neuroimaging data, six control cases are created where a percentage of the nodes (channels or ROIs) in the W_{CCM} matrix are re-ordered using 100 independent random permutations, per participant. The re-ordering percentages used are 0% (no nodes are re-ordered) to 100% (all nodes are re-ordered) by steps of 20%. In all of the computations, the order of the nodes in the PLV matrix remained constant. Therefore, for each participant and node scrambling percentage, 100 similarity metrics are computed, and the mean value is used as a control for the statistical analysis. The mean of the similarity metrics, one for each participant, is implemented in a one-way ANOVA to determine the effect the six different percentages of scrambled nodes has on the similarity metrics. The familywise error rate is set at 0.05 for the Tukey HSD post hoc test.

2.1.4 Toy Dataset Analysis

The toy dataset is analyzed for the specific purpose of understanding how increasing the coupling parameters affected the frequency response of the system and the resulting PLV and CCM networks. As the coupling parameters a_1 and a_2 increase, the resulting x_1 and x_2 time series responses become increasingly similar. In order to show this trend, we compared the frequency responses of x_1 and x_2, for specific a_1 and a_2 combinations. The magnitude components of the frequency response of $x_1(a_1, a_2)$ and $x_2(a_1, a_2)$, for the kth simulation, are defined as $F_{x_1}(k, f_i)$ and $F_{x_2}(k, f_i)$, respectively. The frequencies evaluated in the FFT are f_i where $i = \{1, ..., N\}$, where N is the total number of frequencies used. The mean absolute spectral difference, d_s, between the two responses is computed using

$$d_s(k) = \frac{1}{N F_n(k)} \sum_{i=1}^{N} |F_{x_1}(k, f_i) - F_{x_2}(k, f_i)|, \tag{2.6}$$

$$F_n(k) = \frac{1}{2} \Big[||F_{x_1}(k, f_i)||_2 + ||F_{x_2}(k, f_i)||_2 \Big], \tag{2.7}$$

where F_n is a normalization factor. A higher d_s value indicates a larger difference between the two frequency responses.

In addition, the 2×2 interaction networks determined using PLV and CCM are computed for all the trials in each simulation. The mean and standard deviation of the similarity metrics, over all 1000 simulations, are computed for all coupling strength combinations.

2.1.5 Resting State Neuroimaging Dataset Analysis

After processing the data, networks for the neuroimaging data are computed using both the PLV and CCM algorithms. For the EEG and fMRI data, the library size for the CCM algorithm is set to the entire length of the time series which are 5000 and 255, respectively.

The convergence graphs for the EEG (Figure A.2) and fMRI data (Figure A.3) are shown in Appendix A. The cross-mapped estimation skill is seen to converge for data of this length by visual inspection. The network characteristic measures computed are used to compare the structural features of the resulting graphs. Then, the similarity of the PLV and CCM matrices are compared.

Mean Theta Network Comparisons

Two analyses assess the differences between the derived PLV and CCM networks. First, the range of the edge weights (largest – smallest) in the networks for both PLV and CCM are compared in a one-tailed t-test, over all participants. Second, for each specific link in the network, a t-test is used to compare the CCM and PLV connection strengths, which results in an $[n \times n]$ matrix of uncorrected t-statistic values. For both the EEG and fMRI networks, the links where W_{PLV} and W_{CCM} are significantly different ($p < 0.01$), over all participants, are assessed. Two separate graphs are developed to show the links where $W_{\text{PLV}} > W_{\text{CCM}}$ and $W_{\text{PLV}} < W_{\text{CCM}}$.

Network Characteristics Measures

The PLV and CCM networks are analyzed using four different network measures. The measures are computed at different network densities, which is the number of connected edges over the total number of possible edge connections sorted by edge weight from high to low. For example, at a density of 0.1, only the largest 10% of edge weights in the network are kept and the rest are set to 0. The Brain Connectivity Toolbox (BCT) in Matlab is used to compute the degree, clustering coefficient, betweenness centrality, and efficiency metrics [119]. In order to assess the differences between the PLV and CCM results for each network

characteristic, a t-test is applied at each network density.

1. The degree of the ith node (D_i) is the sum of the edge weights connected to the node. It is a measure of the amount of information coming into the node from other regions, and is computed using

$$\text{D}_i = \sum_{j=1}^{n} w_{ji}, \tag{2.8}$$

where n is the number of nodes.

2. The clustering coefficient of the ith node (CC_i) is the proportion of its adjacent nodes which are interconnected. It is a measure of local connectivity around the node and can be defined using

$$\text{CC}_i = \frac{2}{k_i(k_i - 1)} \sum_{j=1}^{n} \sum_{h=1}^{n} (\tilde{w}_{ij}\tilde{w}_{ih}\tilde{w}_{hj})^{1/3}, \tag{2.9}$$

where $k_i = \sum_{j=1}^{n} |\text{sgn}(w_{ji})|$ is the unweighted degree. The weights are normalized, to ensure that CC_i remains between 0 and 1, using $\tilde{w}_{ij} = w_{ji}/\max_{i,j=1,\ldots,n} w_{ji}$.

3. The betweenness centrality of the ith node (BC_i) is the number of shortest paths between all node pairs that pass through node i. A path of length k from node j to h is a sequence of $k + 1$ distinct nodes with consecutive nodes adjacent with respect to the edges in the graph. A shortest path between j and h minimizes k. The number of shortest paths from j to h is given by σ_{jh} and the number of those paths which include node i is given by $\sigma_{jh}(i)$. The value is scaled between 0 and 1 by the number of nodes in the network, n. The betweenness centrality, defined as

$$\text{BC}_i = \frac{1}{(n-1)(n-2)} \sum_{\substack{h,j \in \mathcal{V} \\ h \neq i \neq j}} \frac{\sigma_{jh}(i)}{\sigma_{jh}}, \tag{2.10}$$

sums the fraction of shortest paths between nodes on which the ith node lies. High betweenness centrality indicates that the node has a large influence on the overall transfer of information through the network.

4. The efficiency (E) of the network is the average of inverse shortest path length, and is inversely related to the characteristic path length. The efficiency is defined as

$$E = \frac{1}{n(n-1)} \sum_{\substack{i,j \in \mathcal{V} \\ i < j \\ i \neq j}} \frac{1}{d(i,j)}, \tag{2.11}$$

where $d(i,j)$ is the length of the shortest path between nodes i and j.

2.2   Results

2.2.1   Toy Data Simulations

For the toy data, the simulated time responses are analyzed to assess the effect of coupling strength on the frequency response and the PLV and CCM networks.

Frequency Response of the Simulations

The comparison of the frequency response of the two coupled time series of the toy data is shown in Figure 2.3. The average spectral difference, over 1000 simulations, is shown as the blue surface. The standard deviation, at each coupling combination, is denoted by the black dots. When the coupling strength is 0%, the difference between the frequency response of two signals is high. However, as both coupling parameters increase, the two signal's frequency responses converge to each other and the difference decreases. In addition, over the 1000

simulations, the resulting mean and standard deviation values are symmetric for both a_1 and a_2. Therefore, the model does not favor one coupling direction over another, which is to be expected since the two systems are identical when unforced and decoupled.
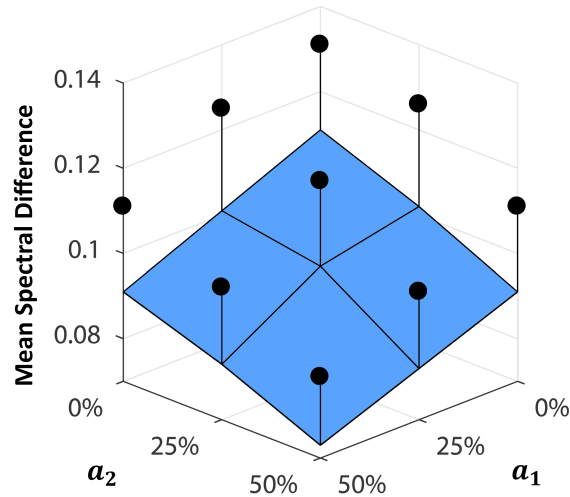
Figure 2.3: The difference between the frequency responses for different coupling combinations. The surface and dots indicate the means and standard deviations, respectively.

Similarity between the PLV and CCM networks

Figure 2.4 shows two examples of the computed PLV and CCM networks for different coupling strengths. The networks follow the same naming convention so the strength from x_1 to x_2 is read as from the 1st column to the 2nd row. The forcing functions used in this simulation are

$$F_1(t) = \sin(4.8t) + \sin(5.7t) + \sin(5.8t) + \sin(6.1t) + \sin(7.1t), \tag{2.12}$$

$$F_2(t) = \sin(4.5t) + \sin(6.7t) + \sin(6.8t) + \sin(7.0t) + \sin(7.2t). \tag{2.13}$$

Figure 2.4a shows a one-way coupling case since only $a_1 > 0$ which means that only the x_1 response is influenced by x_2. The PLV algorithm cannot differentiate the one-way coupling and therefore the network is symmetric. In addition, the PLV algorithm estimated the

strength of the connection to be higher than the output of the CCM algorithm. In the CCM network, the connection strength from x_2 to x_1 is higher than the reciprocal connection. Therefore, the CCM algorithm identified the predominant directionality within the network. In Figure 2.4b, the coupling is present in both directions but is strongest from x_1 to x_2. In this case, the connection strength computed using PLV is closer to those found with CCM. In this case, CCM is able to identify that the connection from x_1 to x_2 is higher than the reciprocal connection. For the CCM algorithm, the library size is set to 2000, which is the maximum length of the dataset. In Appendix A, the convergence graphs, for the two cases, are shown in Figure A.1; the cross-mapped estimation skill is seen to converge for data of this length by visual inspection.
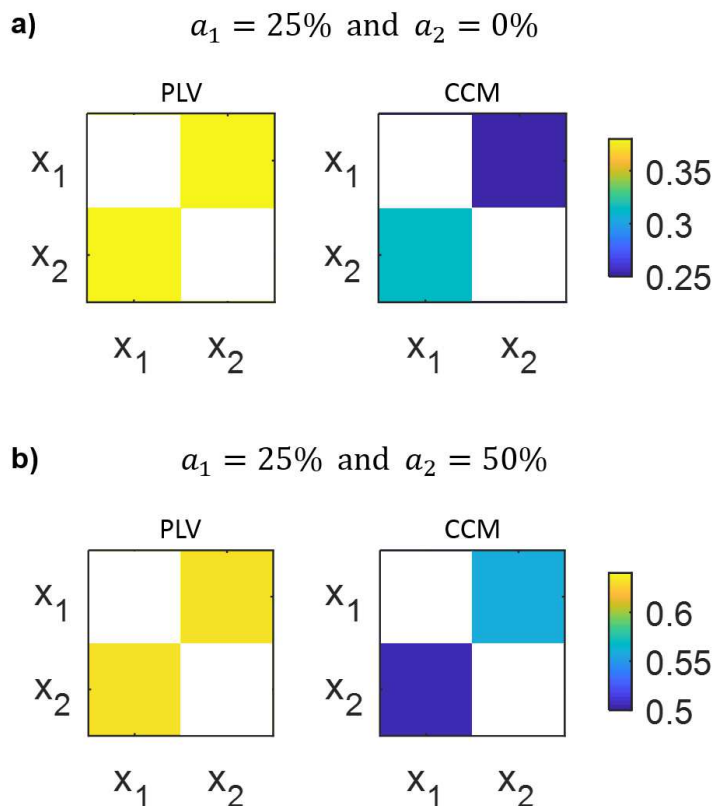
Figure 2.4: Comparison of the PLV and CCM network results for the a) one-way coupling case and b) two-way coupling case. The diagonal is equal to 1 for PLV and 0 for CCM.

The mean and standard deviation of the similarity metric, over the 1000 simulations, for various coupling strengths is shown in Figure 2.5. When the coupling is small, the similarity between the PLV and CCM matrices is approximately 0.9. The lower values are largely due to the fact that CCM can identify lower coupling or one-way coupling while PLV overestimates the strength. However, as the strength of both coupling parameters increase, the similarity metric increases to nearly 1, which is a nearly perfect match between the two matrices. Overall, the standard deviation is very low. The largest variations occur around the lower coupling strengths.
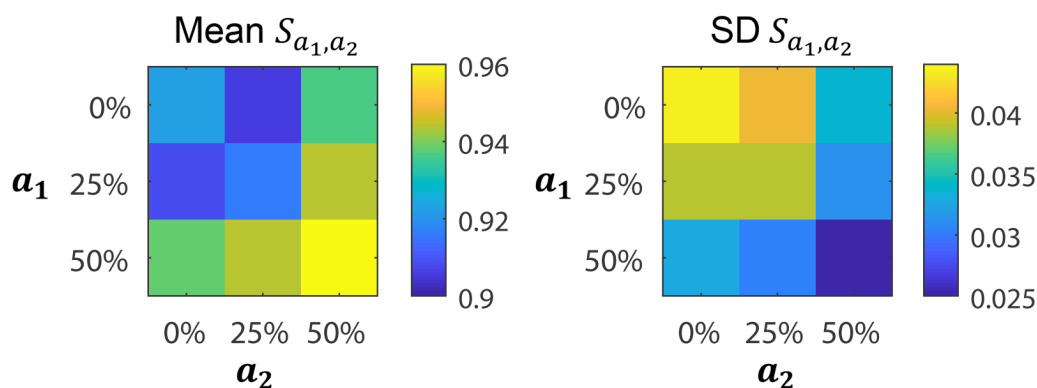
Figure 2.5: The mean and standard deviation of the similarity metric, over the 1000 simulations, for different coupling strengths.

2.2.2   Theta EEG Networks

The mean PLV and CCM networks, over 12 participants, are shown in Figure 2.6. The list of the channels used is located Table A.1 in Appendix A. Both networks exhibit highly similar patterns. However, the range of the edge weight strength in the CCM network (0.960 ± 0.026) is greater than the PLV network (0.936 ± 0.032). A one-tailed t-test showed that the range of the CCM network is significantly higher than the PLV network $(t(22) = 1.97, p = 0.031)$.
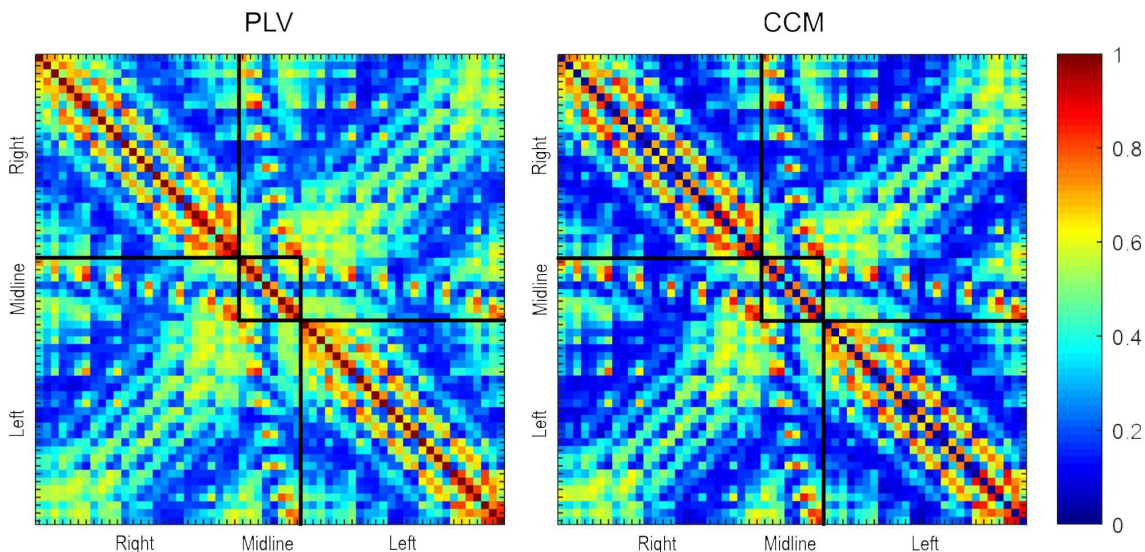
Figure 2.6: Mean PLV and CCM networks from the resting state EEG dataset. Right, Midline, and Left correspond to the electrodes in the right hemisphere, midline, and left hemisphere respectively. The diagonal for PLV and CCM is 1 and 0, respectively.

In addition, Figure 2.7 shows the individual links which are significantly different ($p < 0.01$) between the two networks. The number of links where the edge weight of the PLV network is significantly higher than the CCM network greatly outnumbers the number of links where CCM is greater than PLV. Therefore, the CCM algorithm can detect nuances in the data, which we assume is driven by real changes in network strength structures.

EEG Network Characteristics

The PLV and CCM network characteristics at the previously defined densities are shown in Figure 2.8. For all of the metrics between densities of 0.1 and 0.4, the mean values overlap nearly perfectly. However, as more edge weights are considered at each density, the means diverge but are not significantly different from each other when considered in t-test, for any of the properties. This result indicates that PLV and CCM produce networks with very similar characteristics.
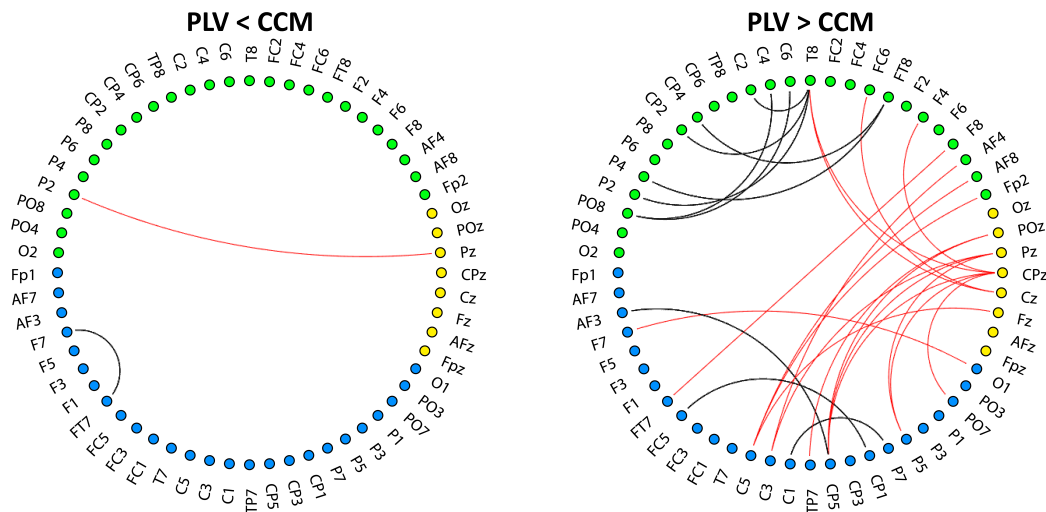
Figure 2.7: The circular graphs show which links have significant differences between the PLV and CCM networks. The left graph shows the connections where the CCM edge weights are significantly stronger than the PLV network. The right graph shows the connections where the PLV edge weights are significantly stronger than the CCM network. The blue, yellow, and green dots represent the left, midline, and right hemisphere, respectively. The black and red lines indicate the intra-hemispheric and inter-hemispheric links, respectively.
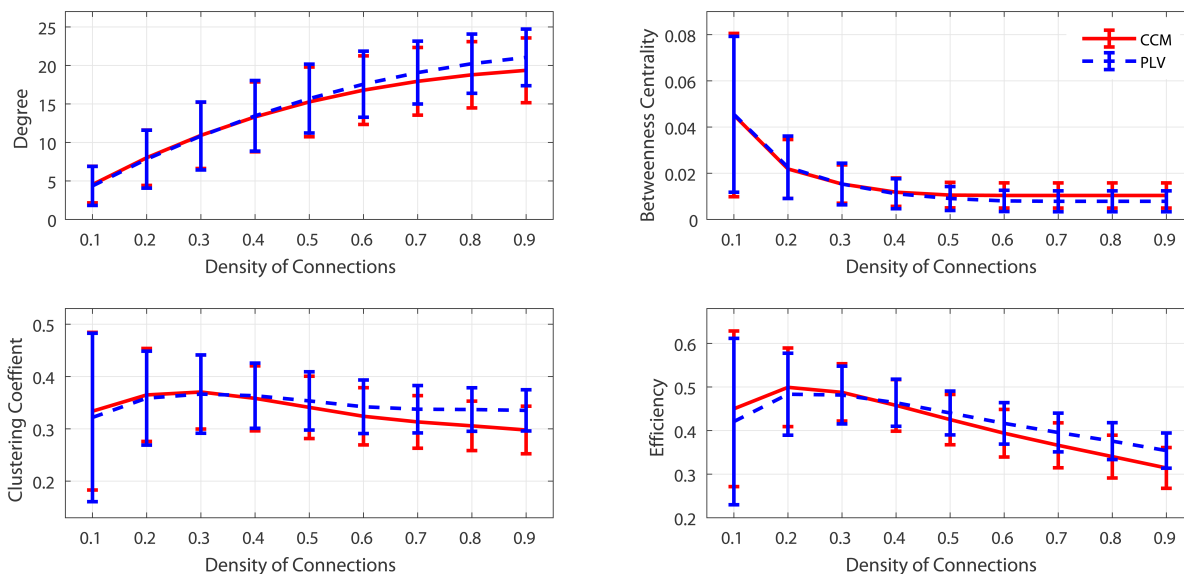
Figure 2.8: The mean and standard deviation of the EEG network characteristics at different network densities.

EEG Network Similarity

In order to statistically assess the agreement between the PLV and CCM networks, we computed the similarity metric for the 12 participants. A percentage of the nodes in the CCM matrix are shuffled, 100 times independently, in the control cases, and the mean of those values are used. The quantiles of the mean similarity metric, for the six cases, are shown in Figure 2.9. The results of the one-way ANOVA ($F(5,66) = 50.9$, $p < 0.0001$) indicates that the original networks (0% shuffled) are significantly more similar when compared to the other randomly shuffled cases. Therefore, based on the results in Figure 2.7 and Figure 2.8, the PLV and the CCM algorithms produce networks with very small differences and this similarity is above a baseline noise value.
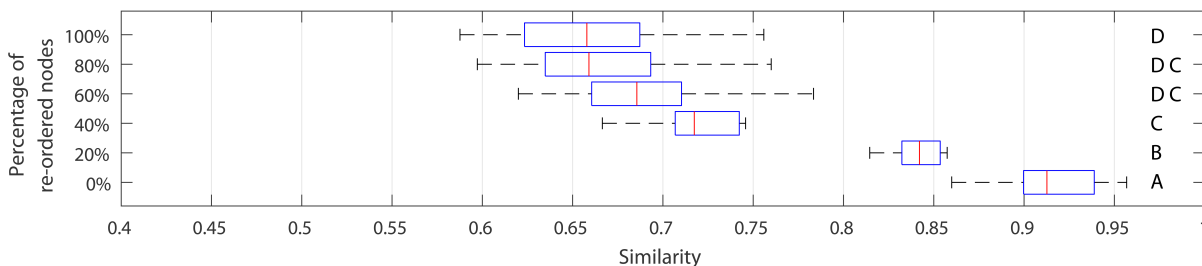
Figure 2.9: The similarity metric for the EEG data and the control conditions with varying percentages of network nodes scrambled. For each non-zero percentage of re-ordered nodes, the average of 100 random permutations of node labels, per each of the 12 participants, are generated for each designated percent of nodes re-ordered. The box and whisker plots show for the results. Conditions marked with different letters, shown on the right vertical axis of the figure, are significantly different.

2.2.3   fMRI Networks

Figure 2.10 shows the mean networks computed using PLV and CCM. The list of the ROIs used is located in Table A.2 in Appendix A. Again, both algorithms produced networks with very similar patterns. Similar to the EEG networks, the range of the edge weights in the CCM network (0.908 ± 0.045) is larger than the PLV network (0.884 ± 0.061). A one-

tailed *t*-test showed that, consistent with the EEG results, the range of the CCM network is significantly larger than the PLV network ($t(98) = 2.19$, $p = 0.015$). Also, Figure 2.11 shows the specific links between nodes which are significantly different ($p < 0.01$) between the PLV and CCM networks. As opposed to EEG results, for the fMRI data, the PLV edge connection strengths are always significantly higher than the CCM network. Consequently, only one graph is shown. Overall, similar to the results observed in the EEG data, the CCM algorithm can detect nuances in the fMRI data better than PLV.
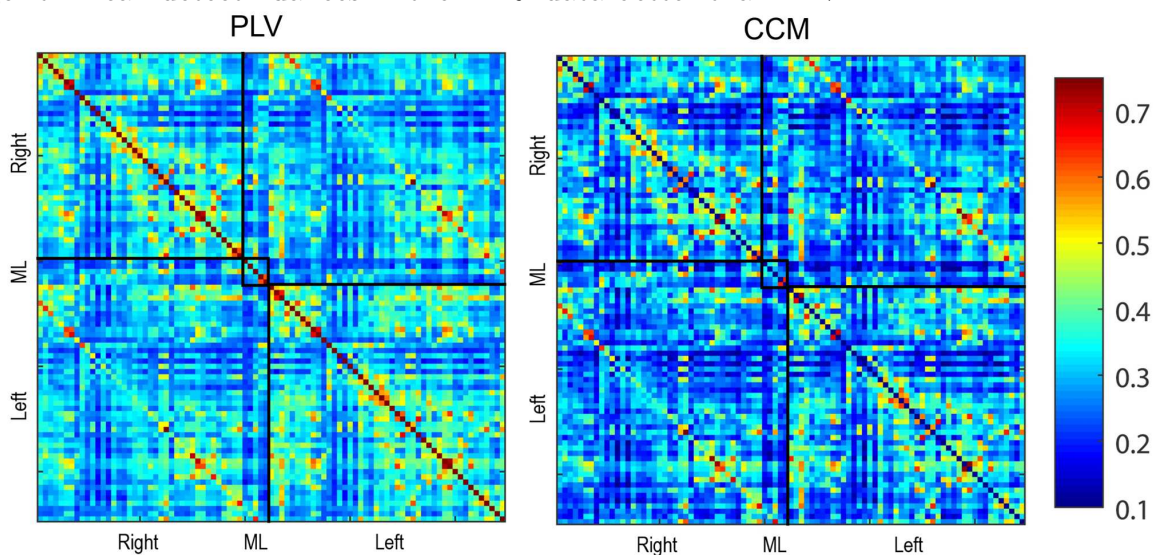
Figure 2.10: Mean resting state fMRI PLV and CCM networks. Right, ML, and Left correspond to the ROIs in the right hemisphere, midline, and left hemisphere respectively. The diagonal for PLV and CCM is 1 and 0, respectively.

fMRI Network Characteristics

The characteristics of the PLV and CCM networks at the defined densities are shown in Figure 2.12. At all of the density values, the mean network characteristic values for CCM and PLV overlap more than is seen with the EEG data. At each network density, none of the network properties are significantly different from each other when considered in *t*-test. Again, this result indicates that the network characteristics are very similar for both the PLV and CCM algorithms.
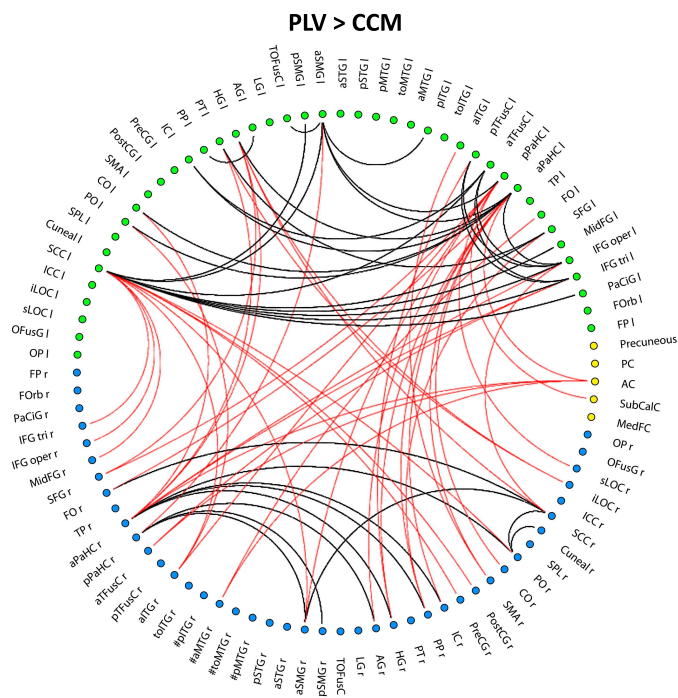
Figure 2.11: The circular graph shows the connections where the PLV edge weights are significantly stronger than the CCM network. The blue, yellow, and green dots represent the left, midline, and right hemisphere, respectively. The black and red lines indicate the intra-hemispheric and inter-hemispheric links, respectively.
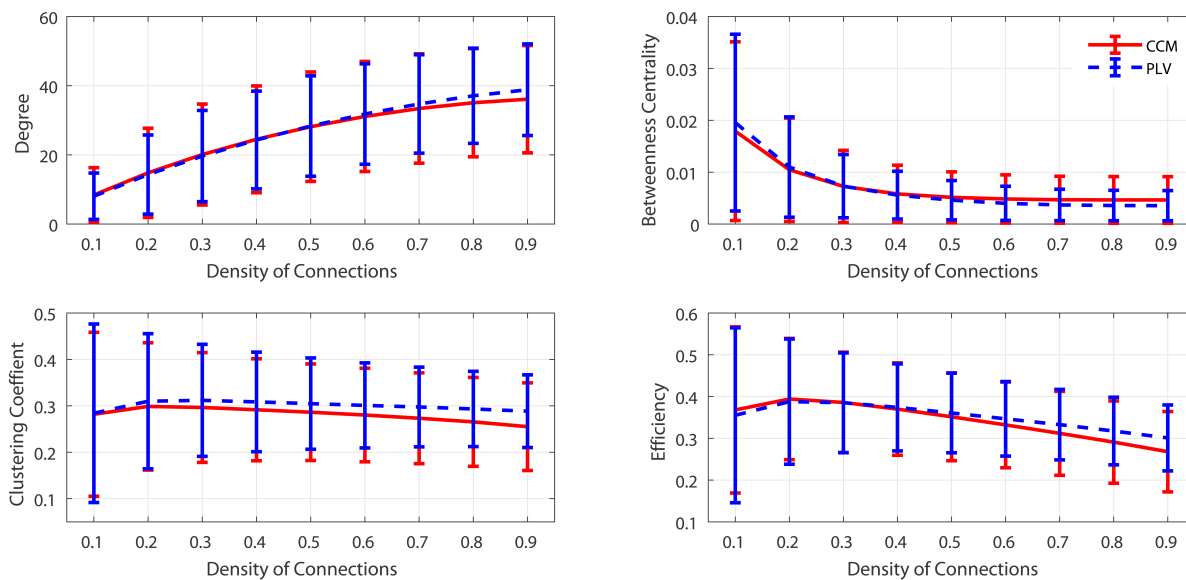
Figure 2.12: The mean and standard deviation of the fMRI network characteristics at different network densities.

fMRI Network Similarity

The similarity metric, between the PLV and CCM networks, is computed for the 50 participants. The control cases shuffle a percentage of nodes in the CCM matrix, 100 times independently, and the mean of those values are used. Figure 2.13 shows the quantiles of the mean similarity metrics for the six cases. In line with the EEG results, the results of the one-way ANOVA ($F(5, 294) = 68.4$, $p < 0.0001$) indicates that the original networks (0% shuffled) are significantly more similar than the other shuffled cases. Therefore, based on the results in Figures 2.11 and 2.12, we conclude that the PLV and the CCM algorithms produce networks with very small differences.
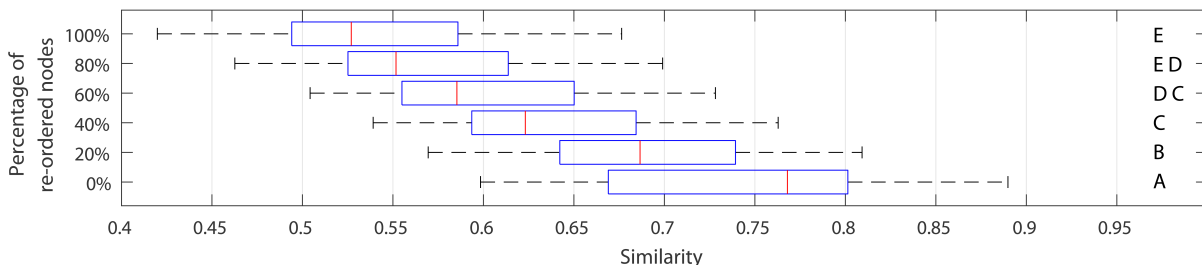
Figure 2.13: The similarity metric for the fMRI data and the control conditions with varying percentages of network nodes scrambled. For each non-zero percentage of re-ordered nodes, the average of 100 random permutations of node labels, per each of the 50 participants, are generated for each designated percent of nodes re-ordered. The box and whisker plots show for the results. Conditions marked with different letters, shown on the right vertical axis of the figure, are significantly different.

2.3   Discussion

The networks derived by the PLV and CCM algorithms provide very similar information. The PLV and CCM algorithms quantify the synchronization between two time series responses using very different methodologies. However, for the toy synchronization dataset and the neuroimaging datasets, the algorithms produced similar results overall.

In the toy dataset, the minimum similarity metric value between the PLV and CCM networks, across 1000 simulations, is 0.9 out of a maximum value of 1, as shown in Figure 2.5. In these simulations, we can see that CCM is able to pick up on one-way or low coupling strengths better than PLV. However, as the coupling strength increased, the similarity between the two responses is nearly identical.

For the EEG and fMRI resting state data, the networks derived by both PLV and CCM provide nearly identical information, as demonstrated by qualitatively comparing patterns of the networks illustrated in Figures 2.6 and 2.10. However, the range of the edge weights is significantly higher in CCM than in PLV, which is consistent with the results observed in the toy dataset that CCM is able to pick up on one-way or low coupling strengths better. In addition, Figures 2.7 and 2.11 corroborate those findings by showing that the edge weights, for particular links, in the CCM network is significantly less than the PLV network. Remarkably, though the CCM approach can detect asymmetric coupling between sources, the data-derived connectivity structures appear to show that symmetric coupling strengths are present in both the EEG and fMRI datasets, given the high similarity between the PLV and CCM connectivity matrices. This suggests that at rest, the brain may recruit reciprocal connections or at least that these reciprocal processes dominate the observable data features for these modalities. This in turn suggests that functional connectivity indices may indeed be appropriate and an adequate representation when studying resting state dynamics.

Overall, the differences between the PLV and CCM network characteristics, for both EEG (Figure 2.8) and fMRI (Figure 2.12) data, are insignificant at all network density values. Furthermore, the similarity between the computed CCM and PLV networks for the EEG (Figure 2.9) and fMRI (Figure 2.13) data is computed for six different cases with different percentages of the nodes that are re-ordered. The mean rate of decay of the similarity metric is shallower for the fMRI data than observed in the EEG data. This suggests that the fMRI

network has finer and more distributed structures than the EEG networks, since increasing the reshuffling is not as detrimental to the similarity metric. However, in both datasets, the similarity between the original computed networks (0% nodes re-ordered) is significantly higher than all of the other cases with the shuffled nodes. Therefore, based on these results, we can conclude that the PLV and CCM algorithms are consistent methods for network computation. However, both algorithms have particular advantages over the other.

Type 1 error is reduced in networks computed using the CCM algorithm. For off-line analysis of neuroimaging data, CCM is potentially a better choice than PLV. Since CCM is model-free, no initial assumptions regarding synchronization are introduced into the network computation. With CCM, Type 1 error is reduced in the network computation because it can more accurately capture the low connections better than PLV. Therefore, the risk of finding falsely high connections is reduced. This may be important to consider when studying patient data where subtle differences in network connectivity structures may emerge more reliably using the CCM approach. In addition, since the output of CCM is not symmetric, unlike PLV, it is potentially a better choice for analyses that are looking at causal, or directed, influences. However, CCM is much more computationally intensive and requires a significantly longer time to run than PLV, as shown in Table 2.1.

The PLV algorithm produces good network approximations for applications requiring fast network identification. Currently, the need for on-line neuroimaging data analysis is increasing for applications such as brain-computer interfaces and therapeutic systems. For such analyses, the ability to identify the network and quantify the connection strength needs to be done quickly. The close correspondence between the CCM and PLV networks validates the use of PLV as a metric of connectivity between brain regions. Therefore, PLV is a viable metric for computing the network strengths to be used as the feedback

signal in a closed-loop control system.

In conclusion, we found that the network computed using both the CCM and PLV algorithms produced comparable results. The characteristics of both the networks follow a very similar trend for the EEG and fMRI data. In addition, the similarity between the two networks is highly significant when compared to control cases where the nodes of the network are shuffled. However, a few key differences do exist in the results between the two methods. PLV is unable to capture low or one-way connection strengths as well as CCM. As a result, for off-line analysis, CCM is potentially the preferred metric because it is able to more accurately capture the directional synchronization of the network. However, PLV is a fast metric to compute which makes it ideal for on-line network identification and as a feedback signal within a closed-loop control system since it is an excellent approximation of the network computed with CCM.

Chapter 3

Visuospatial Working Memory and Binaural Beats

Binaural beats utilize a phenomenon that occurs within the cortex when two different frequencies are presented separately to each ear. This procedure produces a third phantom binaural beat, whose frequency is equal to the difference of the two presented tones and which can be manipulated for non-invasive brain stimulation. The effects of binaural beats on working memory, the system in control of temporary retention and online organization of thoughts for successful goal directed behavior, have not been well studied. In this chapter, we determined the effects of different acoustic stimulation conditions on participant response accuracy and cortical network topology, as measured by EEG recordings, during a visuospatial working memory task. Three acoustic stimulation control conditions and three binaural beat stimulation conditions are used: None, Pure Tone, Classical Music, 5Hz binaural beats, 10Hz binaural beats, and 15Hz binaural beats. We found that listening to 15Hz binaural beats during a visuospatial working memory task not only increased the response accuracy, but also modified the strengths of the cortical networks during the task. The three auditory control conditions and the 5Hz and 10Hz binaural beats all decreased accuracy. Based

on graphical network analyses, the cortical activity during 15Hz binaural beats produced networks characteristic of high information transfer with consistent connection strengths throughout the visuospatial working memory task.

3.1   Materials and Methods

3.1.1   Participants

Twenty-eight healthy adults (12 women, 16 men) aged 19 to 46 yr (mean 27.6 yr) participated in this study. All participants are informed about the task to be completed and provided written consent. The protocols in this study are approved by the Virginia Tech Institutional Review Board. All participants are tested for color blindness and corrected-to-normal vision. In addition, participants self-evaluated their hearing using guidelines from the American Speech-Language-Hearing Association. None of the participants reported any history of neurological disorders or hearing problems.

3.1.2   Auditory Stimulus

A battery of acoustic stimulation conditions are tested during the task. The three control conditions are 1) No Sound, 2) Pure Tone (R: 240Hz, L: 240Hz), and 3) Classical Music (Vivaldi - Spring). The three experimental conditions are 1) 5Hz Binaural Beat (R: 240Hz, L: 245Hz), 2) 10Hz Binaural Beat (R: 240Hz, L: 250Hz), and 3) 15Hz Binaural Beat (R: 240Hz, L: 255Hz). R and L indicate the frequency of the tones in the right and left ear respectively. The experimental binaural beats, 5Hz, 10Hz, and 15Hz, are chosen to represent the theta, alpha, and beta bands, respectively. Figure 1.6b shows an example of the 15Hz binaural beat. The tones are created in Matlab and presented to the participants using

stereo headphones (MDR-NC7, Sony). Before the start of the experiment the volume of the auditory stimuli are set by the participants.

3.1.3 EEG Recordings

A 16 gold cup passive electrode EEG system (OpenBCI, Inc., New York, NY) interfaced with LabVIEW is used to record the data at a sampling frequency of 128Hz. The locations of the electrode channels are Fp1, Fp2, F7, F8, F3, F4, T3, T4, C3, C4, P3, P4, O1, O2, Fz, Cz, which are placed using the 10-20 system [120]. The reference and ground electrodes are placed on the ear lobes. Electrodes are prepared with Ten20 EEG conductive paste (Weaver and Co., Aurora, CO) and electrode impedances are verified < 5 kΩ prior to data collection. The testing took place in a quiet, dimly lit room.

3.1.4 Visuospatial Task

The working memory task selected for this experiment is the delayed match-to-sample visuospatial task [40]. Figure 1.3a shows a match and no match trial. After encoding an initial image, the subject is instructed to retain the image in the absence of continuing input during working memory maintenance. During the retrieval process, the subject is asked to compare the retained and current image and to indicate whether they matched. Capacity, the limit on the 'load' that can be actively maintained, is calculated as $K_C = C(H - F)$, where C is the load, H is the hit rate, and F is the false alarm rate. The hit rate is the percentage of correctly identified matches, and the false alarm rate is the percentage of non-matches identified as matches [40]. Thus, capacity measures how accurately the participants can identify correct matches scaled by the number of targets in each image.

The participants are seated comfortably in front of a computer monitor which presented the

task. Two clearly marked buttons on the keyboard allowed the participant to indicate a match (left arrow) or a no match (right arrow) with their right hand. Before the start of the experiment, an initial load titration test is completed and involved an example practice round (one block of a 2-load task) and then proceeded to increasingly difficult loads (one block each of 3-, 4-, and 5-load versions of the task). The titrated load for the experimental task is determined by finding the load that produced the maximum capacity estimate for each individual participant. If two of the loads resulted in the same capacity, then the load with the highest hit rate is chosen.

After EEG preparations, the participant performed the experimental task at the load determined by the initial titration for 30 minutes. Every 5 minutes, the sound playing though the stereo headphones would change to one of the six different acoustic stimulation conditions. In order to minimize bias, all trials and all conditions are randomized over all participants. The task is presented using a custom script written with the Cogent Graphics Matlab toolbox.

3.1.5   Behavioral Data Processing

The recorded behavioral data is processed for analysis using a custom Matlab script. First, trials on which the participant did not respond or pressed a non-target key are discarded (less than 5%). In order to effectively assess improvement due to oscillatory synchrony in the brain, it is important that each participant be tested at the limit of their individual working memory capacity. Therefore, the metrics used to compare behavior across acoustic stimulation conditions are Δ Accuracy and reaction time. Accuracy is defined as the number of correct trials both matches (Hit) and non-matches (Correct Rejection) divided by the total number of trials. Δ Accuracy is the difference between the accuracy at the end $(3.5 - 5$ mins) as compared to the beginning $(0 - 1.5$ mins) of the acoustic stimulation condition. Reaction

time is the amount of time between when the target image appeared on the screen and when the participant hit a response button.

3.1.6 EEG Data Processing

The raw EEG data is preprocessed using EEGlab [104]. First, the data are bandpassed filtered between 0.5Hz and 50Hz to remove drift and the 60Hz power line noise. Then, the filtered EEG is re-referenced to the average. Afterwards, the maintenance (125 ms – 4125 ms, which corresponded to the time when no visuospatial array is present on the screen between the sample and probe stimuli) and retrieval (4125 ms – 6125 ms) epochs are extracted. The retrieval epoch length remained constant even if the participant responded before the end of the 2 second interval. Finally, the baseline is removed (0-200 ms before stimulus presentation). Only correct trials (i.e. a Hit or Correct Rejection) are used. Epochs are inspected by hand for artifacts from eye blinks, movement, or other sources and are removed. The rejection rate is less than 5%.

Given that the goal is to analyze the overall brain configuration during the different acoustic stimulation conditions, regional links are determined by averaging the connections between the clusters of electrodes over the frontal, temporal, parietal, and occipital lobes. It should be noted that regions, in this context, refers to the average of the surface sites over the different cortices. All of the conditions are normalized against the No Sound results to show the changes in link strengths.

3.1.7 Network Construction and Analysis

The processed EEG signals are filtered again, using EEGlab, into the four common frequency bands: theta (4Hz – 8Hz), alpha (8Hz - 12Hz), beta (12Hz – 25Hz), and gamma (25Hz –

40Hz) [4]. These filtered signals are then used to compute the time-frequency synchronization measure between channels. The time-frequency synchronization measure is PLV which is previously defined in section 2.1.3 in Equations 2.3 and 2.4. The graphical networks are constructed using the channels as the nodes and the time-frequency synchronization measure as the edge weights. Separate networks are created for the maintenance and retrieval epochs and the four different frequency bands.

Graphical Network Measures.Quantifying characteristics of the functional networks derived from neuroimaging data can be achieved using graphical network metrics [86, 121]. The graphical network is undirected and weighted and is constructed using the electrode channels as the nodes ($\mathcal{V} = \{1, ..., n\}$) and the PLV connection strength as the undirected edges ($E = \{(i, j) : \exists \text{ an edge from } i \text{ to } j\}$). The network is undirected and weighted, and can be defined as an adjacency matrix, A, made up of a_{ij} elements and a edge weight matrix, W, made up of w_{ij} elements. The adjacency matrix has $a_{ij} = 1$ if $(i, j) \in E$ and 0 otherwise. The elements of the edge weight matrix are $w_{ij} = \text{PLV}_{ij}$ with the property that $0 \leq w_{ij} = w_{ji} \leq 1$ for $i, j = 1, ..., n, i \neq j$. Note that both A and W are symmetric. The networks are analyzed using three common metrics: degree (Equation 2.8), clustering coefficient(Equation 2.9), and betweenness centrality(Equation 2.10). These metrics are computed using the Brain Connectivity Toolbox (BCT) in Matlab.

Connectivity Ratio. In addition to the standard graphical network measures, a new metric, the connectivity ratio (CR), is defined to investigate the differences between the maintenance and retrieval networks. The 16 x 16 PLV matrices are averaged over all epochs for maintenance and retrieval separately, and the two average matrices which result are given by $\text{PLV}_{\text{Retrieval}}$ and $\text{PLV}_{\text{Maintenance}}$, respectively. To compute the CR, each the elements of the PLV retrieval matrix are is divided by the corresponding maintenance connection values elementwise and the resulting matrix is defined as CR. This metric provides a method of

combining the two graphs into a single graph while maintaining valuable information about the continuity of the strength between them. Based on this definition, the lower the CR value the smaller the change in connection strengths between the maintenance and retrieval networks.

3.1.8   Statistical Methods

The statistical software JMP is used to analyze both the behavioral and EEG data. Multiple ANOVAs are completed to analyze the behavioral response data and the network structures. Henceforward, CONDITION refers to the six acoustic stimulation conditions: None, Pure Tone, Classical Music, 5Hz BB, 10Hz BB, and 15Hz BB. BAND refers to the frequency band: theta, alpha, beta, and gamma. CHANNELS refers to the 16 individual channels of recorded EEG data. LINK refers to the Frontal – Temporal (F – T), Frontal – Parietal (F – P), Frontal – Occipital (F – O), Parietal – Occipital (P – O), Parietal – Temporal (P – T), and Temporal – Occipital (T – O) connections. The post hoc test chosen is the Tukey HSD, which is used to evaluate pairwise comparisons on the marginal means. The familywise error rate is kept at a maximum of 0.05.

For the behavioral data, the original dataset ($N = 28$) is bootstrapped 100 times. This number is chosen so it is on the same order of magnitude as the number of EEG data samples. An alpha level of 0.01 is chosen since all statistical analyses are completed on the bootstrapped behavioral dataset. In addition, the regional links are bootstrapped 100 times due to the large standard deviation of the dataset, and the alpha level is set to 0.0001, to be conservative.

Finally, ordinary least squares (OLS) regression is used to identify key metrics in understanding the relationship between the EEG and the behavioral data. The dependent variable is the

Δ Accuracy. The independent variables included the maintenance and retrieval responses for degree, clustering coefficient, betweenness centrality, the regional link strengths, and the connectivity ratio. Each variable is bootstrapped 10,000 times so that the variation between the regressors and dependent variable could be accounted for. The regression is completed on the bootstrapped dataset. A correlation analysis determined that there is a high degree of multicollinearity between each of these metrics. The correlation coefficient, r, for each pair is either strongly positive (yellow) or negative (blue). The high multicollinearity means that adding more than one parameter to the regression would be both redundant and insignificant, since all parameters would predict similar outputs. Therefore, multiple linear regression models and linear mixed models would not be appropriate for this analysis. Instead, each metric is evaluated separately, using OLS regression, to determine its ability to describe the recorded Δ Accuracy. The dataset, including the behavioral responses and the PLV connectivity networks, have been made publicly available [122].

3.2 Results

3.2.1 Working Memory Task Performance

A one-way ANOVA showed that the effect of CONDITION on the Δ Accuracy is significant ($F_{(5,594)} = 67.184$, $p < 0.0001$). Post hoc pairwise analyses are shown in Figure 3.1. Participants' performance during the 15Hz BB is significantly more accurate over time than all other conditions. It is the only auditory stimulation condition that produced a positive change in accuracy over 5 minutes. All other acoustic stimulation conditions produce negative Δ Accuracy. However, no significant change occurred in the participants' reaction time when compared in an ANOVA using CONDITION ($F_{(5,594)} = 0.194$, $p = 0.965$).
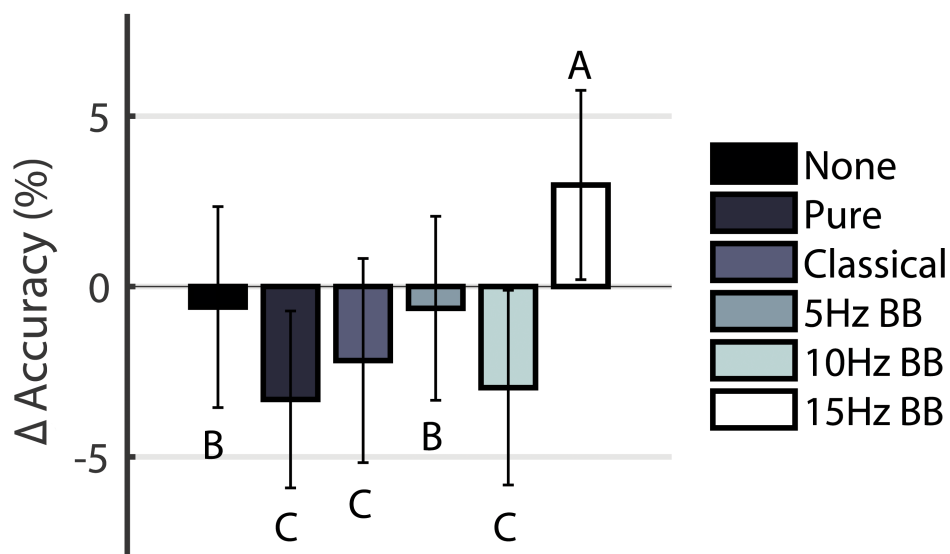
Figure 3.1: Δ Accuracy. Conditions marked with different letters are significantly different.

3.2.2 Connectivity Networks

The first one-way ANOVA examining the EEG data determined that the edge weights of the networks are significantly different between the maintenance (M = 0.472, SD = 0.037) and retrieval networks (M = 0.524, SD = 0.035) (F(1,2878) = 1180.243, p < 0.0001). Therefore, two separate 6 x 4 factorial ANOVAs, for maintenance and retrieval, are completed to determine the effect of CONDITION and BAND on the network structure. Both ANOVAs produced similar significant main effects, as shown in Table 3.1. For both maintenance and retrieval, the main effects of CONDITION and BAND are significant, but their interaction is not significant. Post hoc analyses revealed that the theta band had the largest activations in both the maintenance and retrieval segments (p < 0.0001). No significant effects are found in the other frequency bands. Henceforth, only the theta band will be examined for the rest of this analysis. Figure 3.2 shows the average PLV networks for the six conditions during both maintenance and retrieval as built by the EEG signal in the theta band.
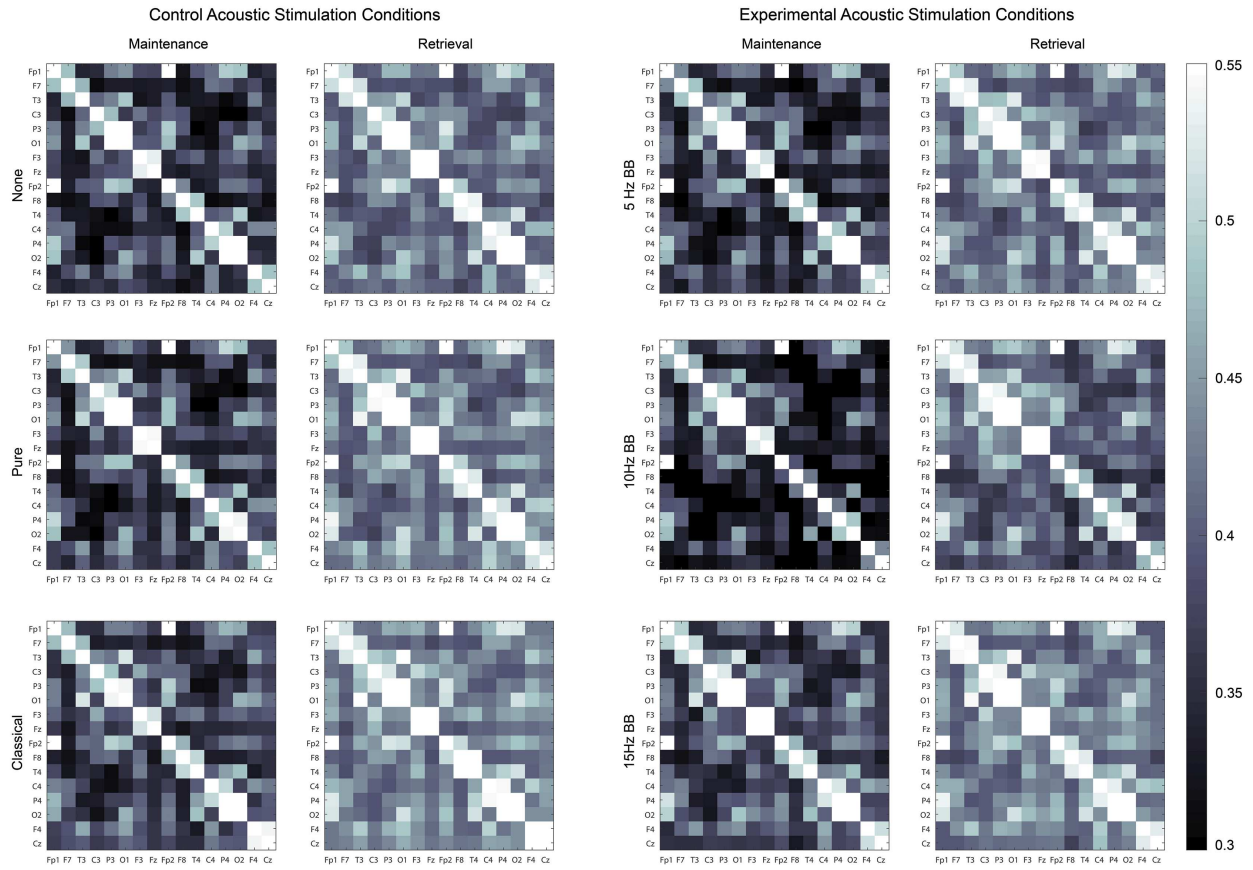
Figure 3.2: Theta band PLV connectivity network weight matrices. For each weight matrix, the diagonal is always equal to one.

Table 3.1: Results from the factorial ANOVA comparing Condition and Frequency Band.

Maintenance

Metric	F-value	p-value
CONDITION	$F(5,5736) = 53.1$	$p < 0.0001$
BAND	$F(3,5736) = 199.1$	$p < 0.0001$
CONDITION × BAND	$F(15,5736) = 0.9$	$p = 0.497$

Retrieval

Metric	F-value	p-value
CONDITION	$F(5,5736) = 53.9$	$p < 0.0001$
BAND	$F(3,5736) = 733.1$	$p < 0.0001$
CONDITION × BAND	$F(15,5736) = 1.1$	$p = 0.266$

Connectivity Ratio. The CR, computed from the weight matrices in Figure 3.2, are analyzed for a significant effect due to CONDITION using a one-way ANOVA. Based on the results, the acoustic stimulation type had a significant effect on the CR ($F(5,1434) = 39.938$, $p < 0.0001$). Significant post hoc pairwise analyses are represented by differing letters in Figure 3.3. The CRs resulting from the 10Hz BB and 15Hz BB conditions are significantly higher and lower, respectively, than all other conditions. This indicates that the change in connection strengths between the maintenance and retrieval networks is smallest for the 15Hz BB condition and largest for the 10Hz BB condition.
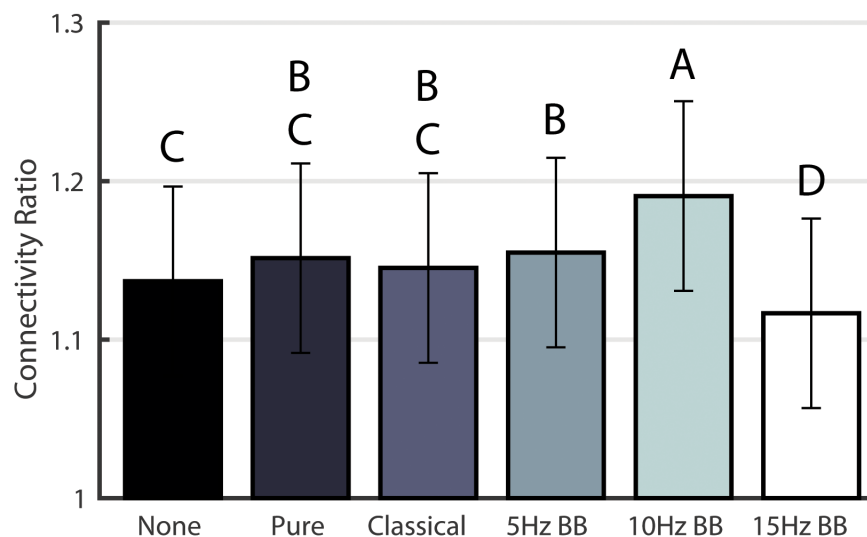
Figure 3.3: Connectivity Ratio for the six acoustic stimulation conditions. Conditions marked with different letters are significantly different.

Graphical Network Measures. To gain a more in-depth evaluation of the network structure in the theta band, two separate two-way ANOVAs (on the maintenance and retrieval segments) are constructed to compare the effect of CONDITION and CHANNELS on degree (Figure 3.4), clustering coefficient (Figure 3.5), and betweenness centrality (Figure 3.6). Table 3.2 shows the F-values from the ANOVAs. All p-values are less than 0.0001. For all network measures, the values from the two hemispheres are generally symmetric.

Maintenance

Metric	Channel	Condition
D	$F(15, 69536) = 57.674$	$F(5, 69536) = 120.473$
CC	$F(15, 69536) = 23.691$	$F(5, 69536) = 147.065$
BC	$F(15, 69536) = 143.793$	$F(5, 69536) = 11.548$

Retrieval

Metric	Channel	Condition
D	$F(15, 69536) = 34.858$	$F(5, 69536) = 58.719$
CC	$F(15, 69536) = 15.058$	$F(5, 69536) = 73.088$
BC	$F(15, 69536) = 37.452$	$F(5, 69536) = 5.662$

Table 3.2: Two-way ANOVA results comparing CONDITION and CHANNELS.
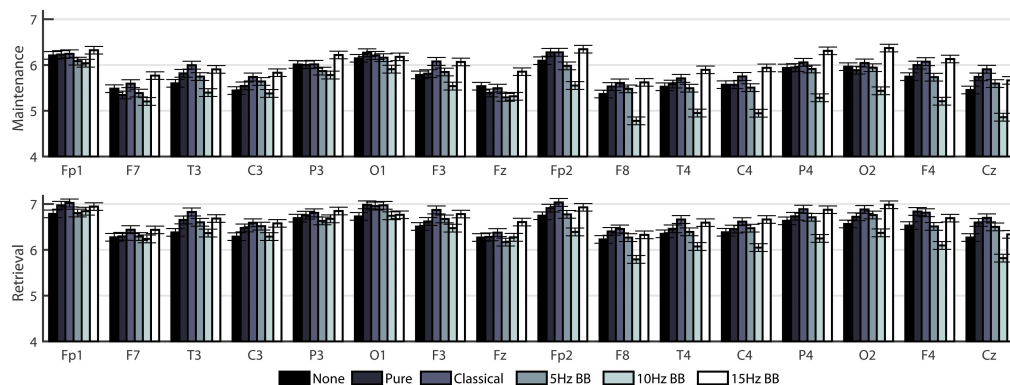
Figure 3.4: Mean degree of EEG nodes in cortical networks for all six acoustic stimulation conditions. Bars indicate standard error.

Figure 3.7 shows a comparison of the three metrics averaged over all the channels for each time segment. The significances are determined from the two-way ANOVAs described previously. For degree and clustering coefficient, the network measure is generally lower and higher for the 10Hz BB and 15Hz BB conditions, respectively, compared to all other conditions. Conversely, the betweenness centrality is higher and lower for the 10Hz and 15Hz BB conditions, respectively, compared to all other conditions.
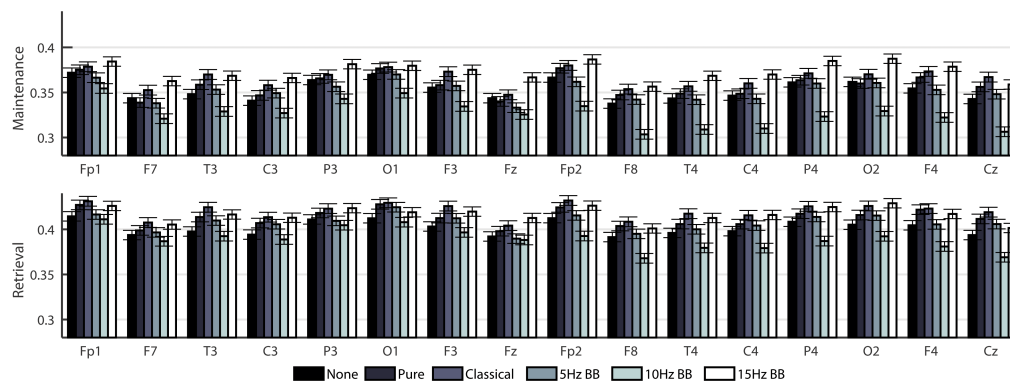
Figure 3.5: Mean clustering coefficient of EEG nodes in cortical networks for all six acoustic stimulation conditions. Bars indicate standard error.
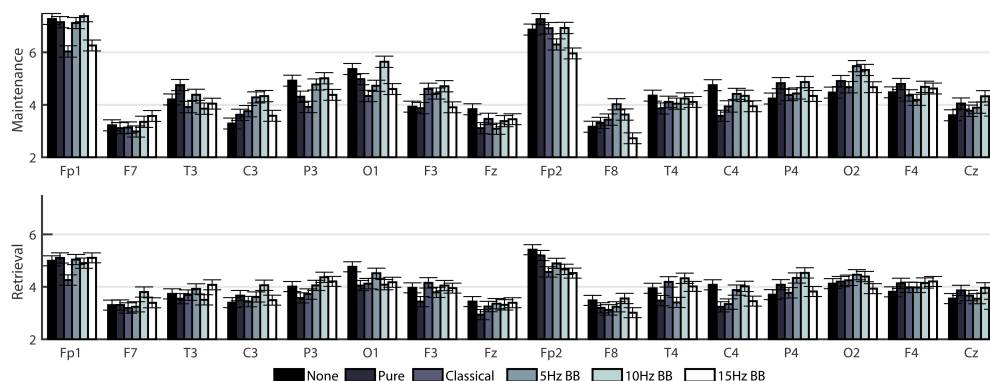
Figure 3.6: Mean betweenness centrality of EEG nodes in cortical networks for all six acoustic stimulation conditions. Bars indicate standard error.

Regional Link Strength

A 6 x 6 factorial ANOVA is constructed to compare the effect of LINK and CONDITION on the PLV link strengths for both maintenance and retrieval segments. Figure 3.8 shows the link strengths for both maintenance and retrieval. For both the maintenance and retrieval networks, the main effects of CONDITION, LINK and the interaction between CONDITION × LINK are significant, as shown in Table 3.3. Notably, the 15Hz BB connection strength values are significantly higher than all other conditions in all connections except for the Temporal – Occipital link during maintenance. This indicates that the 15Hz BB stimulus increased connectivity between the frontal lobe and all other brain regions as well as between
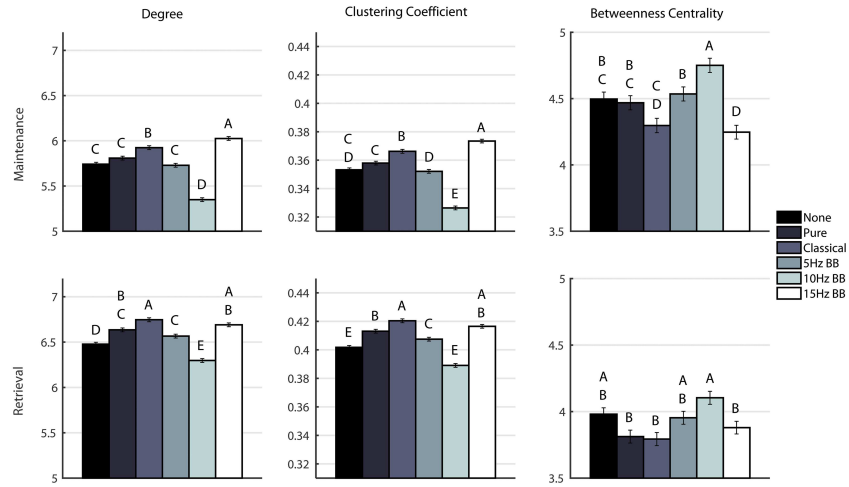
Figure 3.7: Comparison of degree, clustering coefficient, and betweeness centrality for each condition. Conditions marked with different letters are significantly different. The bars show standard error.

the parietal lobe and all other brain regions. The connectivity pattern during retrieval are less clear, although the 15Hz BB link strength values are one of the highest conditions. Thus the effect of 15Hz BB on communication between brain regions is higher, and more distinguishable from other auditory stimuli, during maintenance than it is during retrieval of visuospatial stimuli.

Maintenance

Metric	F-value	p-value
CONDITION	$F(5, 1764) = 2.09\text{E}{+}3$	$p < 0.0001$
LINK	$F(5, 1764) = 1.17\text{E}{+}4$	$p < 0.0001$
CONDITION $\times$ LINK	F(25,1764) = 48.2	$p < 0.0001$

Retrieval

Metric	F-value	p-value
CONDITION	$F(5, 1764) = 1.05\text{E}{+}3$	$p < 0.0001$
LINK	$F(5, 1764) = 8.04\text{E}{+}3$	$p < 0.0001$
CONDITION $\times$ LINK	F(25,1764) = 35.2	$p < 0.0001$

Table 3.3: Results from the factorial ANOVA comparing Condition and Regional Link Strength.
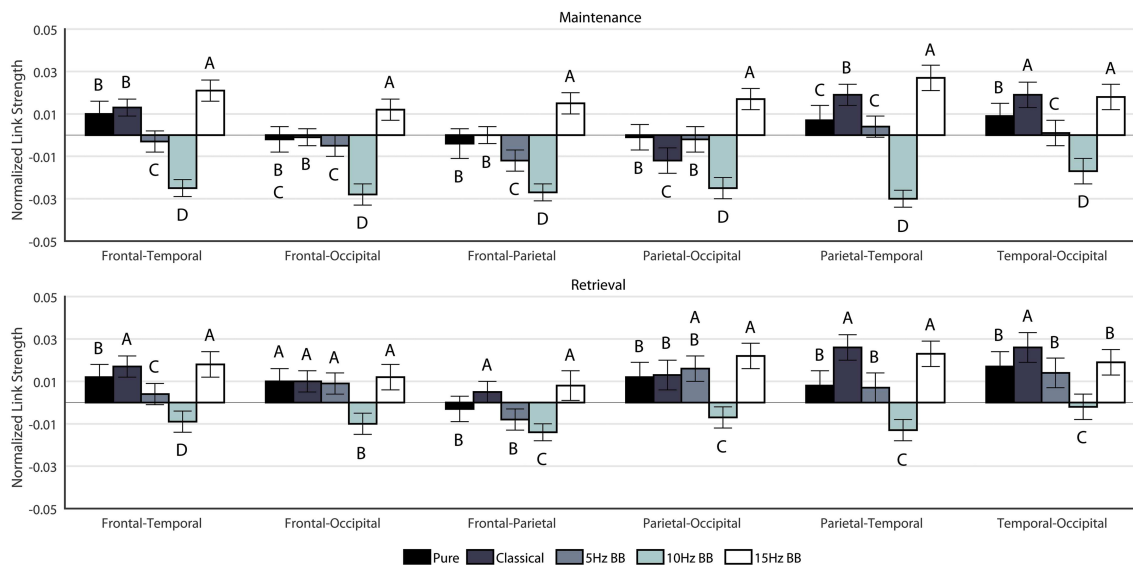
Figure 3.8: Regional Link Strengths. Each condition is normalized against None. The significances are shown for each link individually. Conditions marked with different letters are significantly different.

3.2.3 Correlations Between Behavior and Network Topology

Table 3.4 displays, in order of predictive ability, the coefficient of determination (R^2), intercept, and slope for each metric from the individual OLS regressions. All the metrics, except for betweeness centrality and CR, have a positive correlation with the behavioral changes. Based on the magnitude of the R^2 values, the metrics computed during maintenance generally describe the change in behavioral changes better than those during retrieval.

3.3 Discussion

15Hz binaural beats increases accuracy in a visuospatial working memory task.
Listening to 15Hz BB positively influenced the participants' accuracy during the course of the 5 minutes by 3%. During all other conditions, the participants' accuracy decreased by 1% – 3%. No Sound and 5Hz BB produced a smaller decrease in accuracy while the

Metric	R^2	Intercept	Slope
CR	0.230	0.836	-0.737
$(P-O)_M$	0.210	-0.519	1.099
$(F-P)_M$	0.185	-0.430	1.062
$(F-O)_M$	0.171	-0.445	1.097
$(P-T)_M$	0.145	-0.261	0.689
D_M	0.134	-0.338	0.057
CC_M	0.134	-0.301	0.817
BC_M	0.128	0.305	-0.071
$(F-T)_M$	0.122	-0.302	0.768
$(F-P)_R$	0.088	-0.527	1.164
$(T-O)_M$	0.081	-0.304	0.709
$(P-O)_R$	0.079	-0.442	0.858
$(P-T)_R$	0.076	-0.288	0.653
$(F-T)_R$	0.051	-0.325	0.720
D_R	0.047	-0.311	0.046
CC_R	0.045	-0.274	0.644
$(F-O)_R$	0.037	-0.340	0.741
$(T-O)_R$	0.008	-0.130	0.258
BC_R	0.006	0.077	-0.022

Table 3.4: OLS Regression. M: Maintenance, R: Retrieval

Pure Tone, Classical Music, and 10Hz BB produced the largest decreases. This increase in performance of the working memory task can be explained by noting that 15Hz BB produces high synchronization within the auditory cortex[75] and falls within the beta band which is often associated with active concentration.

Acoustic stimulation significantly affects the relative network connections during maintenance and retrieval in a visuospatial working memory task. Based on the results in Figure 3.3, 15Hz BB induces the smallest relative change in network connection strengths between the maintenance and retrieval portions of the working memory trials. Therefore, the networks are better preserved throughout the working memory task. Working memory maintenance is thought to be driven by reverberatory loops that allow sustained neuronal firing and thereby allow cognitive representations to be held in consciousness [123].

Consequently, sustained neural activity in appropriate networks is the hallmark of working memory task success, as seen in Table 3.4. The CR negatively correlates with the change in accuracy during the working memory task and has the highest R^2 value of 0.23. Therefore, as the accuracy of the performance increases, the relative differences in the network activation between maintenance and retrieval decrease. To our knowledge, this paper is the first to demonstrate that 15Hz BB improves the consistency of relative connection strengths better than the other acoustic stimulation conditions and to use the CR to predict working memory task performance.

Acoustic stimulation consistently impacts regional linkages during both maintenance and retrieval. The strengths of the regional connections offer some insight into the overall functional connectivity of the brain during the working memory task. In previous studies, the interactions between the parietal and prefrontal cortices have been strongly associated with working memory performance [43, 44]. As shown in Table 3.4, the frontoparietal connection for maintenance has a higher correlation ($R^2 = 0.185$) with the performance than during retrieval ($R^2 = 0.088$). Given the increase in working memory performance during exposure to 15Hz BB, we might infer that frontoparietal connectivity is more important during visuospatial working memory maintenance than during retrieval. This inference is consistent with the finding that parietal cortex is involved in storage of visuospatial information [124, 125] whereas the prefrontal cortex itself is important for executive control processes such as decisions made during retrieval. In addition, the regional links between P – O, F – O, and P – T for maintenance are on the same order of magnitude of the R^2 value with the F – P link, as shown in Table 3.4. All of the links have a positive correlation with the behavior. Therefore, if the link strength increases, then working memory performance is positively affected as well.

Stimulation condition significantly changes network structures by introducing

edges that emphasize or de-emphasize the role of certain nodes. As shown in Figures 3.4 – 3.6, there is a high level of symmetry between the left and right hemispheres for the degree, clustering coefficient, and betweenness centrality. When the participants are surveyed after the completion of the session, the majority responded that they remembered the names of the colors which could account for the left hemisphere activation, which is associated with verbal processing. In addition, the channels with the highest values are Fp1, Fp2, F3, F4, P3, P4, O1, and O2 which correspond to the frontal, parietal, and occipital lobes. The 15Hz BB produces a high cumulative transfer of information over the whole network and edge weights which are homogeneously distributed. This is evidenced by Figure 3.7, which shows that 15Hz BB has a high degree and clustering coefficient in addition to a low betweenness centrality value. The low betweenness centrality indicates that all nodes are of more equal importance in the graph. Conversely, when the degree and clustering coefficient are low and the betweenness centrality is high, such as 10Hz BB, then the edge weights are not equally distributed and a few certain nodes are favored in the network. These data demonstrate that binaural beats significantly changes how edge weights, and therefore the structures in the network itself, are assigned. These metrics from the EEG data provide insight into the mechanism driving the behavioral findings that 15Hz BB improved working memory performance whereas 10Hz BB reduced working memory performance. It seems that a visuospatial working memory task is well served by increased communication across brain regions, particularly frontoparietal regions, and by consistency across nodes rather than increased strength in individual nodes.

In conclusion, listening to 15Hz binaural beats during a visuospatial working memory task can not only increase the response accuracy but also change the properties of the the cortical networks supporting task performance. A 3% increase in Δ Accuracy, over the 5 minutes, is found in participants who listened to the 15Hz binaural beat. All other acoustic stimula-

tion conditions produced a negative change. In addition, the best predictor of the working memory performance is the connectivity ratio (CR), which indicates the relative change in network connection strengths between the maintenance and retrieval segments. During 15Hz binaural beats, the network characteristics are better preserved from the maintenance to the retrieval portions of each trial than the other acoustic stimulation conditions. This similarity in the network likely reflects the participants' continued maintenance of the visuospatial pattern through the retrieval phase, when they must report the pattern held in mind. Finally, the 15Hz binaural beats produced the network with the most efficient data transmission. Therefore, a 15Hz binaural beat can be used to successfully augment working memory performance.

Chapter 4

Verbal Working Memory and Binaural Beats

Synchronization in activated regions of cortical networks affect the brain's frequency response, which has been associated with a wide range of states and abilities, including memory. A non-invasive method for manipulating cortical synchronization is binaural beats. Binaural beats take advantage of the brain's response to two pure tones, delivered independently to each ear, when those tones have a small frequency mismatch. The mismatch between the tones is interpreted as a beat frequency, which may act to synchronize cortical oscillations. Neural synchrony is particularly important for working memory processes, the system controlling online organization and retention of information for successful goal-directed behavior. Therefore, manipulation of synchrony via binaural beats provides a unique window into working memory and associated connectivity of cortical networks. In this study, we examined the effects of different acoustic stimulation conditions during an N-back working memory task, and we measure participant response accuracy and cortical network topology via EEG recordings. Six acoustic stimulation conditions are used: None, Pure Tone, Classical Music, 5Hz binaural beats, 10Hz binaural beats, and 15Hz binaural beats. We determined

that listening to 15Hz binaural beats during an N-Back working memory task increased the individual participant's accuracy, modulated the cortical frequency response, and changed the cortical network connection strengths during the task. Only the 15Hz binaural beats produced significant change in relative accuracy compared to the None condition. Listening to 15Hz binaural beats during the N-back task activated salient frequency bands and produced networks characterized by higher information transfer as compared to other auditory stimulation conditions.

4.1 Materials and Methods

4.1.1 Participants

Thirty-four healthy adults (15 women, 19 men) aged 18 to 46 yr (mean 27.1 yr) participated in this study. Each participant provided written consent after being familiarized with the experimental protocols, which are approved by the Virginia Tech Institutional Review Board. Before the start of the task, participants are tested for corrected-to-normal vision and evaluated their hearing using the American Speech-Language-Hearing Association guidelines. No participants reported any previous neurological or hearing problems.

4.1.2 Auditory Stimulus

Multiple acoustic stimulation conditions are evaluated during the course of the session. The control conditions included 1) None, 2) Pure Tone (R: 240Hz, L: 240Hz), and 3) Classical Music (Vivaldi - Spring). The experimental conditions included 1) 5Hz Binaural Beat (R: 240Hz, L: 245Hz), 2) 10Hz Binaural Beat (R: 240Hz, L: 250Hz), and 3) 15Hz Binaural Beat (R: 240Hz, L: 255Hz). The tones presented to the right and left ears are indicated by R

and L, respectively. The binaural beats, 5Hz, 10Hz, and 15Hz, serve as theta, alpha, and beta band stimulation, respectively. The tones are created in Matlab. The stimulus volume, played through stereo headphones (MDR-NC7, Sony), is set by the participants at the start of the session to a comfortably loud level.

4.1.3   EEG Recordings

The EEG data are recorded using a 16 gold cup passive electrode EEG system (OpenBCI, Inc., New York, NY) that is interfaced with LabVIEW. The sampling rate is 128Hz. The chosen 10-20 electrode channel locations [120] are Fp1, Fp2, F7, F8, F3, F4, T3, T4, C3, C4, P3, P4, O1, O2, Fz, Cz. The ear lobes are used for the reference and ground electrodes. Prior to data collection, Ten20 EEG conductive paste (Weaver and Co., Aurora, CO) is used to prepare the electrodes and electrode impedances are verified to be < 5 kΩ.

4.1.4   N-Back Task

Figure 1.3b shows the chosen N-Back verbal working memory task. During the task, each letter is encoded and the sequence is retained in the working memory. For each letter presented on the screen, the subject must compare the retained (no longer visible) and current (visible on-screen) letters and indicate when the current letter on the screen matches the letter that occurred "N" steps prior. Individual cognitive differences determine the limit on the 'load', or number of letters, that can be successfully maintained and manipulated in this task. Capacity is computed using $K_C = C(H - F)$, where C is the load, H is the hit rate (percentage of correctly identified matches), and F is the false alarm rate (percentage of non-matches identified as matches) [40].

Participants completed the N-back test in a quiet, dimly lit room and are seated in front

of a computer monitor. A custom script written for the Cogent Graphics Matlab toolbox presented the task. The participant pressed the left arrow or right arrow on the keyboard to indicate a match or no match, respectively. An initial load titration test is completed, before starting the experiment, and involved a practice round (one block of a 1-back task) and then increased in difficulty (one block each of 1-, 2-, and 3-back task). For each participant, the load used in the experimental task is set by selecting the load which produced the highest capacity estimate. In the event that two loads produced identical capacity values, the load with the largest hit rate less than 100% is used. In case the hit rate equaled 100%, the next highest load is chosen. Each individual is tested at their working memory capacity limit to assess their improvement due to the acoustic stimulation. Of all the participants, thirty-two participants completed the task at a load of 1 and two participants at a load of 2.

Following the EEG setup, each participant performed the task at the selected load for thirty minutes. The sound condition changed every five minutes to one of the six different acoustic stimulation conditions. The binaural beats began precisely with the first working memory trial of a block and ended with the final trial. Between each block is a two-minute break. Over all participants, all trials and sound conditions are randomized to minimize bias.

4.1.5 Behavioral Data Processing and Analysis

A custom Matlab script is used to process the recorded behavioral data. First, trials are discarded if the participant pressed an incorrect key or didn't respond in time (less than 5%). The metrics used to assess performance during each acoustic stimulation condition are accuracy, ranked accuracy, and reaction time. Accuracy is computed by dividing the number of correct trials, both matches (Hit) and non-matches (Correct Rejection), by the total number of trials. To identify relative trends in the accuracy results, of each individual

participant, a new dataset is constructed by ranking the accuracy of the six sound conditions from 1 (lowest accuracy) to 6 (highest accuracy), for each participant. By ranking each participant's accuracy scores, the data is normalized on a standard scale that eliminated the effect of an individual's mean accuracy. Reaction time is defined as the time observed between when the letter appeared on the screen and when the participant pressed a response button. The statistical software JMP (SAS, Cary, NC) is used to analyze the behavioral data. The nonparametric Mann-Whitney U statistical test is used since the data ($N = 34$) is non-normal. The post hoc test chosen is the Steel-Dwass All Pairs, which is the nonparametric equivalent to Tukey HSD, and the familywise error rate is kept at a maximum of 0.05. For the behavioral data, CONDITION refers to all acoustic stimulation conditions: None, Pure Tone, Classical, 5Hz BB, 10Hz BB, and 15Hz BB.

4.1.6   EEG Data Processing

The EEGlab toolbox in Matlab is used to preprocess the raw EEG data [104]. Initially, the EEG recordings are bandpass filtered (0.5Hz – 50Hz) to remove drift and the 60Hz power line noise. Then, the filtered EEG is re-referenced to the average. Two different datasets are then derived from the preprocessed EEG data.

The first dataset contains the continuous five-minute block of EEG recordings used for a frequency analysis. First, artifacts are removed using automatic continuous rejection in EEGlab. Then, independent component analysis (ICA) is used to remove the eye blink components [105]. The resulting dataset contained approximately five minutes of clean EEG data, for each condition, for each of the thirty-four participants.

The second dataset contains the epoched EEG used for the graphical network analysis. The onset (0 ms – 1000 ms, which corresponded to the time when the letter is on the screen)

epochs are extracted using EEGlab. The onset epoch length remained constant even if the participant responded before the end of the one-second interval. Finally, the baseline is removed (0-200 ms before stimulus presentation). Only correct trials (i.e. a Hit or Correct Rejection) are used. Epochs with artifacts from eye blinks, movement, or other sources are removed following manual inspection of the automatically identified artifacts in EEGlab (less than 5% rejection). The resulting dataset contained approximately 100 epochs of clean EEG data, for each of the thirty-four participants, for each condition.

4.1.7 Graphical Network Construction

The processed epoched EEG signals are filtered again, using EEGlab, to focus on the theta (4Hz - 8Hz) band. The time-frequency synchronization measure between channels is computed using the processed EEG signals. The graphical networks are comprised of nodes (the channels) and the edge weights (time-frequency synchronization measure). A measure of synchronization used in the literature is the Phase Locking Value (PLV) which is previously defined in section 2.1.3 in Equations 2.3 and 2.4.

The graphical network is constructed using the electrode channels as the nodes ($\mathcal{V} = \{1, ..., n\}$), where $n = 16$, and the PLV connection strength is associated with the undirected edges as edge weights ($E = \{(i, j) : \exists$ an edge from i to $j\}$). The network is undirected and weighted, and can be defined as an adjacency matrix, A, made up of a_{ij} elements and a edge weight matrix, W, made up of w_{ij} elements. The adjacency matrix has $a_{ij} = 1$ if $(i, j) \in E$ and 0 otherwise. The elements of the edge weight matrix are $w_{ij} = \text{PLV}_{ij}$ with the property that $0 \leq w_{ij} = w_{ji} \leq 1$ for $i, j = 1, ..., n, i \neq j$. Note that both A and W are symmetric. Edge weights in terms of PLV are computed for each epoch and averaged over all epochs to define the graphical network for each participant.

4.1.8   EEG Analysis

Three different EEG data analyses are undertaken. First, a frequency analysis determined the changes in EEG frequency band power. Second, a graphical network measure analysis determined the modulation of the nodes in the network. Third, the regional connection strengths analysis determined the overall changes in the networks. A power analysis conducted for each EEG analysis determined that greater than 1,000 points are necessary for a power of 0.8 and $\alpha = 0.05$. Therefore, we chose to bootstrap the results of each analysis 100 times. The post hoc test chosen is the Tukey HSD, and the familywise error rate is kept at a maximum of 0.05.

Frequency Band Analysis. For each condition, for each participant, the theta (4Hz – 8Hz), alpha (8Hz – 12Hz), beta (12Hz – 25Hz), and gamma (25Hz – 40Hz) band FFT power is computed, for each channel. To determine the effect of the stimulation on the frequency response of the EEG, multiple t-tests are computed comparing, for each channel, the None condition against each of the binaural beat stimuli conditions (5Hz, 10Hz, 15Hz). In addition, a two-way factorial ANOVA is used to determine the effect of the experimental binaural beat stimulation CONDITION (None, 5Hz BB, 10Hz BB, 15Hz BB) and BAND (Theta, Alpha, Beta, Gamma) on the mean FFT power for each channel. Furthermore, looking specifically at Fp1, an electrode placed over a key region involved with verbal working memory, a one-way ANOVA is performed to analyze the effect of CONDITION on the bootstrapped FFT band power.

Graphical Network Measure Analysis. Functional networks built from neuroimaging data can be quantified using traditional graphical network metrics [86, 121]. The networks are analyzed using the degree metric (Equation 2.8) computed by the Brain Connectivity Toolbox (BCT) in Matlab. Multiple ANOVAs are completed to analyze the bootstrapped

degree at the channel and hemispheric level. For this analysis, "regions" refers to the average of the surface sites over the different cortices. We define three bilateral REGIONS to identify overall connectivity: Frontal (F), Centro-temporal (CT), and Parieto-occipital (PO). The Central and Temporal, and Parietal and Occipital channels are combined since the total number of electrodes is low. As an example, the left hemisphere regions are Frontal (Fp1, F7, and F3), Centro-temporal (C3 and T3), and Parieto-occipital (P3 and O1). For the EEG data, CONDITION refers only to the None and 15Hz BB conditions (which will be explained in section 3.3.2). CHANNELS refers to the 16 individual channels of recorded EEG data. HEMISPHERE refers to the electrodes in the left or right hemispheres.

Regional Connection Strength Analysis. The effect of CONDITION (None and 15Hz BB) on the regional connection (LINK) bootstrapped PLV strength is evaluated in a two-way ANOVA. LINK refers to the three anterior - posterior connections (F – CT, F – PO, and CT – PO) for each hemisphere and three bilateral connections (F – F, CT – CT, and PO – PO). The regional links are determined by averaging the regional connections between the clusters of electrodes.

4.2 Results

4.2.1 N-Back Task Performance

No significant changes due to CONDITION are found for the participants' reaction time ($\chi^2(5, 34) = 2.63$, $p = 0.757$) nor for the raw accuracy scores ($\chi^2(5, 34) = 0.59$, $p = 0.968$) when compared in a nonparametric Mann-Whitney U statistical test. Table 4.1 shows the mean accuracy and standard deviation for each condition. Overall, the mean values for the experimental conditions are higher than the control conditions but the differences are not

statistically significant due to high variability. The large variance is likely due to the different load levels or larger age range.

	None	Pure	Classical	5Hz BB	10Hz BB	15Hz BB
Mean	92.95%	92.77%	93.33%	94.39%	93.92%	94.15%
SD	8.08%	11.60%	9.25%	7.04%	7.64%	9.53%

Table 4.1: Average and Standard Deviation of Accuracy

A nonparametric Mann-Whitney U test showed that the effect of CONDITION on the ranked accuracy is statistically significant ($\chi^2(5, 34) = 15.07$, $p = 0.0101$). Post hoc pairwise analyses are shown in Figure 4.1. The only statistically significant result is that, individually, participants' performed significantly better during the 15Hz BB than during the None condition ($p = 0.0041$). The other conditions are not significantly different from either None or 15Hz BB.
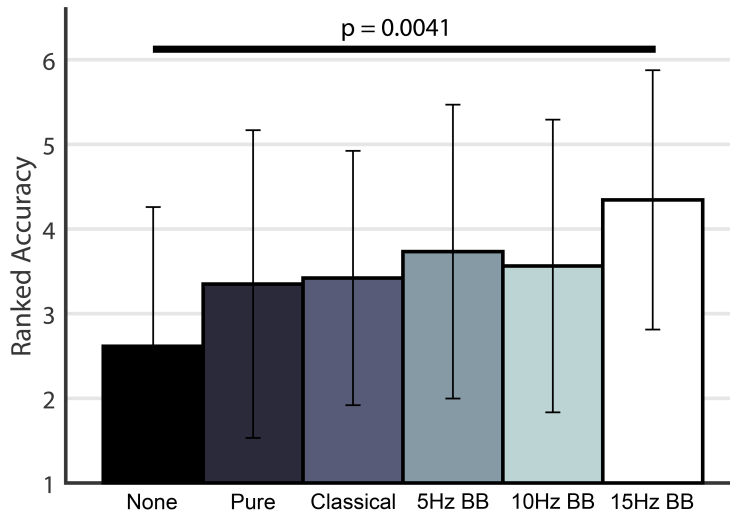
Figure 4.1: Ranked Accuracy for the six acoustic stimulation conditions.

4.2.2 Frequency Band

The results of the frequency band analysis are shown in Figure 4.2. The uncorrected t-statistics, comparing the FFT power for the None condition and the three binaural beat conditions, for each channel, are shown in Figure 4.2A. The results of the two-way factorial ANOVA determined that there are significant effects of CONDITION (F(3,240) = 15.8, $p < 0.0001$), and BAND (F(3,240) = 723.0, $p < 0.0001$) on the mean FFT power but their interaction is not significant (F(9,240) = 1.8, $p = 0.07$). Based on Tukey HSD post hoc analysis, the theta band ($p < 0.0001$) and 15Hz BB ($p < 0.002$) are significantly higher over all other frequency bands and conditions, respectively.
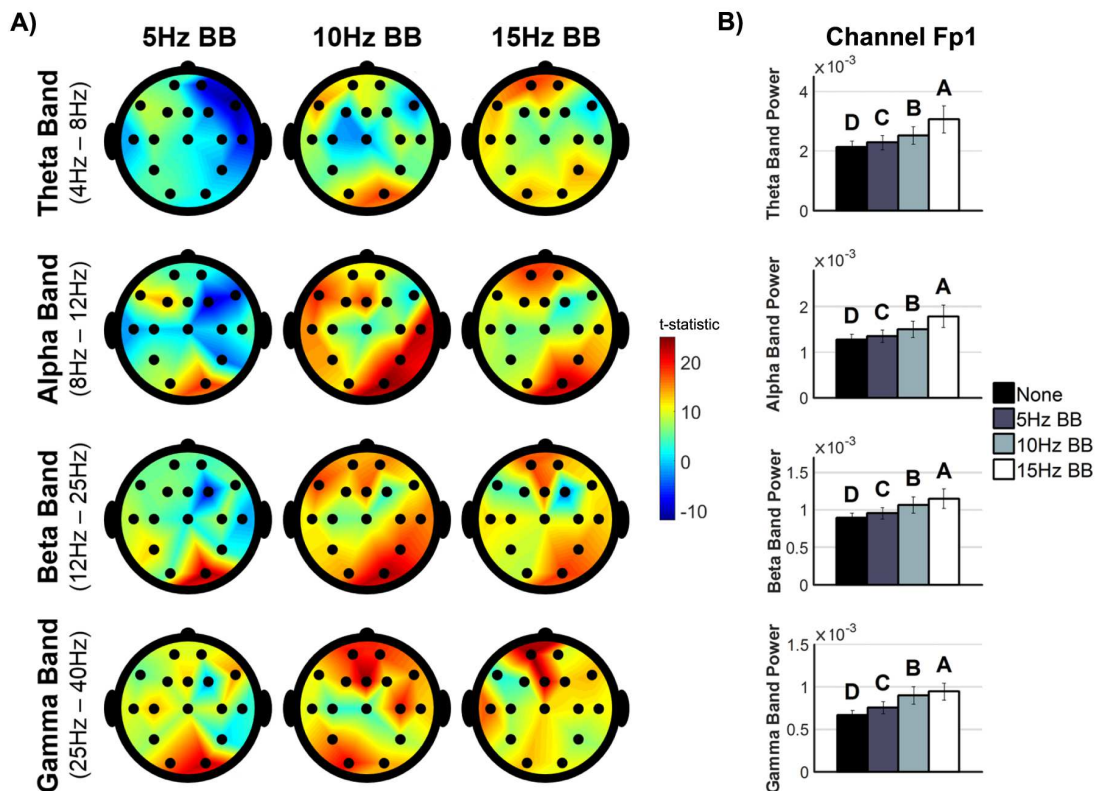
Figure 4.2: A) The uncorrected t-statistic values comparing the FFT power for None against the binaural stimulation conditions. B) The mean and standard deviation for channel Fp1. Conditions marked with different letters are significantly different. Bars show standard error.

In addition, Figure 4.2B shows the FFT power for only the left prefrontal electrode (Fp1). Four one-way ANOVAs, one for each frequency band, analyzed the effect of CONDITION on the bootstrapped FFT power. CONDITION is significant for Theta ($F(3,396) = 165.3, p < 0.0001$), Alpha ($F(3,396) = 165.0, p < 0.0001$), Beta ($F(3,396) = 133.7, p < 0.0001$), and Gamma ($F(3,396) = 230.4, p < 0.0001$).

Therefore, based on the behavioral and frequency response results, only the theta band EEG responses for the None and 15Hz BB conditions are considered for the remaining analysis.

4.2.3 Graphical Network Measure

The mean theta networks, computed over all participants, are shown in Figure 4.3. The networks show, overall, how the networks modified during stimulation.
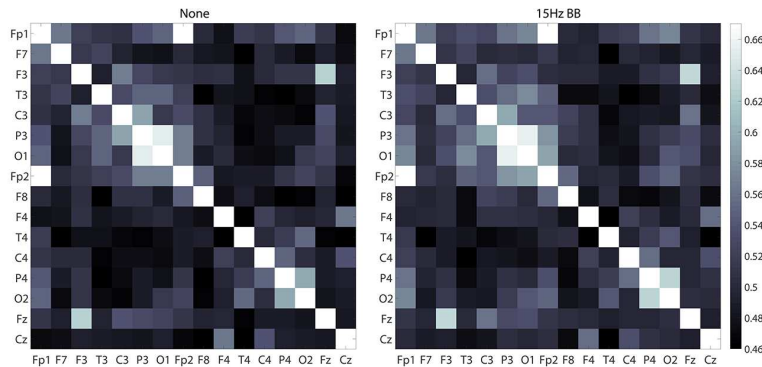
Figure 4.3: Mean theta weight matrices for the None and 15Hz BB acoustic stimulation conditions averaged over all participants.

Specifically looking at the structure of the networks, a two-way ANOVA, shown in Figure 4.4A, is constructed to analyze the effect of CONDITION and CHANNELS on the bootstrapped degree values of the theta networks computed for each participant. CONDITION ($F(1,3168) = 70.6, p < 0.0001$), CHANNELS ($F(15,3168) = 153.5, p < 0.0001$), and their interaction CONDITION $\times$ CHANNELS ($F(15,3168) = 3.8, p < 0.0001$) are significant. Over-

all, the degree values are higher for 15Hz BB when compared against None. Figure 4.4B shows the differences between the two conditions in Figure 3.4A, topographically, for each channel. The prefrontal, parietal, and occipital channels have the largest positive changes between conditions.
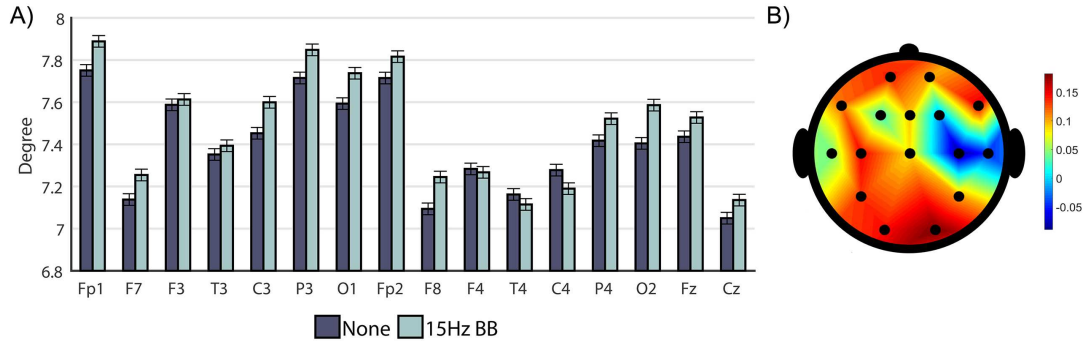
Figure 4.4: A) Mean degree of nodes in connectivity networks averaged over 100 bootstrapped samples. Bars show standard error. B) Difference between conditions (15Hz BB - None).

Furthermore, three separate two-way ANOVAs, one for each REGION, are constructed to determine the effect of CONDITION and HEMISPHERE on degree, and are shown in Figure 4.5. Listed on the graph are the F values from each ANOVA (DOF = 2, N_F = 1197, N_{CT} = 797, and N_{PO} = 797). Generally, the left hemisphere values are higher than the right.
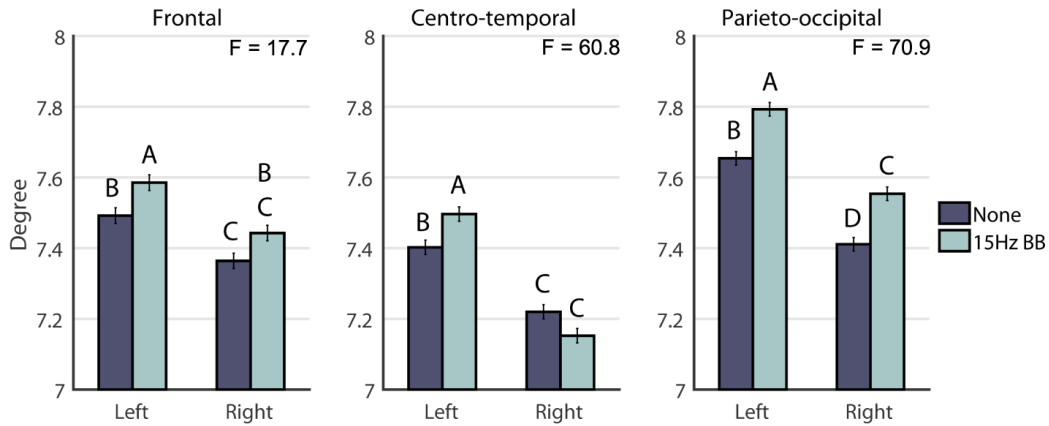
Figure 4.5: Mean degree for each condition across hemispheres averaged over 100 boot-strapped samples. Conditions marked with different letters are significantly different. Bars show standard error.

4.2.4 Regional Connectivity

A 2×9 factorial ANOVA is constructed to compare the effect of LINK and CONDITION on the bootstrapped PLV connection strengths computed from the theta networks from each participant. The main effects of CONDITION ($F(1,1780) = 71.9, p < 0.0001$), LINK ($F(8,1780) = 486.4, p < 0.0001$), and their interaction CONDITION $\times$ LINK ($F(8,1780) = 9.31, p < 0.0001$) are significant. Figure 4.6 highlights the differences in link strengths of the networks between those formed when listening to 15Hz BB versus None. Red indicates that the strength increased during 15Hz BB stimulation, and blue shows a decrease. Regions connected by a dotted line produced insignificant changes between conditions. All connections, except for the right centro-temporal to parieto-occipital and interhemispheric centro-temporal connections, increased when listening to 15Hz BB. Most importantly, the 15Hz BB produced significant increases in the bilateral frontoparietal network and left hemispheric connections. Table 4.2 shows mean and standard deviation of the connection strengths over 100 bootstrapped samples, the mean difference between the two conditions, and the results of the t-tests comparing None to the 15Hz BB for each link.
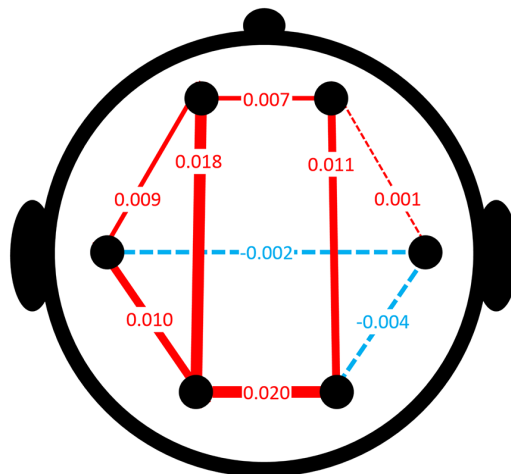
Figure 4.6: Bootstrapped regional PLV connection strength differences between the None and 15Hz BB conditions.

Link	None PLV	15Hz BB PLV	Difference	p-value	t-statistic
PO – PO	0.479 ± 0.019	0.499 ± 0.016	0.020	$< .0001$	8.25
F – PO (L)	0.501 ± 0.027	0.519 ± 0.024	0.018	$< .0001$	5.01
F – PO (R)	0.477 ± 0.016	0.488 ± 0.014	0.011	$< .0001$	5.37
CT – PO (L)	0.554 ± 0.026	0.564 ± 0.024	0.010	0.005	2.84
F – CT (L)	0.501 ± 0.024	0.510 ± 0.023	0.009	0.005	2.82
F – F	0.507 ± 0.017	0.514 ± 0.016	0.007	0.006	2.76
CT – PO (R)	0.526 ± 0.019	0.522 ± 0.016	-0.004	0.130	-1.52
CT – CT	0.456 ± 0.019	0.454 ± 0.018	-0.002	0.416	-0.81
F – CT (R)	0.470 ± 0.018	0.471 ± 0.016	0.001	0.777	0.28

Table 4.2: Regional Connections

4.3 Discussion

15Hz binaural beats increases relative accuracy during an N-Back task. Based on a power analysis, the participant N number is not large enough to determine any significances in raw accuracy scores. However, the ranked accuracy values, shown in Figure 4.1, produced the key result that, individually, participants performed significantly better overall when listening to 15Hz BB than None. Classical Music and Pure Tone produced an insignificant change from None which is consistent with previous literature [126]. In addition, neither the 5Hz or 10Hz BB produced significant changes from the None condition. The increase in performance when listening to 15Hz BB can be potentially explained by noting that 15Hz BB produced the highest change in the theta band frequency response magnitude, increased the degree of the network in prefrontal and parietal channels, and increased synchronization within the frontoparietal network.

15Hz binaural beats impacts EEG frequency response magnitude. As shown in Figure 4.2, binaural stimulation frequency changes the EEG frequency responses over all channels. The theta (5Hz) BB stimulation responses show that, overall, the frequency power is unchanged or decreased when compared to None, except for within the gamma band. The

alpha (10Hz) and beta (15Hz) binaural stimulation frequencies resulted in similar responses across the four bands. However, 15Hz BB produces higher power within the theta band in the left frontal and parietal electrodes. Activation of both regions, within the theta band, is key to working memory performance. Additionally, over all frequency bands, the 15Hz BB produced significantly higher power in the left prefrontal electrode (Fp1) than all other stimulation conditions. Finally, for Fp1, the theta band had the largest change in magnitude between the 15Hz BB and 10Hz BB. These results are consistent with the role of frontal theta networks supporting working memory [25, 48].

15Hz binaural beats modifies network structure. As shown in Figure 4.4A, the channels with the highest degree values, in each hemisphere, correspond to the electrodes over the frontal and parieto-occipital cortices. This result is reflected in Figure 4.4B and Figure 4.5 which shows that, generally, the frontal and parieto-occipital values are higher than the centro-temporal results. The results shown in Figure 4.5 agree with [42, 127] that a verbal working memory task activates both bilateral frontal and parietal regions with additional regions recruited in the left hemisphere. In addition, as shown in both Figure 4.4 and Figure 4.5, 15Hz BB increases the degree values in both the left and right hemispheres. The network of brain activity produced when listening to 15Hz BB, has higher global information transfer than does the baseline network produced by only task performance (no auditory stimulation). The increase in information transfer could explain the change in the behavioral data.

15Hz binaural beats changes regional linkages. 15Hz binaural beats produces the largest change in four links, shown in Figure 4.6: PO – PO, bilateral F – PO, and left CT – PO. Of all the links, the bilateral parieto-occipital connectivity strength increased the most when compared to the None condition. The parietal cortices are involved with early visual signal processing[128] and visual attention feedback [129]. The letters of the N-Back task are encoded as both visuospatial (right hemisphere) and verbal (left hemisphere) objects.

In addition, the bilateral frontoparietal network connectivity strength increased significantly when listening to the 15Hz BB. In previous studies, the interactions between the parietal and prefrontal cortices have been strongly associated with working memory performance [43, 44]. Also, the left hemisphere parieto-occipital to centro-temporal link strength increased. The connection between these two regions is associated with verbal working memory in the form of phonological storage and subvocal rehearsal of the information [39, 130]. Synthesizing these results, we see that the 15Hz BB influences the most important links used within the working memory network which could explain the benefited performance we observe.

In conclusion, this study demonstrates that listening to 15Hz binaural beats can affect cortical network properties during a verbal working memory task. The network produced when listening to 15Hz binaural beats indicates more information transfer than that produced when listening to no sound. Also, the frontoparietal bilateral network increased significantly in connectivity when listening to the 15Hz binaural beats. Furthermore, only the 15Hz binaural beats condition produced significantly more accurate responses, in individuals, when compared to listening to no sound. The other acoustic stimulation conditions produced no significant changes. Therefore, these results indicate that 15Hz binaural beats can be used to change the frequency response and connectivity of cortical networks, and thereby influence verbal working memory task performance.

Future experiments should focus on determining the nonlinear relationship between the binaural beat stimuli and the observed cortical activity and behavior. From previous experiments, it has been shown that 40Hz BB produces maximal responses. If 40Hz BB had been included with the battery of binaural stimulation frequencies tested, then it potentially might have produced a greater modulation of network characteristics. However, it is unknown if it would have produced the desired changes in the behavior, which should be explored.

Chapter 5

Comparison of Visuospatial and Verbal Working Memory Tasks

Beauchene C., Abaid N., Moran R., Diana R.A., Leonessa A., Using non-invasive brain stimulation to augment working memory. Scientific Reports, under review

Synchronization in cortical networks is necessary for complex cognitive function and can be influenced through the auditory system using binaural beats. Binaural beats utilize the brain's response to two pure tones, with a small frequency mismatch, presented separately to each ear. The frequency difference is interpreted as a beating frequency that can manipulate synchrony in connected cortical networks. One such network, the working memory network, is the system responsible for temporarily holding and processing information and may be amenable to modulation via binaural beats. The two experiments presented here show that listening to different sound conditions influenced both participant response accuracy and cortical connectivity during working memory tasks. Different working memory domains, visuospatial and verbal, are tested in each experiment using a delayed match-to-sample task and an N-back task, respectively. The six sound conditions used are None, Pure Tone, Classical Music, 5Hz binaural beats, 10Hz binaural beats, and 15Hz binaural beats. The recorded electroencephalography data is used to quantitatively assess the cortical network topology. The results presented in this chapter are from two recent studies by our group [131, 132]. The objective of these experiments is to quantify the cortical connectivity changes measured

when listening to binaural beats during cognitive tasks. Specifically, both visuospatial and verbal working memory tasks are chosen because binaural beats activate cortical regions key to working memory, which in turn, may impact quantifiable performance.information transfer.

5.1 Methods

5.1.1 Working Memory Tasks

The two different working memory domains, visuospatial and verbal, are tested using a delayed match-to-sample task [40] and an N-back task [133], respectively. Figure 1.3A shows a match and no match trial for the visuospatial task. After encoding an initial image of colored squares, the subject is told to remember that image during a working memory maintenance period of 4 seconds. During retrieval, the subject indicates if the remembered and current image match or not. The spatial layout of the squares does not change on a single trial, only the colors potentially change. Figure 1.3B shows the N-Back task. The sequence of letters is encoded on each trial. The mental set of "N" items must be updated to include a newly presented item and to exclude the oldest item in the set and the set is retained in the working memory. For each letter shown on the screen, the participant is asked to determine if the remembered (no longer visible) and current (visible on-screen) letters match. The participant responds when the current letter on the screen matches the letter that is shown "N" letters prior.

5.1.2   Participants

Thirty-four healthy adults (15 women, 19 men) aged 18 to 46 yr (mean 27.1 yr) are recruited to participate in these studies. Written consent is obtained from each participant after being introduced to the experimental protocols, which are approved by the Virginia Tech Institutional Review Board. All of the experiments were performed in accordance with guidelines and regulations set forth by the Virginia Tech Institutional Review Board. Each participant, before starting the task, is tested to ensure that there are no vision or hearing problems. None of the participants disclosed any previous neurological or hearing problems when asked. Due to equipment malfunction during the visuospatial task, only 28 of the participants (12 women, 16 men) aged 19 to 46 yr (mean 27.6 yr) are included in the analysis of that task. However, for the N-back task, all 34 participants are used in the analysis. The participants used in this comparison are the same used in Chapters 3 and 4.

5.1.3   Auditory Stimulus

During the working memory tests, six different sound conditions are evaluated. The control conditions are chosen to be: 1) None, 2) Pure Tone (R: 240Hz, L: 240Hz), and 3) Classical Music (Stereo: Vivaldi - Spring). The experimental conditions are selected to be: 1) 5Hz Binaural Beat (R: 240Hz, L: 245Hz), 2) 10Hz Binaural Beat (R: 240Hz, L: 250Hz), and 3) 15Hz Binaural Beat (R: 240Hz, L: 255Hz). R and L indicate which tones are played into the right and left ears, respectively. The experimental binaural beat conditions, 5Hz, 10Hz, and 15Hz, are chosen to represent the theta, alpha, and beta band stimulation, respectively. The sound files are created in Matlab and are played through stereo headphones (MDR-NC7, Sony). Each participant set the stimulus volume to a comfortably loud level at the start of the session.

5.1.4   EEG Recordings

An EEG system (OpenBCI, Inc., New York, NY) with 16 gold cup passive electrodes is interfaced with LabVIEW to record the brain activity at a sampling rate of 128Hz. The channel locations are Fp1, Fp2, F7, F8, F3, F4, T3, T4, C3, C4, P3, P4, O1, O2, Fz, Cz, which are set using the 10-20 system [120]. The earlobes are used for the ground and reference electrodes. Prior to data collection, the electrodes are prepared using Ten20 EEG conductive paste (Weaver and Co., Aurora, CO) and each of the electrode impedances are verified to be < 5 kΩ.

5.1.5   Experimental Paradigms

The participants complete the tasks on two separate days. The order that the tasks are given is randomized over all subjects. The same paradigm is used for both sessions, as shown in Figure 5.1, with only the task changing. Participants complete the tasks in a quiet, dimly lit room and sit in front of a computer monitor. A custom script written for the Cogent Graphics Matlab toolbox presents the tasks. The participant presses the left arrow or right arrow on the keyboard to indicate a match or no match, respectively.

Individual cognitive differences determine the limit on each participant's 'load', which is the number of letters or color squares, that can be successfully maintained and manipulated during the tasks. Capacity is computed using $K_\mathrm{C} = \mathrm{C}(\mathrm{H} - \mathrm{F})$, where C is the load, H is the hit rate (percentage of correctly identified matches), and F is the false alarm rate (percentage of non-matches identified as matches) [40]. Before starting the experiment, an initial load titration test is completed for each participant. First, the participant would practice the test at an easy load and then complete the task at increasingly difficult loads. For the visuospatial task, the practice is one block of a 2-load task and then followed by one block

each of the 3-, 4-, and 5-load versions of the task. For the N-Back task, the practice is one block of a 1-back task and then followed by one block each of the 1-, 2-, and 3-back task.

For each participant, the load used in the experimental task is set by selecting the load which produced the highest capacity estimate. In the event that two of the loads produced equal capacity values, the load with the largest hit rate less than 100% is chosen. If the hit rate is equal to 100%, then the next highest load is chosen. The purpose of choosing a titrated load is to ensure that each individual is tested at their working memory capacity limit, hence allowing the identification of any improvement in working memory capacity due to the sound conditions.

After the EEG is setup, each participant performed the task at their selected load for approximately thirty minutes. Every five minutes, the sound condition would switch to one of the other six different sound conditions. For each sound condition, the stimulus began precisely with the first working memory trial of a block and ended with the final trial. Between each block is a two-minute break where no sound is played. Over all participants, each trial and the order of the sound conditions are randomized to minimize bias.
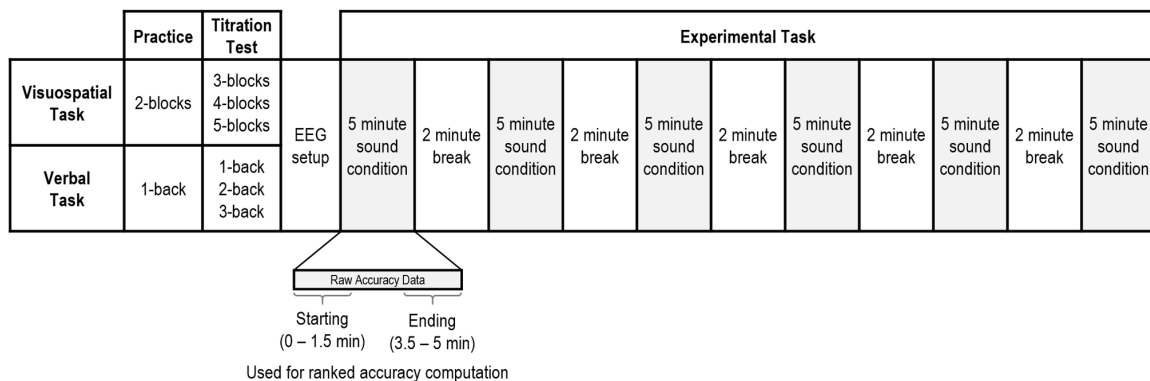
Figure 5.1: An overview of the experimental paradigm used for both tasks.

5.1.6   Behavioral Data Processing

A custom Matlab script processed the recorded behavioral data for analysis. First, the trials where the participant pressed an incorrect key or didn't respond in time are discarded (less than 5%). The behavioral metrics chosen to assess performance during each sound condition are accuracy and ranked accuracy. Accuracy is calculated by dividing the number of correct trials, both matches (Hit) and non-matches (Correct Rejection), by the total number of trials. For each participant, we identify relative trends, over time, in the accuracy results by constructing a new dataset, from the raw accuracy data, by ranking the raw accuracy of the six sound conditions from 1 (lowest accuracy) to 6 (highest accuracy). The ranked accuracy is computed, for each participant, at two segments of time, the start (0 – 1.5 min) and the end (3.5 - 5 min) of each five-minute block. The purpose of ranking each participant's accuracy scores is to normalize the data to a standard scale which eliminates the effect of an individual's mean accuracy. We divide the data into two different time segments in order to assess the change in accuracy over time.

5.1.7   EEG Data Processing

To process the raw EEG data, the EEGlab toolbox in Matlab is used [104]. First, the EEG recordings are bandpass filtered (0.5Hz – 50Hz) to remove both drift and the 60Hz power line noise. The bandpass filter used is a linear FIR filter with an order of 846. Second, the filtered EEG data is re-referenced to the average. Next, the epochs are extracted. For the visuospatial task, the maintenance (125 ms – 4125 ms, which corresponded to the time when no visuospatial array is present on the screen) epochs are extracted. For the N-Back task, the onset (0 ms – 1000 ms, which corresponded to the time when the letter is on the screen) epochs are extracted. Finally, the baseline is removed (0-200 ms before stimulus presentation)

for all epochs. For both tasks, only correct trials (i.e. a Hit or Correct Rejection) are used. Epochs with eye blinks, movement, or other artifacts are removed following manual inspection of the automatically identified artifacts in EEGlab (less than 5% rejection).

5.1.8 Connectivity Network Construction

The processed epoched EEG signals are bandpass filtered, using EEGlab, to focus on the theta band (4Hz – 8Hz). A measure of synchronization is PLV (defined in section 2.1.3 in Equations 2.3 and 2.4), which is used to define the edge weights in a network that considers each EEG channel as a node. The connectivity network is constructed using the EEG channels as the nodes ($\mathcal{V} = \{1, ..., n\}$), where $n = 16$. The network is assumed to be all-to-all, meaning that between every pair of nodes there exists an edge. The weights associated with these edges are determined using the PLV metric. The weighted adjacency matrix is defined as W_{PLV} with elements $w_{ij} = \text{PLV}_{ij}$, $i, j = 1, 2, .., n$. Due to the properties of PLV, w_{ij} is in $[0, 1]$ and W_{PLV} is symmetric since PLV, and therefore the network, is undirected. Edge weights in terms of PLV are computed for each epoch. An average network is computed over all epochs, for each person, to create an average network, for each condition.

5.1.9 Behavioral and EEG Analysis

The behavioral data are analyzed using the statistical software JMP (SAS, Cary, NC). For each task, two one-way ANOVAs, one for each of the starting and ending time segments, are computed to assess the effect of CONDITION on the ranked accuracy. For the behavior analysis, CONDITION refers to all sound conditions: None, Pure Tone, Classical, 5Hz BB, 10Hz BB, and 15Hz BB. The post hoc test chosen is the Tukey HSD, and the familywise error rate is set at 1E-6 to be conservative.

Two different methods are utilized to analyze the EEG data. First, a network measure analysis is used to determine how the nodes in the network are affected by the different sound conditions. Second, the regional connection strengths are analyzed to find the overall changes in the networks between regions. For the EEG analyses, CONDITION refers only to the None and 15Hz BB conditions. Over the two tasks, the None and 15Hz BB conditions had the largest changes when compared to the other conditions. Additional EEG analyses can be found in [131, 132].

A power analysis conducted for all of the behavior and EEG analyses determined that greater than 1,000 points are necessary for a power of 0.8 and $\alpha = 0.05$. Therefore, the results of each analysis are bootstrapped 100 times in order to maintain the same N number for all of the following analyses. The familywise error rate is kept at a maximum of 0.05. The datasets generated during and/or analysed during the current study are available from the corresponding author on reasonable request.

Network Measure Analysis. Characteristics of functional networks computed from neuroimaging data can be quantified using traditional network metrics [86, 121]. The degree metric, defined in Equation 2.8, of the networks is computed the Brain Connectivity Toolbox (BCT) in Matlab. To analyze the bootstrapped degree at the channel and hemispheric level, multiple ANOVAs are used. In this analysis, CHANNELS refers to the 16 individual channels of recorded EEG data. Also, "regions" refers to the average of the surface electrode over the different cortices. We define three bilateral REGIONS to identify overall connectivity: Frontal (F), Centro-temporal (CT), and Parieto-occipital (PO). Since the total number of electrodes is low, the Central and Temporal, and the Parietal and Occipital channels are clustered. As an example, the regions in the left hemisphere include Frontal (Fp1, F7, and F3), Centro-temporal (C3 and T3), and Parieto-occipital (P3 and O1). HEMISPHERE indicates if the electrodes are in the right or left hemispheres.

Regional Connection Strength Analysis. A two-way ANOVA is used to investigate the effect of CONDITION (None and 15Hz BB) on the regional connection (LINK) bootstrapped PLV strength. LINK refers to the three anterior - posterior connections (F – CT, F – PO, and CT – PO) for each hemisphere, and the three bilateral (BL) connections (F – F, PO – PO, and F – PO). The regional links are determined by averaging the regional connections between all of the clusters of electrodes.

5.2   Results

5.2.1   Behavioral Results

No significant changes due to CONDITION are found for the participants' raw accuracy scores, as shown in Table 5.1, in either the visuospatial (VS) task ($\chi^2(5, 28) = 6.37$, $p = 0.27$) or the verbal (VB) task ($\chi^2(5, 34) = 0.59$, $p = 0.97$) when compared in a nonparametric Mann-Whitney U statistical test.

Task	None	Pure	Classical	5Hz BB	10Hz BB	15Hz BB
VS	$80.9 \pm 11\%$	$82.5 \pm 8\%$	$76.8 \pm 9\%$	$76.9 \pm 11\%$	$78.6 \pm 10\%$	80.1 ± 11 %
VB	$93.0 \pm 8\%$	$92.8 \pm 11\%$	$93.3 \pm 9\%$	$94.4 \pm 7\%$	$93.9 \pm 7\%$	94.2 ± 9 %

Table 5.1: Mean and Standard Deviation of the Raw Accuracy.

However, the results of the ANOVA indicate that the effect of CONDITION on the bootstrapped ranked accuracy is statistically significant for both the visuospatial task (Starting: $F(5, 594) = 333.5$, $p < 0.0001$, Ending: $F(5, 594) = 267.1$, $p < 0.0001$) and verbal task (Starting: $F(5, 594) = 1117.1$, $p < 0.0001$, Ending: $F(5, 594) = 675.5$, $p < 0.0001$). Post hoc pairwise analyses, for both tasks, are shown in Figure 5.2.
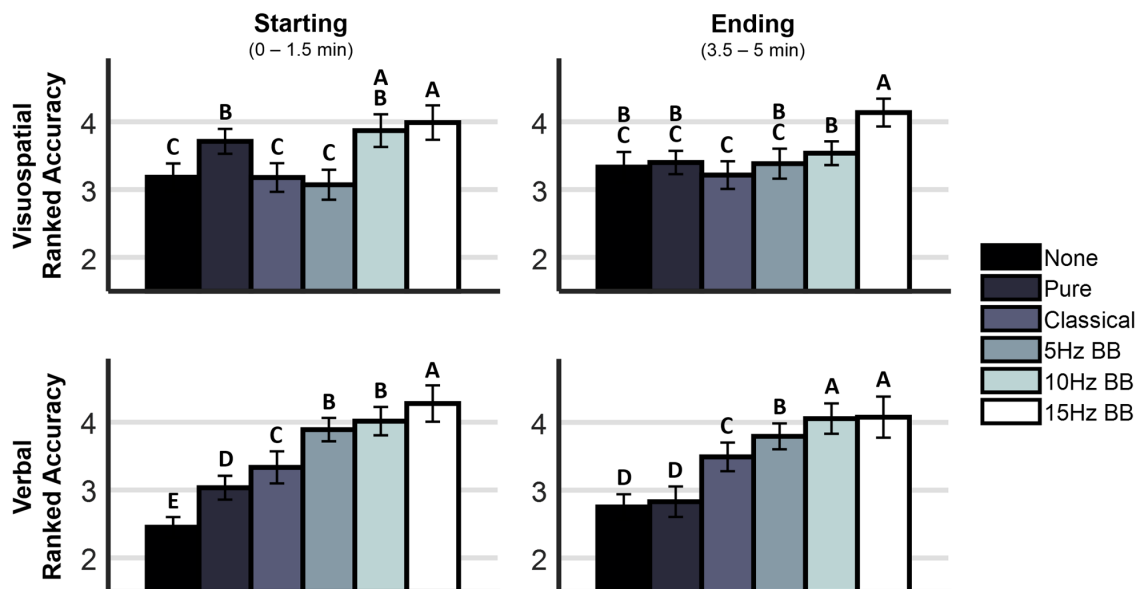
Figure 5.2: Bootstrapped ranked accuracy for the six sound conditions for both the visuospatial and verbal tasks, averaged over all participants. The bars show ± standard deviation. Conditions marked with different letters are significantly different.

The visuospatial task produced more variability, over time, in the relative accuracy of each individual than is observed in the verbal task results. Comparing the two tasks, listening to 15Hz BB produced the largest increase in relative accuracy from the None condition. Given our goal of analyzing how changes in brain network synchrony cause behavioral changes, further analyses focus only on the None and 15Hz BB conditions that represent the extremes of performance on the task.

5.2.2 Mean Theta Connectivity Networks

The mean theta PLV connectivity networks for the visuospatial (Figure 5.3) and verbal (Figure 5.4) tasks show similar structures but also illustrate task-related differences. The networks show that the connection strengths change when listening to 15Hz BB when compared to the no sound condition.
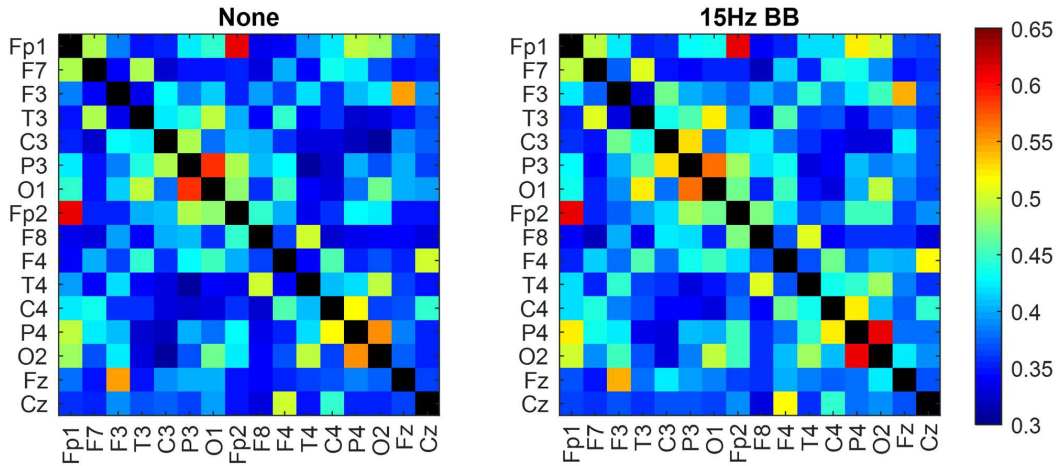
Figure 5.3: Mean theta weight matrices, for the visuospatial task, for the None and 15Hz BB sound conditions averaged over all participants. The diagonal is equal to 1.
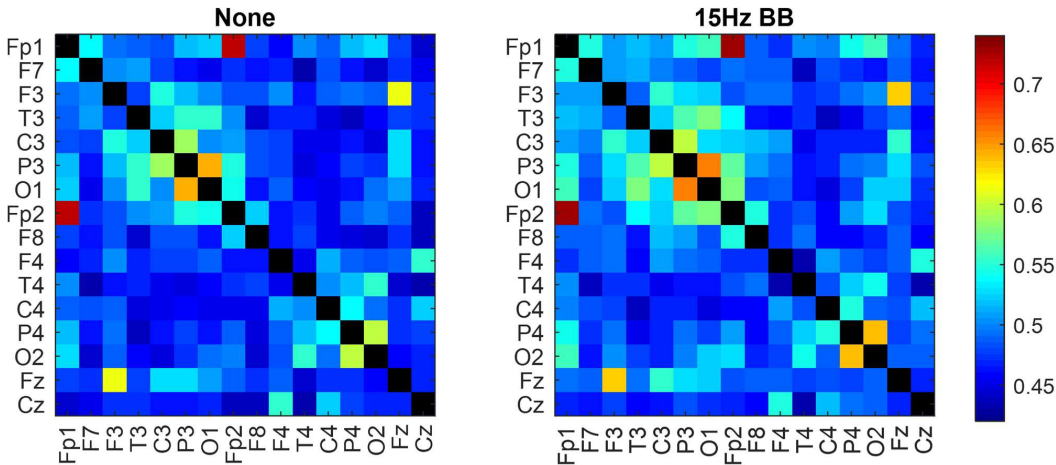
Figure 5.4: Mean theta weight matrices, for the verbal task, for the None and 15Hz BB sound conditions averaged over all participants. The diagonal is equal to 1.

5.2.3   Network Analysis

To analyze the network structures, two different two-way ANOVAs, are constructed to analyze the effects of CONDITION and CHANNELS on the bootstrapped degree values of the theta PLV networks, for each task. The F statistics are reported in Table B.1) in Appendix B and for each effect p is always less than 0.0001. Figure 5.5A and Figure 5.5C show the

degree values, at each node, for the visuospatial and verbal tasks, respectively. Comparing the F values between the tasks, the degree as a function of CONDITION is greater than CHANNELS for the visuospatial task. The opposite is true for the verbal task. Overall, for both tasks, the degree values for 15Hz BB are generally higher than the None condition.
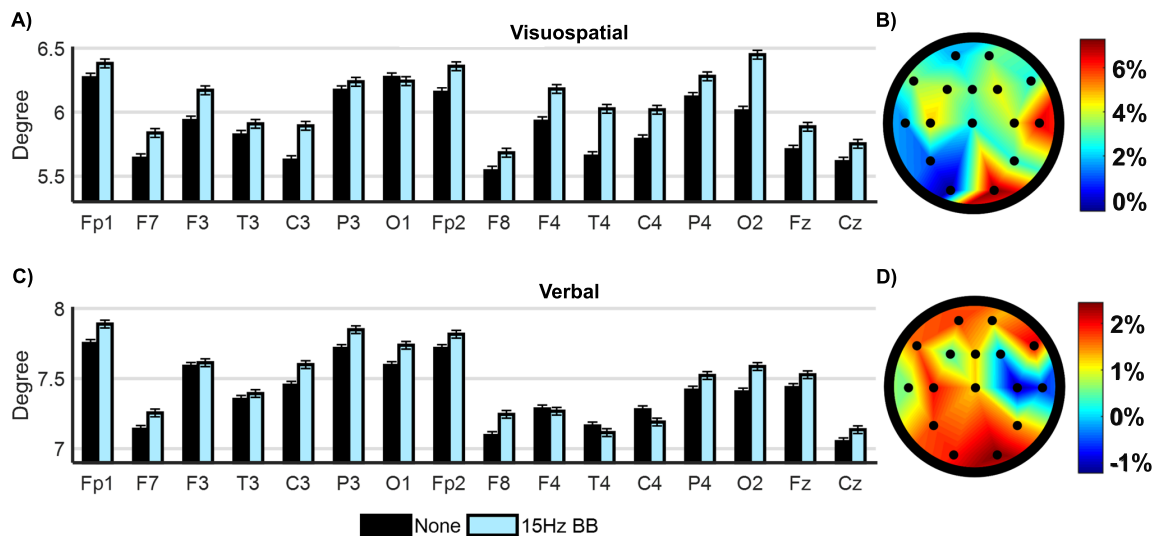
Figure 5.5: Mean degree of the nodes averaged over the 100 bootstrapped samples for the visuospatial (A) and verbal (C) tasks. Bars show ± standard error. The percent difference between conditions is shown for the visuospatial (B) and verbal (D) tasks.

In addition, Figure 5.5B and Figure 5.5D show the percent difference between the degree values computed for the None and 15Hz BB networks, topographically. For the visuospatial task, the larger increase is found in the right hemisphere and the opposite is found for the verbal task. The right occipital (O2) channel has the largest increase in both tasks. In order to find the hemispheric differences in the degree values, three separate factorial two-way ANOVAs, one for each REGION, are constructed, for each task. The purpose is to isolate the effects of CONDITION and HEMISPHERE on the degree values. Figure 5.6 shows the results for the visuospatial (Figure 5.6A) and the verbal (Figure 5.6B) tasks. On each graph is listed the F values from each two-way ANOVA (DOF = 3, $N_{\mathrm{F}} = 1196$, $N_{\mathrm{CT}} = 1196$, $N_{\mathrm{PO}} = 796$). Similar to the results found in Figure 5.5, for the visuospatial task, the degree
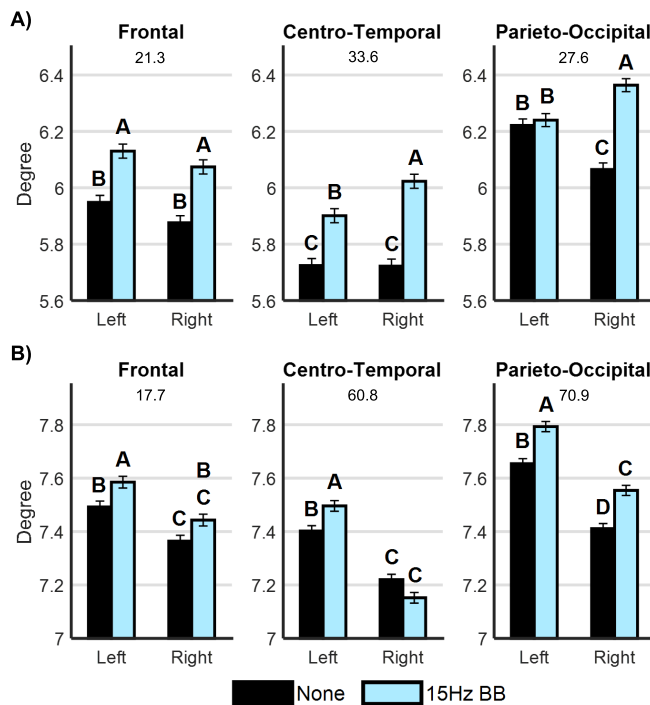
Figure 5.6: Mean degree for each hemisphere averaged over the bootstrapped samples for the visuospatial (A) and verbal (B) tasks. Conditions marked with different letters are significantly different. Bars show ± standard error.

values in the right hemisphere are generally higher than in the left. For the frontal region, the hemispheric difference is minimal but 15Hz BB is significantly higher than None. In addition, the parieto-occipital region shows that there is no significant difference between the None and 15Hz BB conditions in the left hemisphere, but the right hemisphere has the largest change of any region. The opposite effect is seen in the verbal task since the left hemisphere is generally higher than the right. The differences, across hemispheres and conditions, is greater in the frontal and parieto-occipital regions than the visuospatial task.

5.2.4   Regional Connectivity

A 2×9 factorial ANOVA is constructed to compare the effects of LINK and CONDITION on the bootstrapped PLV connection strengths computed from the mean theta networks,

from each participant. The F statistics are reported in Table B.2) in Appendix B and for each effect p is always less than 0.0001. Figure 5.7 shows the differences in the regional link strengths between those formed when listening to 15Hz BB versus None. The lines indicate that the strength increased significantly during 15Hz BB stimulation in comparison to None. The line thickness indicates the amount of change. The hemispheric specialization, due to the working memory domain, can be seen in Figure 5.7. For the visuospatial task, all the connections increased significantly during the 15Hz BB condition when compared to no sound. Most importantly, the 15Hz BB produced significant increases in the right hemisphere frontoparietal connection and right hemispheric connections. For the verbal task, all connections, except for the right centro-temporal connections, increased when listening to 15Hz BB. Most notably, the 15Hz BB produced significant increases in the bilateral frontoparietal network and left hemispheric connections. Table B.3) and Table B.4 in Appendix B show the statistical results from the visuospatial and verbal tasks, respectively. Included in the tables are the mean and standard deviation of the connection strengths over 100 bootstrapped samples, the mean difference between the two conditions, and the results of the two-tailed t-tests comparing None to the 15Hz BB for each link.
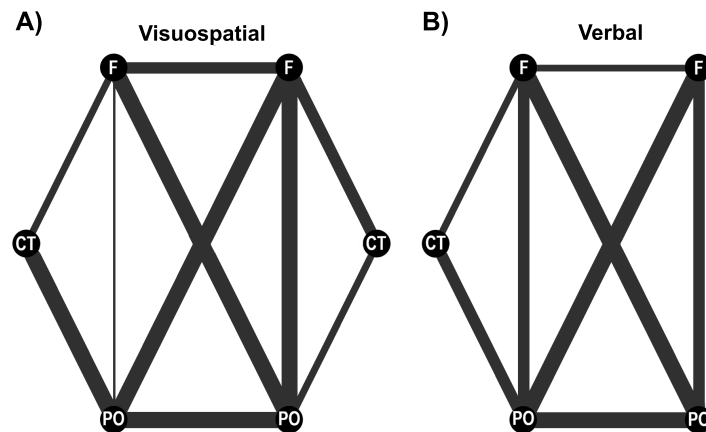
Figure 5.7: Bootstrapped regional PLV connection strength differences between the None and 15Hz BB conditions. The verbal task network does not include the right centro-temporal node because no significant changes in the connected links are observed.

5.3   Discussion

Based on a power analysis, the number of participants is not large enough to determine any significances in raw accuracy scores. However, the bootstrapped ranked accuracy values, shown in Figure 5.2, produced the key result that, individually, participants performed significantly better overall when listening to 15Hz BB than None. For the visuospatial task, the conditions which produced higher relative accuracy changed over time. In the beginning of the five-minute condition block, listening to a Pure Tone, 10Hz BB, and 15Hz BB all produced high relative accuracy. However, by the end of the five minutes, all other conditions had dropped but 15Hz BB remained significantly higher. Therefore, even though other conditions produced high accuracy at the beginning of the task block, 15Hz BB is the only condition to sustain that relative accuracy. This pattern is similar to the results observed in [131] which found a mean 3% increase in the change in raw accuracy over the 5 minutes. For the verbal task, the same general pattern is seen in the ranked accuracy in the beginning and at the end of the task. Overall, the key result is that listening to 15Hz BB consistently outranked all of the other conditions. The increase in performance when listening to 15Hz BB can be potentially explained by noting that 15Hz BB increased both the degree of the network in prefrontal and parietal channels and synchronization within the frontoparietal network which would suggest that more information is able to travel over the connected network. Additionally, listening to 15Hz BB might be able to maintain network function across an interval in the face of either fatigue or interference from previous trials.

The results in Figure 5.5, which shows the degree values for each channel, agree with the previous literature which supports hemispheric specialization depending on the working memory domain. The degree values in the right and the left hemisphere are higher in the visuospatial and verbal task, respectively. Also, regardless of the task, the channels with the highest degree values correspond to the electrodes over the frontal and parieto-occipital cortices, which

are the dominant regions in the working memory network. This result is reflected in Figure 5.6 which shows that, generally, the frontal and parieto-occipital values are higher than the centro-temporal results. The results in Figure 5.6 also show an activated bilateral frontal and parietal regions with additional regions recruited in the right and left hemisphere, for the visuospatial and verbal working memory task, respectively. However, regardless of the task, the 15Hz BB consistently produced higher degree values than the None condition. The network of brain activity produced when listening to 15Hz BB has higher global information transfer than does the baseline network produced by only task performance (no auditory stimulation). The increase in information transfer could explain the changes in the observed behavior.

Significant increases in the frontoparietal network are observed in both tasks, due to listening to 15Hz BB, as shown in Figure 5.7. The change during the verbal task is symmetric. However, in the visuospatial task, the dominant increase is observed in the right hemisphere. Between the two tasks, listening to 15Hz BB produces the largest change in the bilateral PO – PO, bilateral F – PO, right F – PO, and left CT – PO connections. The parietal cortices are involved with early visual signal processing[128] and visual attention feedback [129]. In previous research, the co-activation of the parietal and prefrontal cortices is strongly associated with increased working memory performance [43, 44]. The connection between the parieto-occipital to centro-temporal regions is associated with working memory in the form of phonological storage and subvocal rehearsal of the information [39, 130]. Combining all of the results together, we see that the 15Hz BB promotes and enhances the most important links within the working memory network, which could explain the observed increase in performance.

The results of these studies demonstrate that listening to 15Hz binaural beats can affect cortical network properties during both a verbal and visuospatial working memory task.

The networks evidenced during the 15Hz binaural beats condition show that more information is transferred across the network than when listening to no sound. In addition, the connectivity of the frontoparietal network increased significantly when listening to the 15Hz binaural beats. Hemispheric specialization, which is known to be involved in working memory processing, is observed in both tasks with the visuospatial task recruiting more regions in the right hemisphere and the verbal task in the left hemisphere. In both tasks, the 15Hz binaural beats condition produced the largest significant change in accurate responses, in individuals, when compared to listening to no sound. Therefore, the combination of these results shows that listening to 15Hz binaural beats can be used to modify the connectivity of cortical networks, and thereby influence verbal and visuospatial working memory task performance.

Chapter 6

The Virtual Brain Controller Testing Environment

Beauchene C., Roy S., Simon J., Abaid N., Leonessa A., Closed-Loop Control of the Frequency Response of The Virtual Brain Model. Proceedings of the ASME DSCC - Dynamic Systems and Control Conference, October 11-October 13, 2017, Tysons Corner, Virginia, USA.

The brain is a highly complex network and analyzing brain connectivity is a nontrivial task. Consequently, the neuroscience community created a large-scale, customizable, mathematical model which simulates brain activity called The Virtual Brain (TVB). Using TVB, we seek to control electroencephalography (EEG) measured brain states using auditory inputs, through TVB. This chapter details the development and proof-of-concept testing of a simulation environment for an EEG-based closed-loop control of TVB using BB. Results suggest that the connectivity networks, constructed from simulated EEG, may change with certain BB stimulation frequency. In this work, we demonstrate that a linear and an adaptive controller can successfully modulate TVB connectivity.

6.1   The Virtual Brain

The Virtual Brain (TVB), schematized in Figure 6.1, is a large scale brain network model which can be used to simulate brain activity [134, 135]. The completely open-source architecture of TVB is implemented in Python. TVB approximates brain activity using a graphical network made up of nodes, which represents partitioned areas of the brain. The connectivity matrix, based on structural MRI or diffusion tensor imaging data, defines the edge weights and time delays between all nodes in the network. Neural mass models are used to define the local dynamics at each node. TVB can simulate the EEG response, using a forward head model, from the computed local field potentials at each node. In addition, regional stimulation can be simulated by applying a series of pulses to any node. The combination of the neural mass models at each node, the connectivity matrix, and the 3D brain structure create the full virtual brain model. We use TVB to determine the effect of the binaural beat by apply a regional stimulus and evaluating the simulated EEG response.
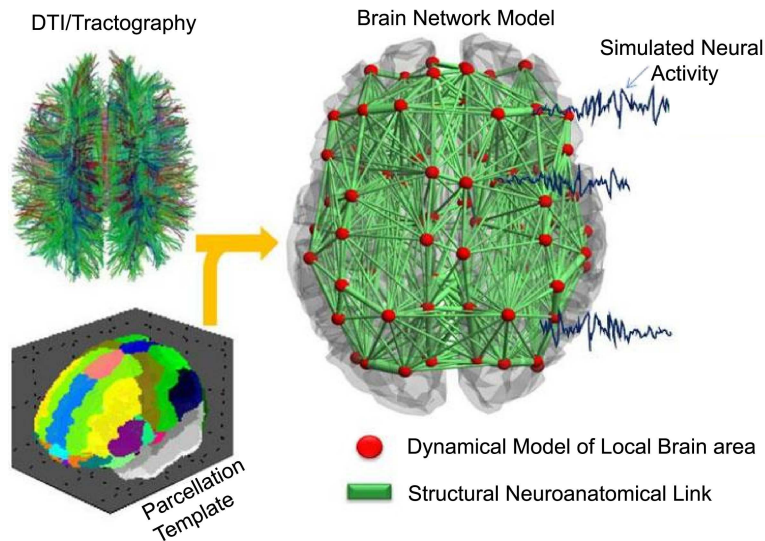
Figure 6.1: The Virtual Brain Model [1].

6.1.1   Neural Mass Model

One of the neural mass models integrated into TVB is the Generic 2D Oscillator model [134]. This model is capable of generating different phenomena that neuronal populations can exhibit. The equations governing the dynamics are given by

$$\dot{V} = d\tau[-fV^3 + eV^2 + gV + \alpha W + \gamma I], \tag{6.1}$$
$$\dot{W} = \frac{d}{\tau}[cV^2 + bV - \beta W + a], \tag{6.2}$$

where V and W can be considered to be the neuron's membrane potential and recovery variable, respectively. I is the external current which contains inputs from the local and long-rang connectivity. For this application, we are using the parameters from [135], so $a = -0.5$, $b = -10$, $c = 0$, $d = 0.2$, $e = 3$, $f = 1$, $g = 0$, $I = 0$, $\alpha = 1$, $\beta = 1$, $\gamma = 1$, $\tau = 1$.

6.1.2   Binaural Beat Stimulus

Based on previous literature [75, 136, 137], the neural response to the binaural beat input, as shown in Figure 6.2a, is completely dependent on the interaural phase difference (IPD) produced. The period of the IPD, T_{IPD}, is determined by the amount of time required for the IPD to cycle through 360º, as shown in Figure 6.2b. The neurons in the inferior colliculus (IC), which is contained within the auditory pathway, are tuned so that the firing rate spikes for approximately half the IPD cycle, as shown in Figure 6.2c. The overall phase difference information is preserved from the IC to the primary auditory cortex (A1) by the periodic neural firing at the binaural beat frequency. TVB does not include the brainstem so we need to bypass the auditory pathway and stimulate the model directly at the cortex level at A1. The input to the TVB, as shown in Figure 6.2d, is based on the temporal Gaussian bump (TGB). The TGB is an approximation of the graded action potential input
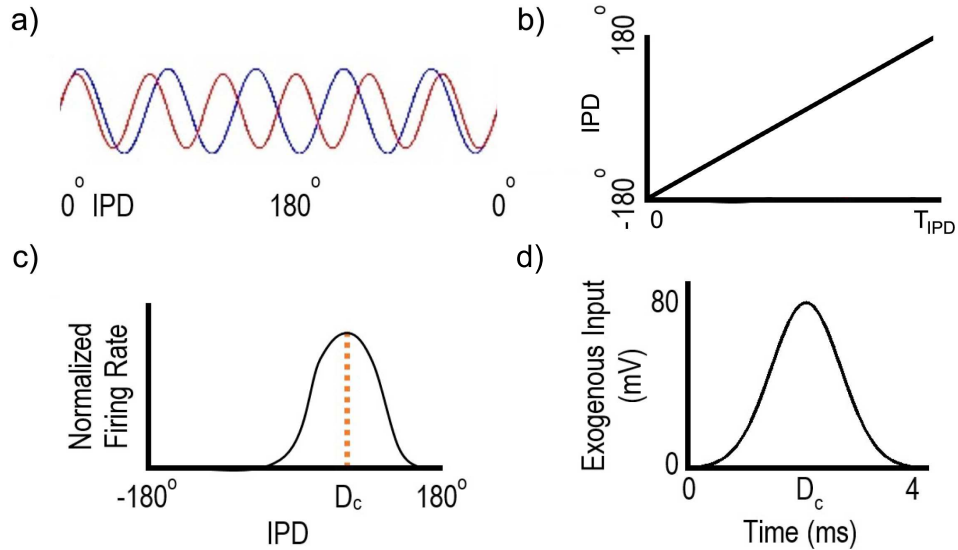
Figure 6.2: a) Two sin wave inputs for a binaural beat period T_{IPD}. b) The IPD per T_{IPD}. c) The IC normalized firing rate per T_{IPD}. d) The exogenous TGB input for every T_{IPD}.

that is received by A1 from the IC neurons. The TGB is centered on the maximal firing rate, D_C, and is 4ms long. For more information on the TGB, please refer to [138]. Within the TVB framework, we can approximate the TGB with a pulse. Therefore, we mimic binaural beats using the same pulse train, with the specific binaural beat period, at the left and right A1 nodes. From the simulated EEG results, we can compute the connectivity networks to analyze the differences due to the changing frequency. The simulated EEG channels are shown in Appendix C in Table C.1.

6.1.3   Connectivity Network Construction

In order to see changes in the networks in the different frequency bands, the simulated EEG data is filtered into the theta (4Hz − 8Hz), alpha (8Hz − 12Hz), beta (12Hz − 25Hz), and gamma (25Hz − 40Hz) bands. The time-frequency measure between channels is computed using the filtered EEG signals. The graphical networks are comprised of nodes (the channels) and the edge weights (Phase Locking Value) defined in section 2.1.3. The graph-

ical network is constructed using the electrode channels as the nodes ($\mathcal{V} = \{1, ..., n\}$), where $n = 60$, and the PLV connection strength defines the edge set ($E = \{(i, j) : \exists$ an edge from node i to node$j\}$). The network can be defined as a weighted adjacency matrix, W, made up of elements $\omega_{ij} = \text{PLV}_{ij}$ with the property that $0 \leq \omega_{ij} \leq 1$ for $i, j = 1, ..., n$. An edge of weight ω_{ij} exists between nodes i and j when $\omega_{ij} \neq 0$, and doesn't otherwise. The network is undirected and weighted, so W is symmetric.

6.1.4 TVB Model Parameters

The frequency response of the TVB under both open-loop and closed-loop control are evaluated and compared. The closed-loop simulation environment implemented around TVB is developed in Matlab. The platform could have a wide range of applications and can be used to test different controller types and feedback signals.

TVB is highly customizable and can be fit to different simulation requirements. For an in-depth explanation of the mathematical description and and implementation of TVB, please refer to [134, 135]. We have chosen the use the model configuration as shown in Table 6.1. TVB is able to simulate 60 channels of EEG. The location of the stimulus is at left and right primary auditory cortex (A1) nodes. One of the TVB stochastic integrators is used to compute dynamics and introduce noise (a scaled derivative of a Wiener process). The seed of the noise can be defined *a priori*.

6.2 Open-Loop Simulations

In order to characterize the response of the model to different stimuli, a random sweep of the binaural beat frequency input, between 4Hz and 40Hz, is simulated. The binaural beat

Model Components	Name	Parameters
Coupling	Linear	Default
Connectivity	76 nodes	Default
Neural Mass Model	2D Generic oscillator	[135]
Integrator	Heun Stochastic	dt $= 2^{-4}$ sec
Noise	Additive	Scaling = 5e-4
Monitor	EEG	Fs = 1024Hz
Stimulus	Pulse Train	BB frequencies

Table 6.1: Model Configuration

frequency changed after 8 seconds. The EEG data is filtered using a IIR filter with two bands at theta (4Hz – 8Hz) and gamma (25Hz – 40Hz). These bands are chosen because previous studies have shown that to successfully remember information during a working memory task, increased phase synchronization in the theta and gamma bands is needed [22, 53, 54]. The PLV network is computed using the filtered EEG data. The Frontal (F) – Parietal (P) PLV connection strength is computed by averaging all the connections between the frontal and parietal electrodes. Six simulations are run, using a different seed for the noise, to compute a mean and standard deviation for each frequency.

6.3   Closed-Loop Simulation Platform

The testing platform can be used to test various controllers such as linear (PID, LQR, etc) and nonlinear (extremum seeking control [139] , predictor-based adaptive output feedback control [140], etc). For this application, a proportional-integral (PI) controller and an adaptive augmented PI controller are implemented to control the network strength between the frontal and parietal electrodes. The following algorithm, which is shown in Figure 6.3, describes the general process used to implement TVB within a closed-loop controller. Pulse trains of different frequencies can be applied to any node within TVB.

```
Define model

Define initial stimulus frequency

for i = 1:N for N simulation steps

    Run simulation for Ts seconds

    Compute feedback signal

    Update feedback to the controller

    Update stimulus frequency

end
```

The same network analysis procedure described in the previous section is used. For each stim-
ulation step, the EEG data is filtered, then the F-P PLV connection strength is computed.
We currently have implemented the closed-loop framework in both Matlab and Simulink.
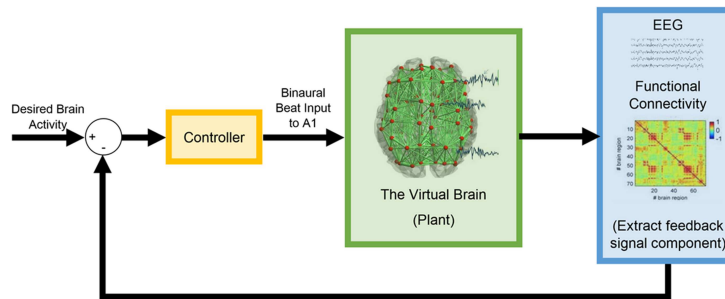
Figure 6.3: Closed-loop simulation platform for controller testing

6.4 Proportional-Integral (PI) Controller

For each of the results shown in this analysis, the simulations are run for 8 seconds. The
simulation time is chosen because the transient response of changing from one binaural beat
stimulus frequency to another ends after approximately 3 seconds. Therefore, the networks

are computed on the steady state response during the last 4 seconds of data. To show that it is possible to regulate the F-P PLV connection strength, a PI controller is implemented within the developed closed-loop simulation environment. The controller output BB_j, at each simulation step, is defined as

$$BB_j = K_\mathrm{P}e_j + K_\mathrm{I}e_{I_j} + BB_0, \quad \text{for} \quad j = 1, 2, ..., N. \tag{6.3}$$

where BB_0 is the starting binaural beat frequency, at $t = 0$. K_P is the proportional gain and K_I is the integral gain. The error e_j is the difference between the desired F-P PLV connection strength and is the current F-P PLV connection strength. The integral of the error, e_{I_j}, is defined as $e_{\mathrm{I}_j} = \sum_{k=1}^{j} e_k$. The K_P and K_I gains are tuned using an iterative process to balance the settling time and overshoot for a variety of starting frequencies. The final gains chosen are $K_\mathrm{P} = 0.1$ and $K_\mathrm{I} = 1.8$. The controllers ability to track a desired F-P PLV connection strength value is tested in a number of simulations. The tracking error of is evaluated at four initial frequencies (BB_0): 5Hz, 13Hz, 22Hz, 30Hz.

6.5   Adaptive Augmented PI Controller

A summary of the adaptive augmented PI controller developed by [141] is detailed in this section. Using this control strategy allows for the classical PI controller to provide the linear contribution which is augmented by adding an adaptive control effort. The adaptive gains, current state of the system, desired trajectory, and a set of structures functions of the state all affect the adaptive control effort. A first-order model is used to describe the behavior of the connectivity in the brain. The system is given by

$$\dot{x}(t) = ax(t) + b\lambda^*(u(t) + W^{*\mathrm{T}}\phi(x(t)), \tag{6.4}$$

where $a \in \mathbb{R}$ is a known state constant, $b \in \mathbb{R}$ is a known input constant, $\lambda^* > 0$ is a constant of known sign but unknown magnitude, $u(t) \in \mathbb{R}$ is the control effort, $W^* \in \mathbb{R}^p$ is an unknown constant vector where $p > 0$ is the number of linear and nonlinear functions contained in $\phi(x(t))$ No loss in generality occurs when assuming the state constant a is known as a vector of basis functions $\phi(x(t))$ will also contain the linear functions $x(t)$, which provides and overall uncertainty on the linear coefficient of the dynamics of the system.

The PI controller relies on the integration of the error between the desired and current state. Therefore, another state is introduced, $x_{\mathrm{I}}(t) \triangleq \int_0^t (x(\tau) - x_{\mathrm{d}}(\tau))d\tau$ where x_d is the desired trajectory. The new model of the system, which includes the integral state, is described as

$$\dot{x}_{\mathrm{a}}(t) \triangleq \begin{bmatrix} a & 0 \\ 1 & 0 \end{bmatrix} x_{\mathrm{a}}(t) + \begin{bmatrix} b \\ 0 \end{bmatrix} \lambda^* (u(t) + W^{*\mathrm{T}}\phi(x(t)) + \begin{bmatrix} 0 \\ -1 \end{bmatrix} x_{\mathrm{d}}(t), \tag{6.5}$$

where $x_{\mathrm{a}}(t) \triangleq [x(t) \ x_{\mathrm{I}}(t)]^{\mathrm{T}}$. In order to use the adaptive control algorithm, a reference system must be defined. We chose to use the known dynamics of Equation 6.5 which can be written as

$$\dot{x}_{\mathrm{lin}}(t) \triangleq \begin{bmatrix} a & 0 \\ 1 & 0 \end{bmatrix} x_{\mathrm{lin}}(t) + \begin{bmatrix} b \\ 0 \end{bmatrix} u_{\mathrm{lin}}(t) + \begin{bmatrix} 0 \\ -1 \end{bmatrix} x_{\mathrm{d}}(t). \tag{6.6}$$

where $x_{\mathrm{lin}}(t) \triangleq [x_{\mathrm{l}}(t) \ x_{\mathrm{l_I}}(t)]^{\mathrm{T}}$. The PI controller chosen to guarantee that Equation 6.6 tracks the desired trajectory is defined by

$$u_{\mathrm{lin}}(t) \triangleq -K^{*\mathrm{T}} (x_{\mathrm{lin}}(t) - r(t)), \tag{6.7}$$

where $K^* \triangleq [K_{\mathrm{P}} \ K_{\mathrm{I}}]^{\mathrm{T}}$ and $r(t) = [x_{\mathrm{d}}(t) \ 0]^{\mathrm{T}}$. Substituting equation 6.7 into 6.6 results in the following closed-loop linear system, which is chosen as the reference system for the adaptive

controller design,

$$\dot{x}_{\text{lin}}(t) = A_{\text{r}}x_{\text{lin}}(t) + \begin{bmatrix} bK_{\text{P}} \\ -1 \end{bmatrix} x_{\text{d}}(t), \tag{6.8}$$

where A_{r} is defined as

$$A_{\text{r}} \triangleq \left(\begin{bmatrix} a & 0 \\ 1 & 0 \end{bmatrix} - \begin{bmatrix} b \\ 0 \end{bmatrix} K^{*\text{T}} \right). \tag{6.9}$$

To guarantee that the augmented system Equation 6.5 converges to the reference system Equation 6.8, a tracking error is given by

$$e_{\text{a}}(t) \triangleq x_{\text{a}}(t) - x_{\text{lin}}(t), \tag{6.10}$$

The total control effort applied to the system, $u(t)$ is the combination of the linear and adaptive part and is described as

$$u(t) \triangleq u_{\text{lin}}(t) + u_{\text{ad}}(t). \tag{6.11}$$

$u_{\text{ad}}(t)$ is designed by analyzing the error dynamics [141]. The resulting adaptation laws are defined as

$$\dot{\hat{K}}(t) = \text{sign}(\lambda^*)\Gamma_K \left(x_{\text{a}}(t) - r(t) \right) e_{\text{a}}^{\text{T}}(t) P \begin{bmatrix} b \\ 0 \end{bmatrix}, \tag{6.12}$$

$$\dot{\hat{W}}(t) = \text{sign}(\lambda^*)\Gamma_W \phi(x(t)) e_{\text{a}}^{\text{T}}(t) P \begin{bmatrix} b \\ 0 \end{bmatrix}. \tag{6.13}$$

where $\hat{K}(t) \triangleq [\hat{K}_1(t) \ \hat{K}_2(t)]^{\text{T}}$ and the adaptation gains are $\Gamma_K > 0$ and $\Gamma_W > 0$. The adaptive control law implemented into the closed-loop system is given by

$$u_{\text{ad}}(t) \triangleq -\hat{W}^{\text{T}}(t)\phi(x(t)) - \hat{K}^{\text{T}}(t) \left(x_{\text{a}}(t) - r(t) \right), \tag{6.14}$$

is Lyapunov stable and the tracking error $e_a(t)$ converges to zero.

6.6 Adaptive Augmented Controller Implementation

6.6.1 Integration

The standard forward Euler method for numerical integration is not capable of accounting for the large time steps. Therefore, the backwards, or implicit, Euler method is implemented for this system. If we define a differential equation $\frac{dy}{dt} = f(t, y)$ where f is the function with an initial value $y(t_0) = y_0$. Applying a numerical integration method produces a sequence $y_0, y_1, y_2, ...$ such that y_k approximates $y(t_0 + kh)$, where h is the step size. The backward Euler method algorithm computes the approximation of the function using

$$y_{k+1} = y_k + hf(t_{k+1}, y_{k+1}). \tag{6.15}$$

For this implementation, the integral of $\dot{x}_I(t)$, $\dot{x}_{lin}(t)$, $\dot{\hat{K}}(t)$, and $\dot{\hat{W}}(t)$ are computed using the backward Euler integration method.

6.6.2 Selection of Controller Parameters

The parameters of the linear reference system are $a = 0.1$, $b = 0.1$ and $\lambda^* = 1$, where a and b are determined using PI controller results from TVB. The gains for the linear controller were originally chosen so that $K_P = 1$ is an order of magnitude larger than $K_I = 0.1$. After an iterative tuning process to balance the settling time and overshoot for a variety of starting frequencies, the adaptive gains Γ_W and Γ_K are set to 0.002. In order to compare to the results of the PI controller, the desired trajectory, $x_d(t)$ is equal to 0.9.

6.7   Results

6.7.1   Open-Loop Control Results

The results of the open-loop controlled simulations are used to understand frequency response of the model and to help inform the controller choice for the closed-loop control implementation. Figure 6.4 shows the response of the F-P PLV connection strength of the TVB model as a function of input binaural beat frequency. Several maxima occur in the F-P PLV connection strength at approximately 8Hz, 15Hz, and 25Hz and ranges between 0.85 and 0.98, which indicates the EEG signals are highly synchronized.
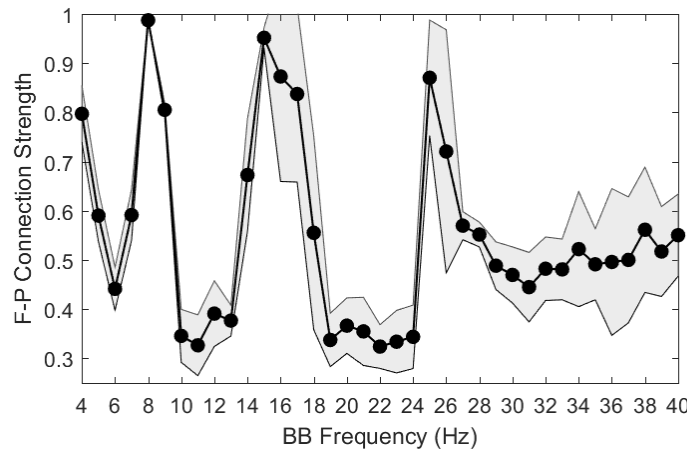
Figure 6.4: The average and standard deviation of the frontal-parietal PLV connection strength values as a function of the binaural beat frequency

6.7.2   PI Controller Results

A PI controller is successfully implemented and tested within the developed closed-loop simulation environment. The PI controller is able to drive the F-P PLV connection strength to the desired value of 0.9. The desired value is arbitrarily chosen to represent the approximate

maximum responses of the system. However, due to the multiple maxima in the response shown in Figure 6.4, the controller drives the binaural beat frequency to different values depending on the initial starting frequency value. Figure 6.5 shows the mean and standard deviation, over five simulations, of the controller starting from four different initial frequencies. The results for $BB_0 = 5$, $BB_0 = 13$, $BB_0 = 22$, and $BB_0 = 30$ are shown in red, blue, green, and gray, respectively. The controller is able to successfully drive the tracking error to approximately zero for the first three starting conditions. However, the fourth starting frequency, $BB_0 = 30$, is unable to converge because the PI controller is unable to detect the maximum value which is at a frequency less than the initial starting frequency. Since the initial error and the gains are positive, then the PI controller will start searching higher so it will not converge.

6.7.3   Adaptive Augmented PI Controller Results

The Adaptive Augmented PI controller is able to drive the F-P PLV connection strength to the desired value of 0.9. Similar to the results of the PI controller in Figure 6.5, the controller drives the binaural beat frequency to different values. Figure 6.6 shows the simulation results for four different initial binaural beat frequencies. The results for $BB_0 = 6$, $BB_0 = 13$, $BB_0 = 22$, and $BB_0 = 30$ are shown in blue, yellow, green, and purple, respectively. Two simulations are run for each initial frequency. The controller is able to successfully drive the tracking error to approximately zero for all the starting conditions. Figure 6.7 shows how the adaptive laws evolve over time.
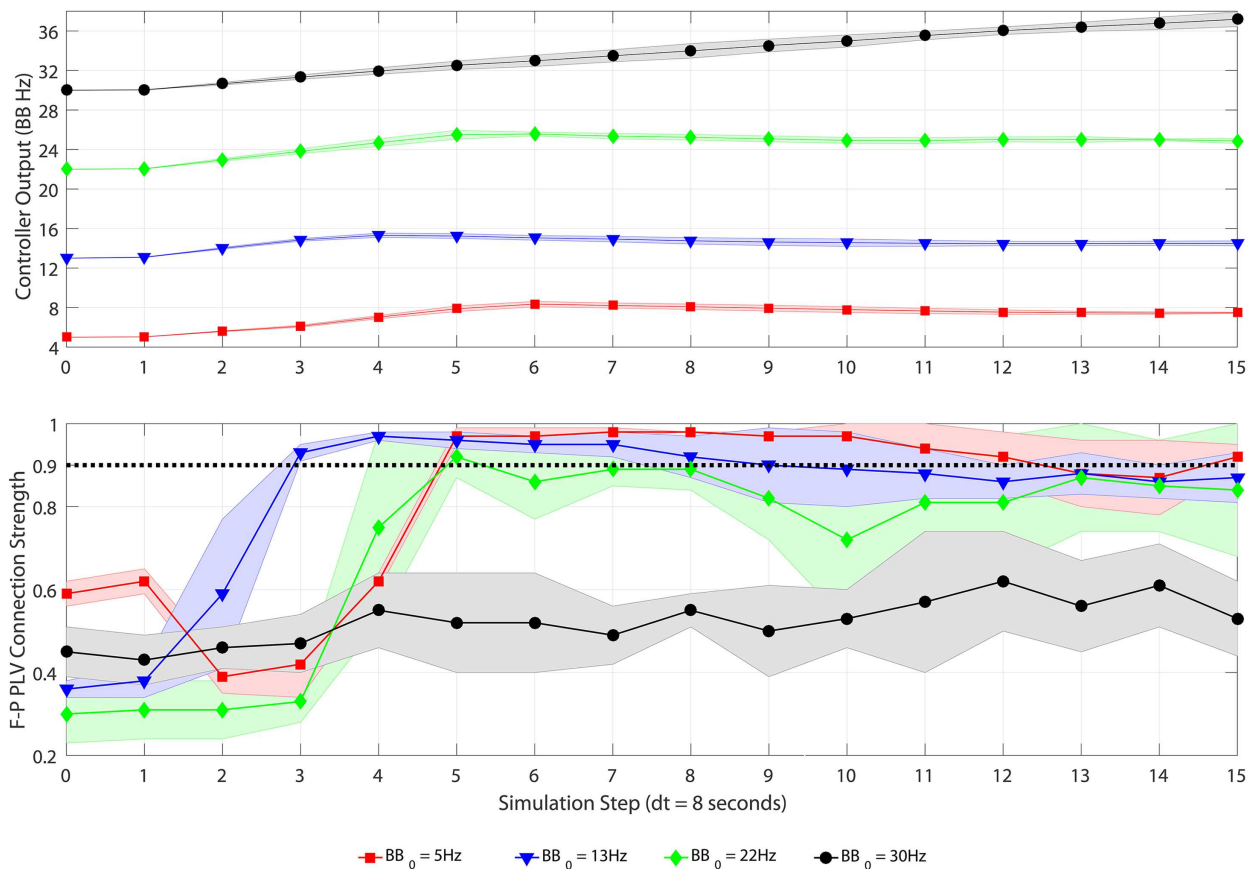
Figure 6.5: The binaural beat output of the PI controller and the resulting F-P PLV connection strength values for four starting frequencies : $BB_0 = 5$ (red), $BB_0 = 13$ (blue), $BB_0 = 22$ (green), and $BB_0 = 30$ (gray). The shaded areas are one standard deviation.

6.8 Discussion

A controller can change the binaural beat frequency to modify the strengths of the connectivity network. The closed-loop simulation environment is developed to be customizable to fit a range of applications. The stimulus input and feedback signal can be modified depending on the chosen controller.

The implemented PI controller is an example of how well a linear controller is able to drive a response of the model to a certain desired value. However, the PI controller is not able to necessarily find the closest maximum value. For example, if the initial starting frequency is
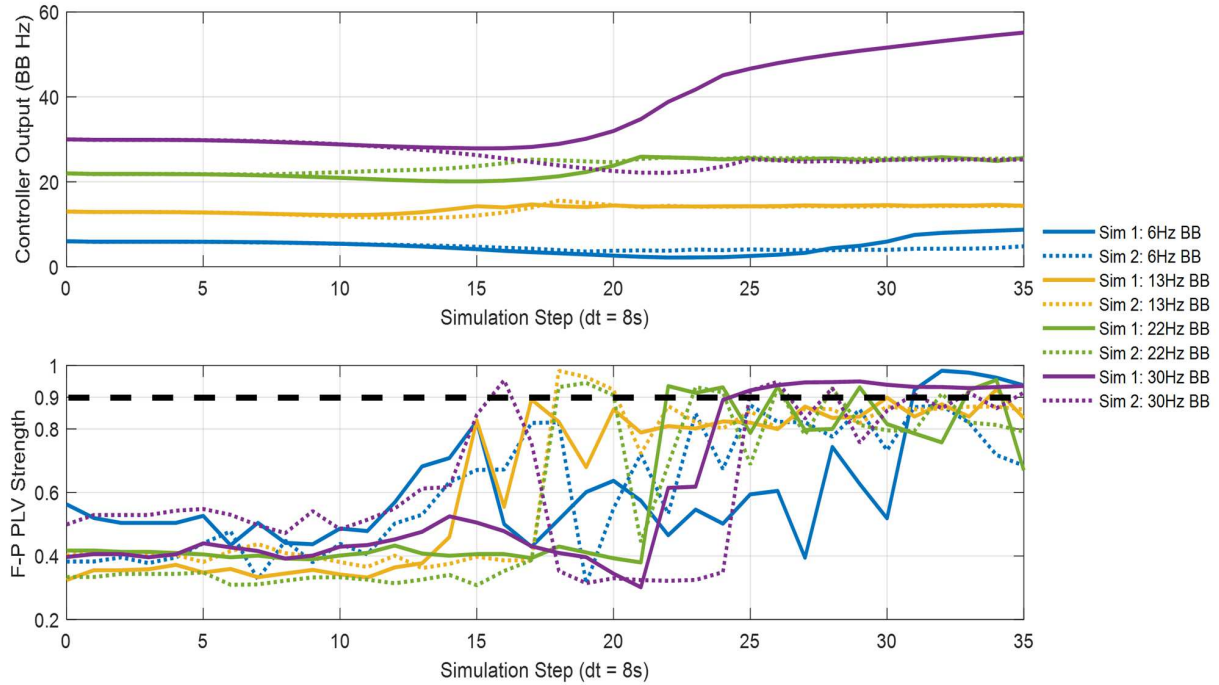
Figure 6.6: The binaural beat frequency output of the Augmented Adaptive PI controller and the resulting F-P PLV connection strength values for four starting frequencies: $BB_0 = 6$ (blue), $BB_0 = 13$ (yellow), $BB_0 = 22$ (green), and $BB_0 = 30$ (purple).
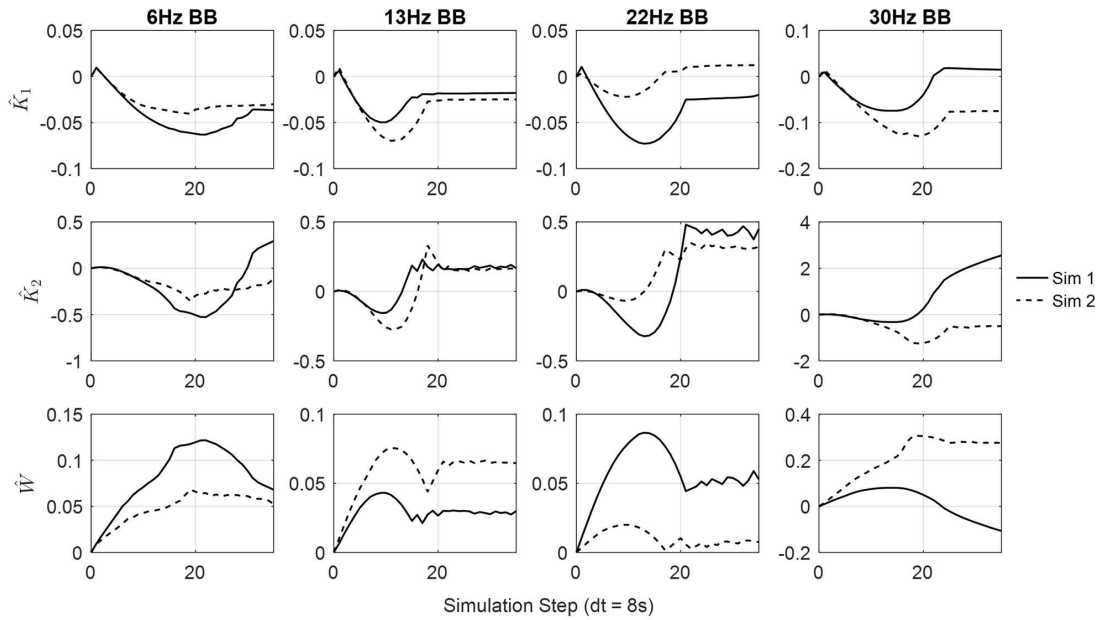
Figure 6.7: The adaptive laws for each of the simulations.

18Hz, then, according to Figure 6.4, the closest maximum would be around 15Hz. However, with a PI controller, it would drive the frequency to approximately 25Hz, since it primarily pushes upward.

The adaptive augmented PI controller is also able to drive the frontal-parietal PLV values to the desired connection strength. A major advantage over the simple PI controller is that the adaptive augmented PI controller is able to find the desired F-P PLV value below the initial starting frequency.

In conclusion, a both a simple PI controller and an adaptive augmented PI controller are able to drive the binaural beat frequency to produce a higher frontal-parietal connection in TVB. Using non-invasive stimulation within a closed-loop controller is a new and emerging field within neuroscience. Our developed closed-loop simulation environment is a valuable tool because it has the ability to test various controllers and allows for major parameter tuning outside of a clinical setting. It is both a cheaper and safer option for initial controller testing, since it does not require a human participant. Closed-loop non-invasive brain stimulation, including binaural beats, can modulate depending on the brain-state of the user, which can change over shorter and longer time scales. For example, cognitive abilities of persons with MCI change over time so an open-loop stimulation protocol might be ineffective a couple hours or six months later. Therefore, a closed-loop stimulation protocol is the best option for a therapeutic system.

Chapter 7

Closed-Loop Binaural Stimulation Results

The objective of this chapter is to show that there exists a controller that changes the synchronization between the frontal and parietal regions of the brain. We focused on finding an effective control strategy, laying the foundation for future research on control optimization.

The overall purpose of this system, shown in Figure 7.1, is to augment the user's working memory capacity using binaural beat stimulation. First, the EEG data is collected and processed in real-time. Then, the behavioral data and the EEG data is used to evaluate the working memory state of the user and the frontal-parietal PLV connection strength is fed to the controller. The control action is fed to the binaural beat generator whose output is played to the user through stereo headphones.
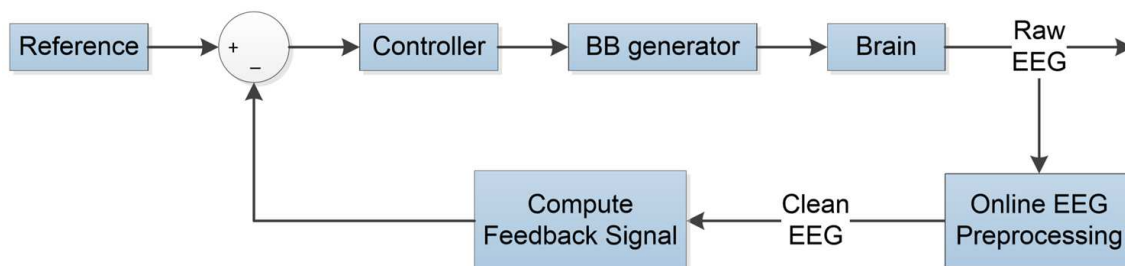
Figure 7.1: An overview of the EEG=based closed-loop controller developed for the experiment.

7.1   Experimental Paradigm

In total, 30 people are recruited to participate in this study. The first 14 participants (23.8 ± 4.6, 8 male) are used to tune the controller. The last 16 people were tested after the controller parameters are set (25.7 ± 3.6, 7 male). Written consent is obtained from each participant after being introduced to the experimental protocols, which are approved by the Virginia Tech Institutional Review Board. All of the experiments are performed in accordance with guidelines and regulations set forth by the Virginia Tech Institutional Review Board. Each participant, before starting the task, is tested to ensure that they have no vision or hearing problems. None of the participants disclosed any previous neurological or hearing problems when asked.

The working memory task that the participants completed during the test is the same delayed match-to-sample visuospatial working memory task described in Chapter 3. Additionally, the load, or number of color blocks, is titrated to each person individually (for details see section 3.1.4).

After the load is selected, the EEG is set up. OneStep Cleargel (H + H Medizinprodukte GbR Munster, Germany) is injected into each hole in the cap, which contains the electrode, using a blunt needle syringe. The skin under the left eye is cleaned using the Nuprep skin prep gel (Weaver and Co. Aurora, CO, USA). The EOG channel is placed under the left eye using OneStep Adhesive Conductive Paste (H + H Medizinprodukte GbR Munster, Germany) and a bandaid to keep it in place. The EEG electrodes are verified to be less than < 20 kΩ prior to data collection. The testing took place in a quiet, dimly lit room. For three participants, the impedance of the EEG electrodes is much greater than < 20 kΩ so they are not included in the final analysis.

After the EEG setup is complete, the initial step is to connect the DAQ to the OpenViBE

software [142] which is used to record and process the EEG data. Next, we record a minute of EEG data where the participant is blinking approximately every second. The recorded EEG file is used to calibrate the de-noising block in OpenViBE, which is used to remove the eye blink artifacts [143]. Next, the volume of the binaural beats is adjusted by the participants to their comfort level.

Finally, the experiment begins and the participant performs the visuospatial working memory task for a total of 20 minutes at their previously determined titrated load. For the initial 4 minutes no sound is played and this time acts as a baseline control. Then, for the remaining 16 minutes, the adaptive augmented PI controller modifies the binaural beat frequency that the participant listens to.

7.2 Experimental System

For this application, a eego sports system (ANT Neuro, Philadelphia, PA USA) is used. The system has the capability of recording EEG data at a sampling frequency of up to 2kHz. The cap has 63 EEG electrodes and an EOG channel to record eye blinks. The layout of the channels and the order of the recordings are shown in Appendix D in Figures D.1 and D.2. The default reference channel is CPz which is used for this application.

7.2.1 EEG Processing

In OpenViBE, the sampling rate of the EEG is set to 512Hz. In addition, OpenViBE processed the EEG data using the following steps.

1. The EEG is downsampled to 128Hz.

2. An initial 4th order Butterworth bandpass filter between 1Hz and 40Hz is applied to the data to remove drift and powerline noise.

3. The eye blink artifacts are minimized using the EOG denoising block [143]. To use the EOG denoising box, first, the denoising matrix is calibrated off-line using the file where the participant blinks a lot. The fundamental principle of the algorithm to estimate the matrix, d is based on regression analysis where $d =< U^{\text{T}}U >^{-1}< U^{\text{T}}S >$ with U being the noise (EOG electrode) and S the source (EEG electrodes) [143]. The EEG signals can be processed, on-line, using the EOG denoising block which computes the clean EEG as $S_{\text{processed}} = S - bU$.

4. The processed signals are re-referenced to a common average.

5. The frontal and parietal EEG channels are selected for further processing in order to reduce the computational load.

6. An additional 4th order Butterworth bandpass filter between 4Hz and 8Hz is applied to the data to focus on the theta band.

7. The clean EEG signals are epoched using a sliding window of 20 seconds that shifts every one second.

8. The Matlab scripting block calls a script which uses the processed epoched data to first compute the bipartite network using PLV as the edge weights. A total of 50 connections are computed. For each epoch, $x(t)$ is equal to the average of all the PLV edge weights. Second, the integration of the adaptive augmented PI controller is computed. The states, adaptive laws, and the desired trajectory are updated to compute the controller effort. Finally, based on the current control action, tones are generated and played to the participant to produce the binaural beats.
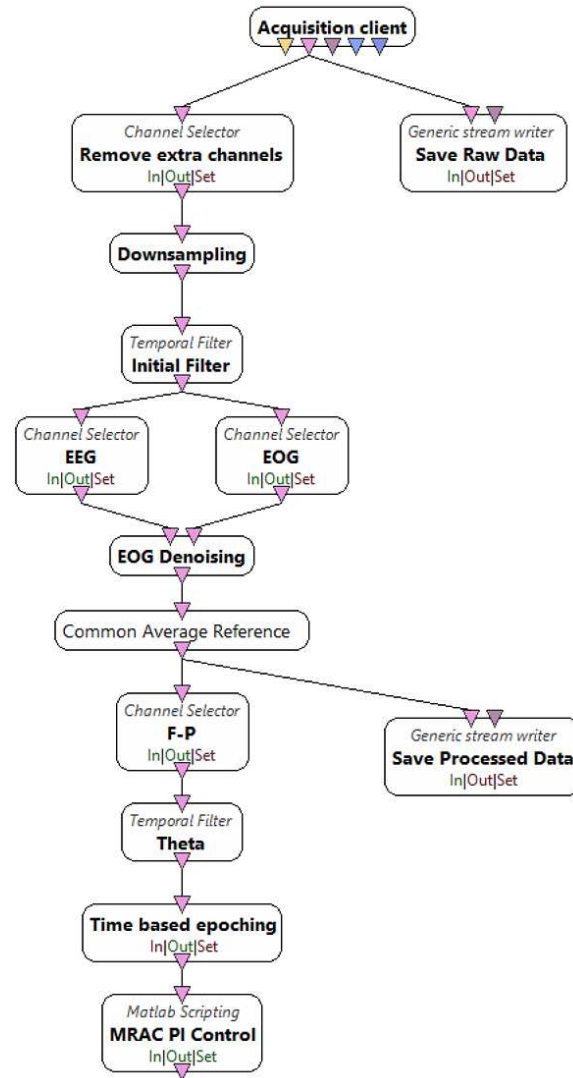
Figure 7.2: A screen shot of the OpenViBE block diagram used to process the data and call the Matlab script.

7.2.2   Auditory Stimulation

The tones that the participant listens to during the experiment are generated in Matlab. The tone played into the right ear is always 240Hz. Depending on the output of the controller, the tone played into the left ear is the sum of 240Hz and $u(t)$. The tones are presented to the participants using stereo headphones (QuietComfort 35 (Series II), Bose). The sounds are

kept constant for 20 seconds in order to allow the brain connectivity to modulate. In order that the changing tones do not overlap, the sound is ramped up and down over 1 second in the beginning and end of the 20 seconds, respectively.

7.3 Implementation

The implementation of the controller for the experimental system is more complicated than is described in section 6.6. The numerical integration algorithm is still the backwards Euler method since it is stable at large time steps. However, one major difference is that the controller effort must remain constant for 20 seconds in order for the brain to adapt. Therefore, a zero-order hold is applied to the controller effort which leads to the development of the reference trajectory, $r(t)$. After initial implementation during the tuning phase, additional filters were added to the adaptive laws and the controller output.

7.3.1 Filtering the Adaptive Laws

Due to the noise in the system, adaptation laws previously defined in Equations 6.12 and 6.13 are modified to be

$$\dot{\hat{K}}(t) = \text{sign}(\lambda^*)\Gamma_K \left(x_\text{a}(t) - r(t)\right) e_\text{a}^\text{T}(t) P \begin{bmatrix} b \\ 0 \end{bmatrix} - \alpha \hat{K}(t), \tag{7.1}$$

$$\dot{\hat{W}}(t) = \text{sign}(\lambda^*)\Gamma_W \phi(x(t)) e_\text{a}^\text{T}(t) P \begin{bmatrix} b \\ 0 \end{bmatrix} - \alpha \hat{W}(t), \tag{7.2}$$

where $\alpha = 0.1$ acts as a low pass filter. The parameter α was tuned by first setting the value to 0.5 and slowly decreasing it over the initial 14 participants.

7.3.2 Approximations Using the Backwards Euler Algorithm

The approximations of the linear reference system using the backwards Euler algorithm is easily found to be

$$
x_{\text{lin}}(t+1) = \begin{bmatrix} 1 - h(a - bK_{\text{P}}) & hbK_{\text{I}} \\ -h & 1 \end{bmatrix}^{-1} \left(x_{\text{lin}}(t) + h \begin{bmatrix} bK_{\text{P}} \\ -1 \end{bmatrix} x_{\text{d}}(t+1) \right). \tag{7.3}
$$

Additionally, the approximations of the adaptive laws are described as

$$
\hat{K}(t+1) = \frac{\hat{K}(t) + h \left(\text{sign}(\lambda^*)\Gamma_K \left(x_{\text{a}}(t+1) - x_{\text{d}}(t+1) \right) e_{\text{a}}(t+1)^{\text{T}}(t) P \begin{bmatrix} b \\ 0 \end{bmatrix} \right)}{1 + h\alpha}, \tag{7.4}
$$

$$
\hat{W}(t+1) = \frac{\hat{W}(t) + h \left(\text{sign}(\lambda^*)\Gamma_W \phi(x(t+1)) e_{\text{a}}(t+1)^{\text{T}}(t) P \begin{bmatrix} b \\ 0 \end{bmatrix} \right)}{1 + h\alpha}. \tag{7.5}
$$

7.3.3 Vector of Nonlinearities

Initially, the nonlinearities was simply $\phi(x(t)) = x(t)$. However, based on the results for the first 14 participants used during the tuning process showed very slow oscillations in the PLV connection strength. Therefore, the vector of nonlinearities used for the experiments is defined as $\phi(x(t)) = [x(t), \sin(0.005x(t)), \sin(0.01x(t)), \sin(0.02x(t)), \sin(0.03x(t))]$. The frequency of the sine waves are determined using a frequency analysis of $x(t)$. A potential reason behind the very slow oscillations is due to the timing of the task. Another viable reason is due to the long periodicity of the resting state networks which oscillate around 0.001Hz to 0.1Hz [144, 145, 146].

7.3.4   Selection of the Desired Trajectory

As stated previously, the first four minutes of the test are silent to act as a baseline mea-
surement. From this data, the mean and standard deviation of the frontal-parietal PLV
connection strength is determined from the last minute of baseline data. The desired trajec-
tory, $x_{\mathrm{d}}(t)$, which is the desired frontal-parietal (F-P) PLV connection strength, is computed
by adding two times the standard deviation to the mean value. Therefore, the adaptive
augmented PI controller will work to drive the PLV connection strength to be significantly
higher than the baseline values.

7.3.5   Zero-Order Hold on the Controller Effort

Since the controller input can only be changed every 20 seconds, we have implemented a
zero-order hold on the controller effort. In essence, when the controller is held constant, the
reference trajectory, $r(t)$, and the control output, $u(t)$ are switched.

Therefore, when $t = 20, 40, 60, ...$ seconds,

1. The reference trajectory is set to $r(t) = [x_{\mathrm{d}}(t)\ 0]^{\mathrm{T}}$, where $x_{\mathrm{d}}(t)$ is the previously defined
   desired trajectory.

2. A simple first order filter is applied to the controller and is computed as

$$u(t) = \beta\big(u_{\mathrm{lin}}(t) + u_{\mathrm{ad}}(t) + \mathrm{BB}_0\big) + (1 - \beta)u(t - 1) \qquad (7.6)$$

   where $\mathrm{BB}_0 = 13\mathrm{Hz}$ is the initial binaural beat frequency and $\beta = 0.95$. The parameter
   β was tuned by first setting the value to 0.5 and slowly increasing it over the initial 14
   participants.

3. The new $u(t)$ is set as u_{prev} to keep constant for the next 20 seconds.

4. The integral terms $x_{\text{I}}(t)$ and $x_{l_{\text{I}}}(t)$ are reset to zero.

For all other t,

1. $u(t)$ is set equal to u_{prev}

2. The reference trajectory is derived from the controller equation and is given by

$$r(t) = \begin{bmatrix} \frac{(u(t)-\text{BB}_0)+K^{*\text{T}}x_{\text{lin}}(t)+\hat{W}^{\text{T}}(t)\phi(x(t))+\hat{K}^{\text{T}}(t)x_{\text{a}}(t)}{K_{\text{P}}+\hat{K}_1(t)} \\ 0 \end{bmatrix} \tag{7.7}$$

3. Recompute $u_{\text{lin}}(t)$ and $u_{\text{ad}}(t)$ using the new $r(t)$ and states.

7.3.6   Selection of Controller Parameters

An iterative process is implemented to tune the parameters for the first 14 participants. Over all the participants, the parameters are increased until the response began to oscillate or grow unbounded and then the values are reduced. For K_{P} and K_{I} the initial values are 1 and 0.1 respectively. Only K_{P} is tuned and the final value is set $K_{\text{P}} = 1.7$. The adaptive gains Γ_W and Γ_K are initially set at 0.001 and increased to $\Gamma_W = 0.01$ and $\Gamma_K = 0.01$. The parameters of the reference system are still $a = 0.1$, $b = 0.1$ and $\lambda^* = 1$. The initial binaural beat frequency is arbitrarily selected to be 13Hz.

7.4   Statistical Analysis

To assess the effectiveness of the controller, the response $x(t)$ is divided into 48 twenty-second epochs corresponding to the time when the controller output is held constant. For each of the 48 epochs, a one-tailed t-test is used to determine if the controller driven F-P PLV connection strength response is significantly higher than the baseline PLV response. In order to be conservative, α is set to 0.001. An overall summary of the controller response, S, is computed by summing the number of significant epochs and dividing by the total number of epochs.

7.5   Results

Overall, the controller is able to modulate the frontal-parietal PLV connection strength. The results, for all of the participants, are shown in Table 7.1. All of the participants, except for one, showed some amount of increase in the frontal-parietal PLV connection strength when compared to baseline. The median $S = 47.9\%$ indicates that, over all the participants, nearly 48% of the time the controller has driven the frontal-parietal PLV connection strength significantly higher than baseline. However, large variability exists between participants since the standard deviation of S is 26.3%. In addition, the overall accuracy during the 20 minutes is listed. Accuracy is defined as the number of correct trials both matches (Hit) and non-matches (Correct Rejection) divided by the total number of trials. The median accuracy over all the participants is $80.3\% \pm 7.1\%$.

The following three results showcase the variability observed among participants. All of the responses are shown in Appendix D.

Table 7.1: Summary of Experiments

ID (Load)	S	Accuracy
1(3)	41.6%	80.3%
2(4)	12.5%	77.4%
3(4)	58.3%	82.4%
4(3)	47.9%	81.2%
5(5)	70.8%	70.8%
6(5)	20.8%	70.1%
7(4)	87.5%	73.4%
8(3)	72.9%	83.8%
9(5)	0%	92.4%
10(5)	25.0%	66.4%
11(5)	35.5%	88.4%
12(4)	70.8%	84.6%
13(4)	52.1%	73.6%

7.5.1   Case 1: Tracking the Reference and Achieving Steady State

The frontal-parietal PLV connection strength response to the controller for participant 8 is shown in Figure 7.3. In this case, the PLV response towards the end of the 20 minutes is oscillating around the desired reference value. In addition, the binaural beat frequency achieves steady state around 900 seconds. In addition, the person answered more accurately towards the end of the task once the F-P PLV connection strength is consistently higher. The adaptive law updates are shown in Figure 7.4. The values varied a lot over the 16 minutes but achieved an oscillatory steady state at the end.

7.5.2   Case 2: Achieving Steady State

The frontal-parietal PLV connection strength response to the controller for participant 1 is shown in Figure 7.5. In this case, at around 800 seconds, the PLV response is oscillating around a steady state value but is lower than the reference. Similar to Case 1, the participant

was more likely to answer correctly towards the end of the session when their PLV was significantly higher. The controller output also remains relatively constant around 18Hz after 600 seconds. The adaptive laws are shown in Figure 7.6 and remain relatively consistent 300 seconds after the controller started to modulate the binaural beats.

7.5.3   Case 3: Remained at Baseline

The frontal-parietal PLV connection strength response to the controller for participant 2 is shown in Figure 7.7. In this case, the PLV response very rarely moves from oscillating around the baseline, which is not the desired result. However, over time, the PLV connection strength did not decay below the baseline. Therefore, the controller is able to maintain the connection strength even if it is not improved. The controller output remains relatively constant around 20Hz after around 300 seconds. The adaptive laws are shown in Figure 7.8 and remain relatively consistent 100 seconds after the controller starts.
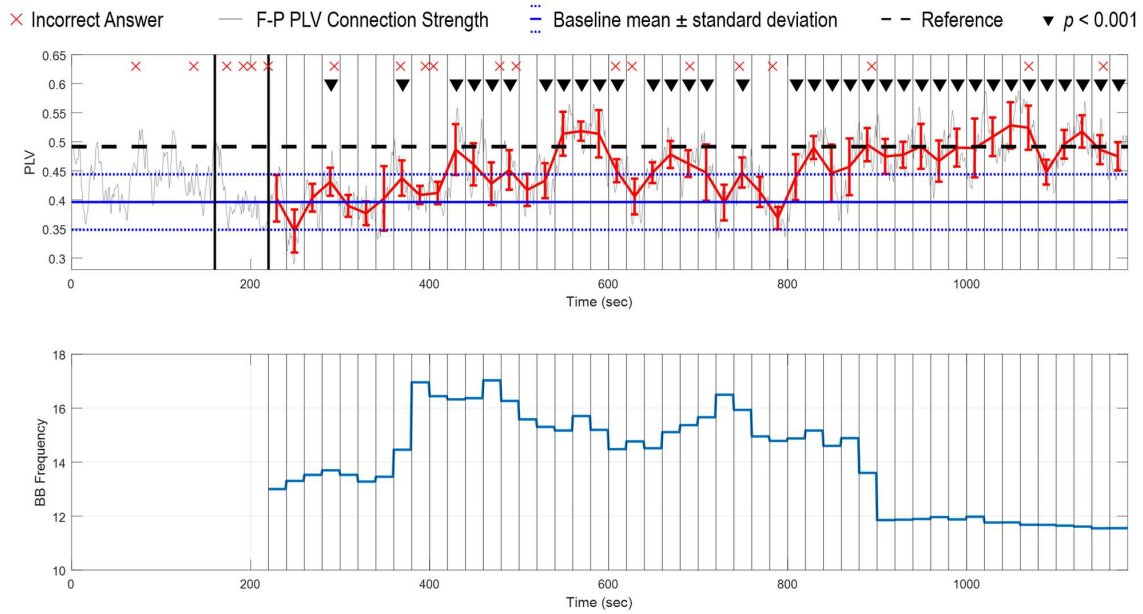
Figure 7.3: The F-P PLV connection strength as a function of time and the corresponding controller output for Participant 8. The mean and one standard deviation of the PLV, for each epoch, is shown by the error bars in red.
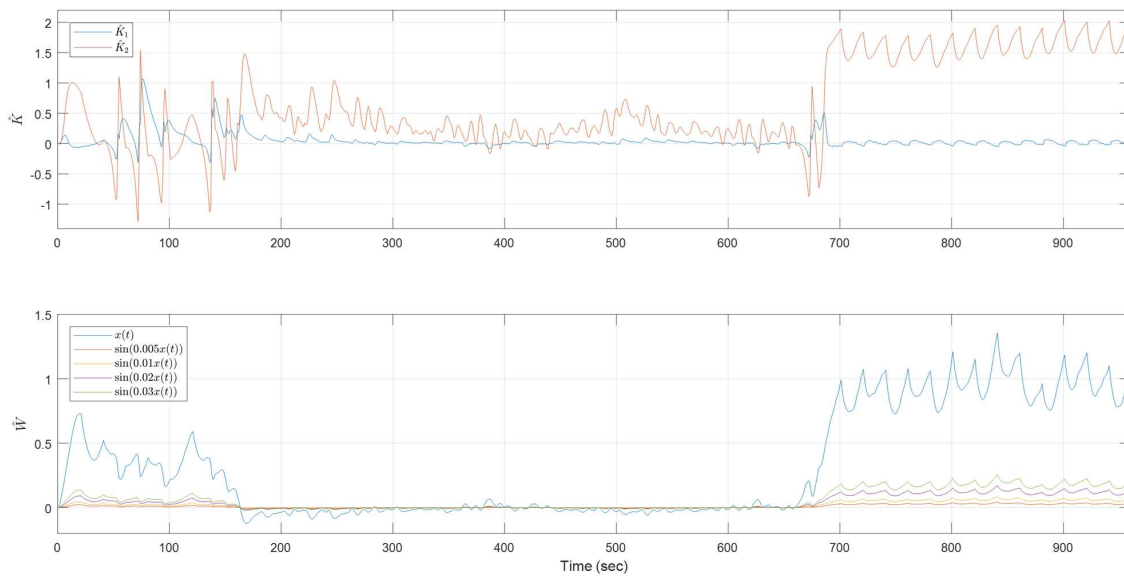
Figure 7.4: The adaptive laws for Participant 8. 0s indicates the start of the controller.
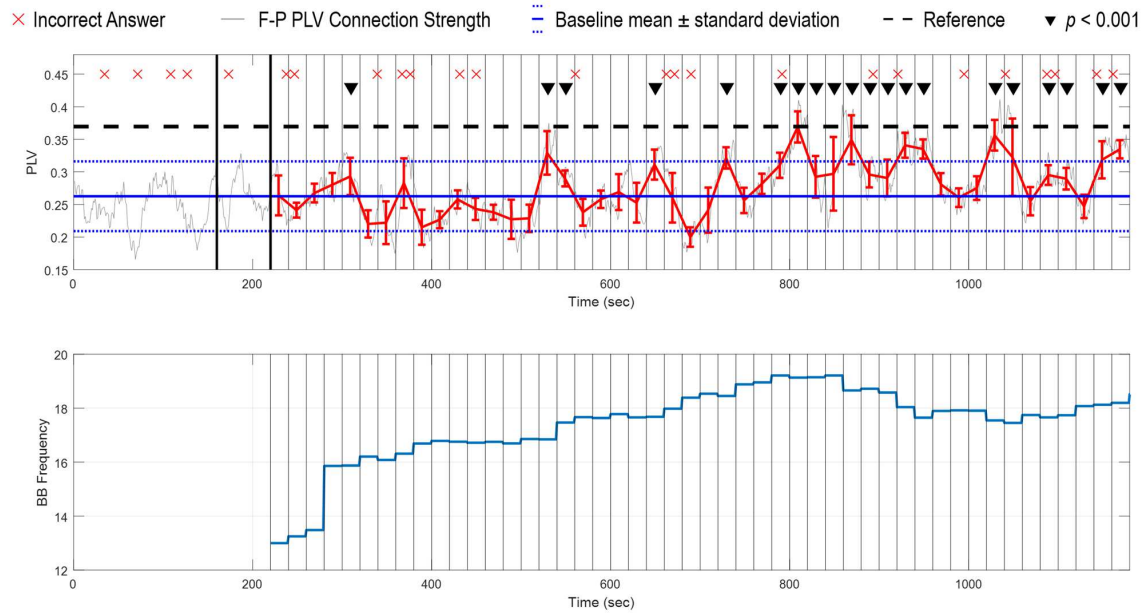
Figure 7.5: The frontal-parietal PLV connection strength as a function of time and the corresponding controller output for Participant 1. The mean and one standard deviation of the PLV, for each epoch, is shown by the error bars in red.
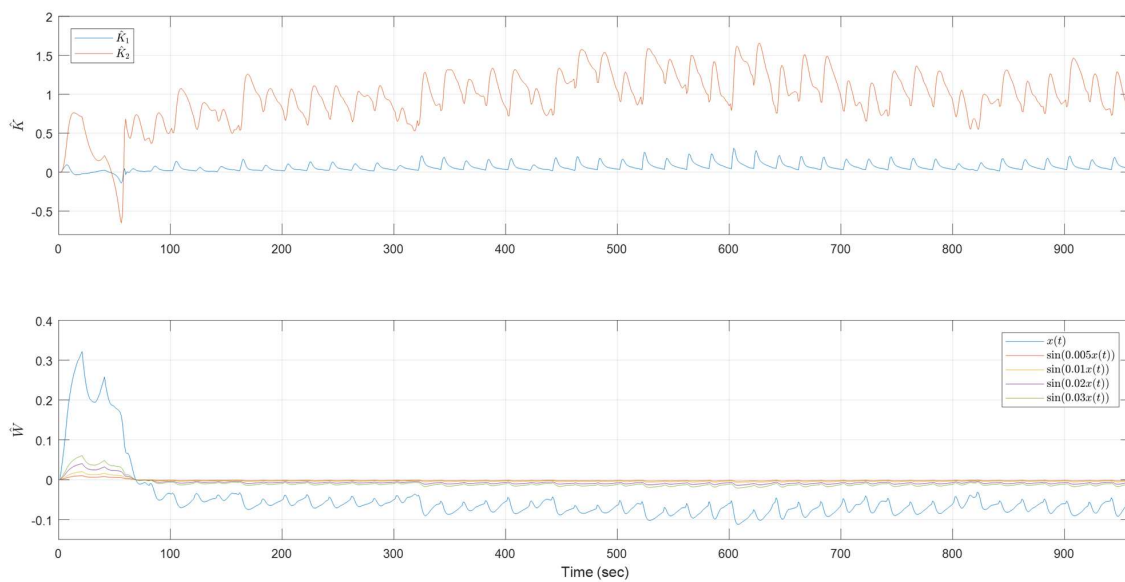
Figure 7.6: The adaptive laws for Participant 1. 0s indicates the start of the controller.
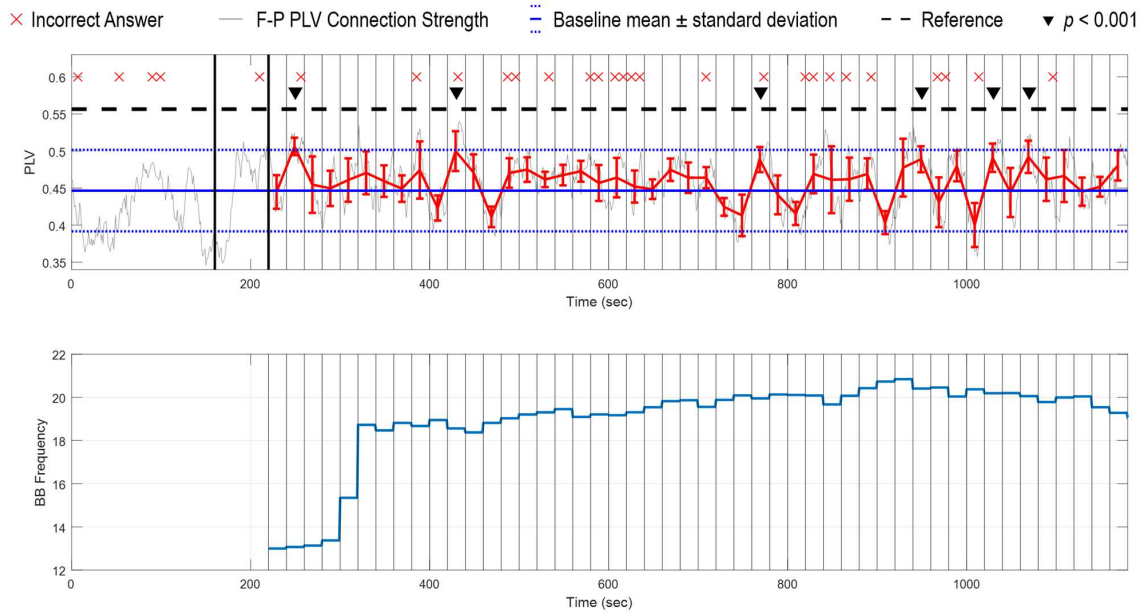
Figure 7.7: The frontal-parietal PLV connection strength as a function of time and the corresponding controller output for Participant 2. The mean and one standard deviation of the PLV, for each epoch, is shown by the error bars in red.
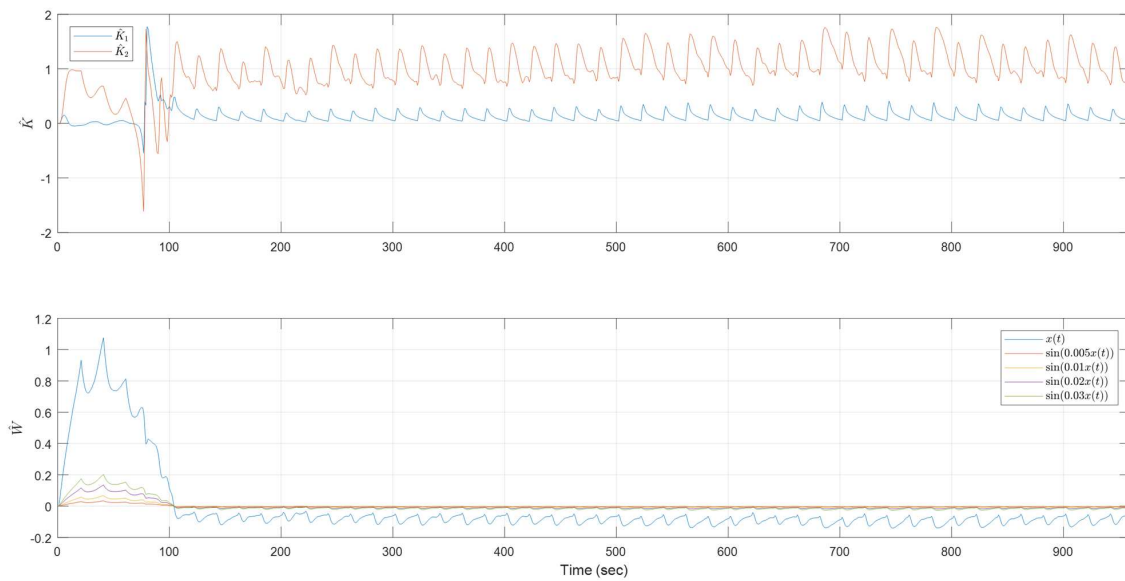
Figure 7.8: The adaptive laws for Participant 2. 0s indicates the start of the controller.

7.5.4   Tracking Analysis of the Controller

Figure 7.9 shows the histograms of the controller output and the measured PLV output, for each participant. The large peak in the histogram of the controller output corresponds with the initial binaural beat frequency at 13Hz. For each participant, the PLV values are normalized by the desired trajectory value. If the normalized PLV response is equal to one, then the PLV is equal to the desired trajectory. The normalized PLV values for the majority of the participants is centered around 0.9. Therefore, the measured PLV values are similar to the desired trajectory value for most participants.
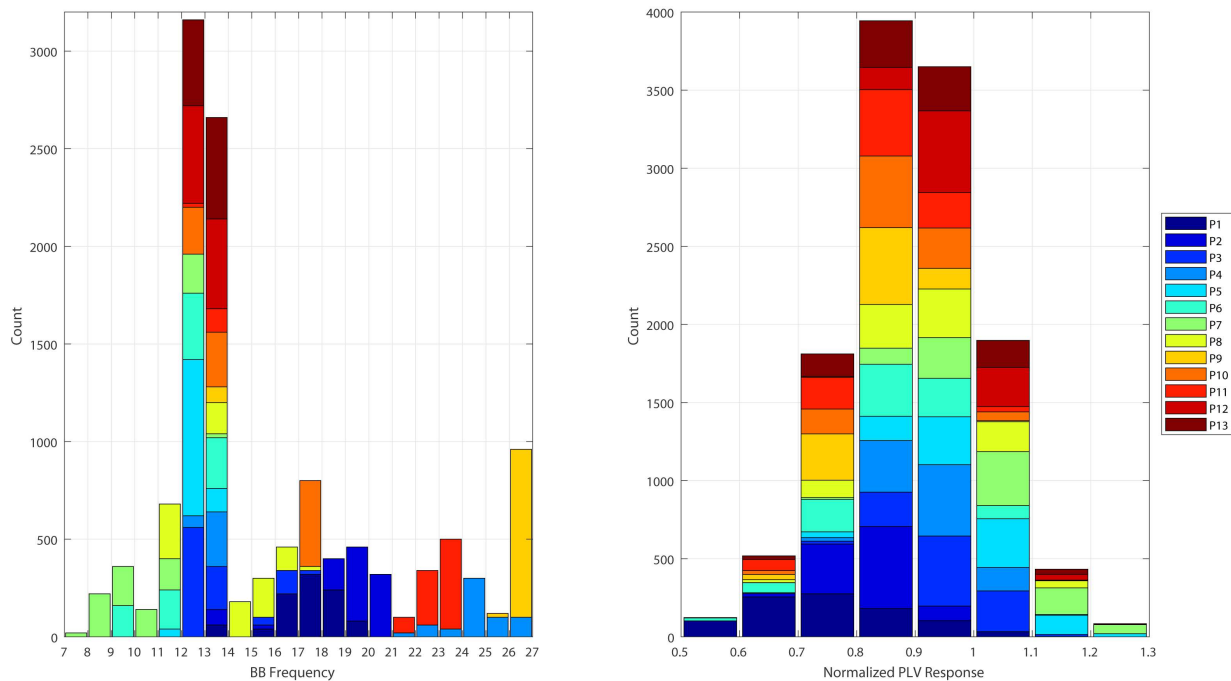
Figure 7.9: The histogram results, for each participant, of the binaural beat frequency controller output and the measured PLV response normalized by the desired trajectory.

7.5.5 Example Controller Outputs

Figure 7.10 shows the results of the measured PLV output, $x(t)$, the reference system, x_l, and the reference trajectory, $r(t)$. At the beginning of each 20 second period the reference trajectory system increases rapidly to try to force the system to reach the desired trajectory. Since the controller effort is maintained throughout the 20 seconds, the reference system must adjust accordingly which produced the large peaks in the response.
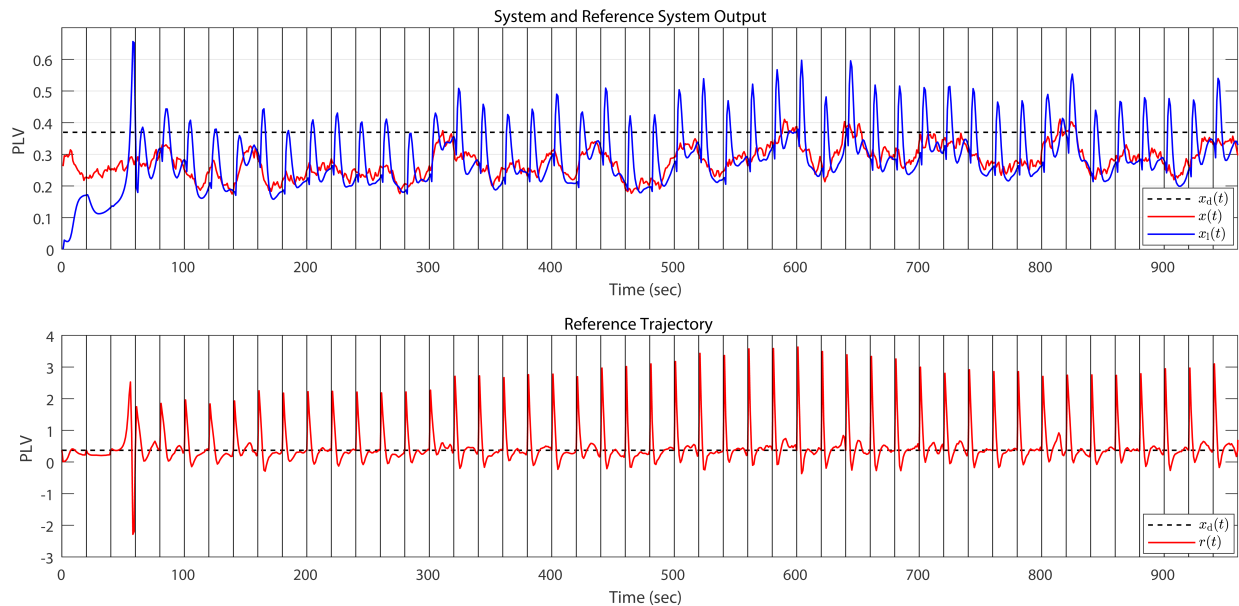
Figure 7.10: The top plot shows a comparison of the reference system to the PLV values computed from the EEG signals in relation to the desired trajectory. The bottom plot shows the reference trajectory in comparison to the desired trajectory.

7.6 Discussion

Overall, the controller is effective in modulating the brain connectivity using binaural beats. In many of the cases, the controller is able to find a binaural beat frequency that worked for that individual at that period in time. If the participants are tested again, then the results

may vary. Many different factors could impact the response of the participants including the time of day, fatigue, response to the binaural beats, and many more which are very hard to quantify or control for.

For most participants, the trials in which they answered incorrectly, indicated by the red "x", is often when their frontal-parietal PLV connection strength is low. Previous research has shown that increased synchronization between the between the frontal and the parietal regions of the brain corresponds to better working memory task performance [22, 50, 51, 52, 53, 54, 55].

All participants, except for one, showed some significant increase in the frontal-parietal PLV connection strength when compared to the baseline measurement. Over all the participants, the controller has driven the frontal-parietal PLV connection strength significantly higher than baseline for nearly 48% of the 16 minutes. However, the change in brain connectivity that the controller is able to achieve is dependent on the individual and there is a large variability between participants since the standard deviation is 26%.

7.7   Future Work

One aspect of the future work for this project which should be addressed the arbitrarily chosen parameters which are the desired trajectory and the initial binaural beat frequency. The desired frontal-parietal PLV value is chosen to be two standard deviations above the mean baseline PLV value. A large amount of variability is observed in the thirteen participants. For some, the controller is able to drive the PLV to the desired value, for others it is unable to do so. For future implementations, the desired value could be adjusted based on the past PLV values. Therefore, if the person responds well to the binaural beats (i.e Participant 6) then the desired trajectory could be set higher. In addition, potentially more than the

last minute of the 4 minutes of no sound should be used for determining the baseline PLV values. For example, with Participant 9, if the baseline computation had been over the last 2 minutes, then the mean would have reflected a more accurate connection strength. However, using the current method, the desired value is set too high which resulted in none of the epochs being significantly above baseline.

In addition, the initial binaural beat frequency is chosen to be 13Hz. For most of the participants, the binaural beat frequency at the end of the 16 minutes is different from 13Hz. However, in two of the cases (i.e Participants 12 and 13), the frequency barely deviated from 13Hz because the initial binaural beat frequency worked well in driving the PLV connection strength to the desired value so the controller essentially isn't required. A more systematic way of choosing the initial binaural beat frequency should be determined.

Future applications should also address the current limitations of the system which includes the computational processing load limit and the movement of the participant. First, the processing of the EEG data in OpenViBE has limitations. The software lags behind if the EEG data is not downsampled to 128Hz and the time shift for the epoching window is less than one second. In addition, the code that is called within the Matlab scripting block must be completed within 1 second or else OpenViBE crashes. In addition, a problem which was not addressed in this work are the movement artifacts in the EEG. Even though the participants are instructed to keep as still as possible, movement artifacts still occurred. The artifacts can affect the PLV computation and therefore affect the controller results.

In the future, a controller which does not require a model could be implemented, such as in [147, 148, 149, 150]. The fundamental idea of the algorithm is that when the system model is unknown and the state vector is unmeasured, the construction of the model dynamics and and estimation of the full state is not necessary if all we need to control is the output (i.e. the measurements). Instead, an output predictor is used to predict the system output

using the history of the input and output stored in autoregressive filtered vectors. Therefore, designing an output tracking control for the unknown system is equivalent to developing a tracking control for the predictor, which is a system with known dynamics and states. With this approach, the tracking task can be achieved by designing a tracking controller for a linear time varying system, using one of many approaches existing in the literature.

Chapter 8

Conclusions

In conclusion, this dissertation details theoretical, computational, and experimental research at the intersection of neuroscience, system dynamics, and controls.

The second chapter compares the results of using PLV and CCM to develop resting-state brain connectivity networks. The results suggest that the network characteristics follow the same trends and the similarity between the computed networks, for both algorithms, is highly significant. However, CCM can identify low or one-way connection strengths better than PLV but takes exponentially longer to calculate.

The next three chapters detail the results of the use of open-loop binaural beats used to entrain specific brain structures utilized during visuospatial (Chapter 3) and verbal (Chapter 4) working memory tasks. We determined the effects of different acoustic stimulation conditions on participant response accuracy and cortical network topology, as measured by EEG recordings. We found that listening to 15Hz binaural beats during both working memory tasks not only increased the response accuracy but also modified the strengths of the cortical networks during the task. Chapter 5 shows additional analysis which compares the networks developed for each task. Overall, these results suggest that this safe and accessible stimulation method can modulate behavioral performance and cortical connectivity.

Chapter 6 describes the large-scale brain network model called The Virtual Brain used to assess closed-loop controller performance. We developed the first simulation environment

for an EEG-based closed-loop control of TVB using binaural beats. Results suggest that the connectivity networks, constructed from simulated EEG, may change with certain binaural beats stimulation frequency. The simulations are used to test both a linear and adaptive controller's ability to change cortical responses using the controlled binaural beat stimulus.

Chapter 7 details the development and testing of the first experimental closed-loop EEG-based controller which modulates the binaural beat stimulus played to the participant during a working memory task. Each person's brain functions in slightly different ways, so an open-loop control system for brain stimulation is impractical from a control engineering perspective. The input of the system is the binaural beats delivered through headphones. Entrainment of the beat frequency throughout the brain is recorded using EEG.

8.1 Significance of Work

Only a limited number of studies have investigated the effects of binaural beats on working memory, which controls the temporary retention and online processing of information. Furthermore, no studies, before this work, have evaluated the effects of binaural beats on brain connectivity during working memory tasks.

Compared to current methods of brain stimulation both for system identification or therapeutic interventions (i.e. transcranial alternating/direct current, transcranial magnetic stimulation, and ultrasound), binaural beats capitalize on existing brain structures to entrain higher-level areas of the cortex. In addition, binaural stimulation does not require large equipment or a clinical setting to be used safely. As a result, this system has the potential to be further developed into a medical device to identify and control working memory disorders indicative of cognitive impairment even outside clinical settings. Thus, any associated therapies developed in the future have a strong potential for wide application and usability.

8.2 Open Questions

This research seeks to answer the question of whether binaural beats can be used to identify and control working memory using both open and closed-loop control. However, many open questions for future research exist, for example,

1. What is the time constant for when the brain starts to respond to the binaural beats? Additionally, after the binaural beats stop, how long does the brain remain in that state? Qualitatively assessing the previous research, the time constants appear to be small, meaning that the brain reacts fairly quickly to the binaural beats but also reverts back quickly after the sounds stop.

2. How do closed-loop binaural beats affect other cognitive tasks such as attention or long-term memory?

3. How does the past history of binaural beat frequency affect the response? From the results of the closed-loop experiment shown in Chapter 7 it would appear that the previous binaural beats that the person listened to does matter.

4. What are the long term effects of listening to binaural beats? For example, a longitudinal study could be undertaken to evaluate the long term effects of listening to both open-loop and closed-loop binaural beats.

5. What is the nonlinear relationship between the input binaural beat frequency and the brain's response?

6. Why do some people respond better to the binaural beat frequency than others?

The work in this dissertation lays a foundation for exploring these questions with the experimentally-tested hardware and control infrastructure in the future.

Bibliography

[1] Roxana A Stefanescu and Viktor K Jirsa. A low dimensional description of globally coupled heterogeneous neural networks of excitatory and inhibitory neurons. *PLoS Comput Biol*, 4(11):e1000219, 2008.

[2] Ronald C Petersen, Glenn E Smith, Stephen C Waring, Robert J Ivnik, Eric G Tangalos, and Emre Kokmen. Mild cognitive impairment: clinical characterization and outcome. *Archives of Neurology*, 56(3):303–308, 1999.

[3] Michael Grundman, Ronald C Petersen, Steven H Ferris, Ronald G Thomas, Paul S Aisen, David A Bennett, Norman L Foster, Clifford R Jack Jr, Douglas R Galasko, Rachelle Doody, et al. Mild cognitive impairment can be distinguished from alzheimer disease and normal aging for clinical trials. *Archives of Neurology*, 61(1):59–66, 2004.

[4] Hans Berger. Über das elektrenkephalogramm des menschen. *European Archives of Psychiatry and Clinical Neuroscience*, 87(1):527–570, 1929.

[5] D Corydon Hammond. What is neurofeedback: An update. *Journal of Neurotherapy*, 15(4):305–336, 2011.

[6] C.A. Simpkins and A.M. Simpkins. *Neuroscience for Clinicians: Evidence, Models, and Practice*. Springer, 2012.

[7] Ole Jensen, MA Idiart, and John E Lisman. Physiologically realistic formation of autoassociative memory in networks with theta/gamma oscillations: role of fast nmda channels. *Learning & Memory*, 3(2-3):243–256, 1996.

[8] Ole Jensen, Jochen Kaiser, and Jean-Philippe Lachaux. Human gamma-frequency oscillations associated with attention and memory. *Trends in Neurosciences*, 30(7):317–324, 2007.

[9] Rosalyn J Moran, Pablo Campo, Fernando Maestu, Richard B Reilly, Raymond J Dolan, and Bryan A Strange. Peak frequency in the theta and alpha bands correlates with human working memory capacity. *Frontiers in Human Neuroscience*, 4:200, 2010.

[10] Erika Nyhus and Tim Curran. Functional role of gamma and theta oscillations in episodic memory. *Neuroscience & Biobehavioral Reviews*, 34(7):1023–1035, 2010.

[11] Olaf Sporns. *Networks of the Brain.* MIT press, 2011.

[12] Hae-Jeong Park and Karl Friston. Structural and functional brain networks: from connections to cognition. *Science*, 342(6158):1238411, 2013.

[13] Karl J Friston. Functional and effective connectivity: a review. *Brain Connectivity*, 1(1):13–36, 2011.

[14] Alfons Schnitzler and Joachim Gross. Normal and pathological oscillatory communication in the brain. *Nature Reviews Neuroscience*, 6(4):285–296, 2005.

[15] Michael G Rosenblum, Arkady S Pikovsky, Jürgen Kurths, Grigory V Osipov, István Z Kiss, and John L Hudson. Locking-based frequency measurement and synchronization of chaotic oscillators with complex dynamics. *Physical Review Letters*, 89(26):264102, 2002.

[16] Peter A Tass. Transmission of stimulus-locked responses in two coupled phase oscillators. *Physical Review E*, 69(5):051909, 2004.

[17] Andreas K Engel, PR Roelfsema, P Fries, M Brecht, and W Singer. Role of the temporal domain for response selection and perceptual binding. *Cerebral Cortex*, 7(6):571–582, 1997.

[18] Bernardo Perfetti, Clara Moisello, Eric Carl Landsness, Svetlana Kvint, Simona Lanzafame, Marco Onofrj, Alessandro Di Rocco, Giulio Tononi, and M Felice Ghilardi. Modulation of gamma and theta spectral amplitude and phase synchronization is associated with the development of visuo-motor learning. *The Journal of Neuroscience*, 31(41):14810–14819, 2011.

[19] Stephan Salenius and Riitta Hari. Synchronous cortical oscillatory activity during motor action. *Current Opinion in Neurobiology*, 13(6):678–684, 2003.

[20] Tommaso Costa, Elena Rognoni, and Dario Galati. Eeg phase synchronization during emotional response to positive and negative film stimuli. *Neuroscience Letters*, 406(3):159–164, 2006.

[21] Gennady G Knyazev. Motivation, emotion, and their inhibitory control mirrored in brain oscillations. *Neuroscience & Biobehavioral Reviews*, 31(3):377–395, 2007.

[22] Jürgen Fell, Peter Klaver, Klaus Lehnertz, Thomas Grunwald, Carlo Schaller, Christian E Elger, and Guillén Fernández. Human memory formation is accompanied by rhinal–hippocampal coupling and decoupling. *Nature Neuroscience*, 4(12):1259–1264, 2001.

[23] Paul Sauseng, Wolfgang Klimesch, Walter R Gruber, and Niels Birbaumer. Cross-frequency phase synchronization: a brain mechanism of memory matching and attention. *NeuroImage*, 40(1):308–317, 2008.

[24] B Schack, W Klimesch, and P Sauseng. Phase synchronization between theta and

upper alpha oscillations in a working memory task. *International Journal of Psychophysiology*, 57(2):105–114, 2005.

[25] Juergen Fell and Nikolai Axmacher. The role of phase synchronization in memory processes. *Nature Reviews Neuroscience*, 12(2):105–118, 2011.

[26] Yoshiki Kuramoto. *Chemical Oscillations, Waves, and Turbulence*, volume 19. Springer Science & Business Media, 2012.

[27] Chai Wah Wu. *Synchronization in Complex Networks of Nonlinear Dynamical Systems*, volume 76. World Scientific, 2007.

[28] Francisco Varela, Jean-Philippe Lachaux, Eugenio Rodriguez, and Jacques Martinerie. The brainweb: phase synchronization and large-scale integration. *Nature Reviews Neuroscience*, 2(4):229–239, 2001.

[29] Jean-Philippe Lachaux, Eugenio Rodriguez, Jacques Martinerie, Francisco J Varela, et al. Measuring phase synchrony in brain signals. *Human Brain Mapping*, 8(4):194–208, 1999.

[30] AR Mclntosh and F Gonzalez-Lima. Structural equation modeling and its application to network analysis in functional brain imaging. *Human Brain Mapping*, 2(1-2):2–22, 1994.

[31] Karl J Friston, Lee Harrison, and Will Penny. Dynamic causal modelling. *NeuroImage*, 19(4):1273–1302, 2003.

[32] Thomas Schreiber. Measuring information transfer. *Physical Review Letters*, 85(2):461, 2000.

[33] Clive WJ Granger. Investigating causal relations by econometric models and cross-spectral methods. *Econometrica: Journal of the Econometric Society*, pages 424–438, 1969.

[34] George Sugihara, Robert May, Hao Ye, Chih-hao Hsieh, Ethan Deyle, Michael Fogarty, and Stephan Munch. Detecting causality in complex ecosystems. *Science*, 338(6106):496–500, 2012.

[35] Karin Schiecke, Britta Pester, Diana Piper, Martha Feucht, Franz Benninger, Herbert Witte, and Lutz Leistritz. Advanced nonlinear approach to quantify directed interactions within eeg activity of children with temporal lobe epilepsy in their time course. *EPJ Nonlinear Biomedical Physics*, 5:3, 2017.

[36] Yoshito Hirata, José M Amigó, Yoshiya Matsuzaka, Ryo Yokota, Hajime Mushiake, and Kazuyuki Aihara. Detecting causality by combined use of multiple methods: Climate and brain examples. *PloS one*, 11(7):e0158572, 2016.

[37] Axel Wismüller, Anas Z Abidin, Adora M DSouza, and Mahesh B Nagarajan. Mutual connectivity analysis (mca) for nonlinear functional connectivity network recovery in the human brain using convergent cross-mapping and non-metric clustering. In *Advances in Self-Organizing Maps and Learning Vector Quantization*, pages 217–226. Springer, 2016.

[38] Alan D Baddeley and Graham J Hitch. Working memory. *The Psychology of Learning and Motivation*, 8:47–89, 1974.

[39] Alan Baddeley. The episodic buffer: a new component of working memory? *Trends in Cognitive Sciences*, 4(11):417–423, 2000.

[40] Edward K Vogel, Andrew W McCollough, and Maro G Machizawa. Neural measures reveal individual differences in controlling access to working memory. *Nature*, 438(7067):500–503, 2005.

[41] Edward E Smith and John Jonides. Storage and executive processes in the frontal lobes. *Science*, 283(5408):1657–1661, 1999.

[42] Manaan Kar Ray, Clare E Mackay, Catherine J Harmer, and Timothy J Crow. Bilateral generic working memory circuit requires left-lateralized addition for verbal processing. *Cerebral Cortex*, 18(6):1421–1428, 2008.

[43] Clayton E Curtis and Mark D'Esposito. Persistent activity in the prefrontal cortex during working memory. *Trends in Cognitive Sciences*, 7(9):415–423, 2003.

[44] Bradley R Postle. Working memory as an emergent property of the mind and brain. *Neuroscience*, 139(1):23–38, 2006.

[45] GD Honey, CHY Fu, J Kim, MJ Brammer, TJ Croudace, J Suckling, EM Pich, SCR Williams, and ET Bullmore. Effects of verbal working memory load on corticocortical connectivity modeled by path analysis of functional magnetic resonance imaging data. *NeuroImage*, 17(2):573–582, 2002.

[46] Peter König, Andreas K Engel, and Wolf Singer. Integrator or coincidence detector? the role of the cortical neuron revisited. *Trends in Neurosciences*, 19(4):130–137, 1996.

[47] MR Mehta, AK Lee, and MA Wilson. Role of experience and oscillations in transforming a rate code into a temporal code. *Nature*, 417(6890):741–746, 2002.

[48] Paul Sauseng, Wolfgang Klimesch, Michael Doppelmayr, Simon Hanslmayr, Manuel Schabus, and Walter R Gruber. Theta coupling in the human electroencephalogram during a working memory task. *Neuroscience Letters*, 354(2):123–126, 2004.

[49] György Buzsáki and Andreas Draguhn. Neuronal oscillations in cortical networks. *Science*, 304(5679):1926–1929, 2004.

[50] Sabine Weiss and Peter Rappelsberger. Long-range eeg synchronization during word encoding correlates with successful memory performance. *Cognitive Brain Research*, 9(3):299–312, 2000.

[51] Christopher Summerfield and Jennifer A Mangels. Coherent theta-band eeg activity predicts item-context binding during encoding. *NeuroImage*, 24(3):692–703, 2005.

[52] Karim Benchenane, Adrien Peyrache, Mehdi Khamassi, Patrick L Tierney, Yves Gioanni, Francesco P Battaglia, and Sidney I Wiener. Coherent theta oscillations and reorganization of spike timing in the hippocampal-prefrontal network upon learning. *Neuron*, 66(6):921–936, 2010.

[53] Juergen Fell, Eva Ludowig, Timm Rosburg, Nikolai Axmacher, and Christian E Elger. Phase-locking within human mediotemporal lobe predicts memory formation. *NeuroImage*, 43(2):410–419, 2008.

[54] Michael J Jutras and Elizabeth A Buffalo. Synchronous neural activity and memory formation. *Current Opinion in Neurobiology*, 20(2):150–155, 2010.

[55] Naoyuki Sato and Yoko Yamaguchi. Theta synchronization networks emerge during human object–place memory encoding. *Neuroreport*, 18(5):419–424, 2007.

[56] J Sarnthein, Hellmuth Petsche, P Rappelsberger, GL Shaw, and A Von Stein. Synchronization between prefrontal and posterior association cortex during human working memory. *Proceedings of the National Academy of Sciences*, 95(12):7092–7096, 1998.

[57] Werner Lutzenberger, Barbara Ripper, Laura Busse, Niels Birbaumer, and Jochen

Kaiser. Dynamics of gamma-band activity during an audiospatial working memory task in humans. *The Journal of Neuroscience*, 22(13):5630–5638, 2002.

[58] Claudio Babiloni, Fabio Babiloni, Filippo Carducci, Febo Cincotti, Fabrizio Vecchio, Benedetta Cola, Simone Rossi, Carlo Miniussi, and Paolo Maria Rossini. Functional frontoparietal connectivity during short-term memory as revealed by high-resolution eeg coherence analysis. *Behavioral Neuroscience*, 118(4):687, 2004.

[59] Sylvie Belleville, Stephanie Sylvain-Roy, Chloe de Boysson, and Marie-Claude Menard. Characterizing the memory changes in persons with mild cognitive impairment. *Progress in Brain Research*, 169:365–375, 2008.

[60] Charles Flicker, Steven H Ferris, and Barry Reisberg. Mild cognitive impairment in the elderly predictors of dementia. *Neurology*, 41(7):1006–1006, 1991.

[61] MC Tierney, JP Szalai, WG Snow, RH Fisher, A Nores, G Nadon, E Dunn, and PH St George-Hyslop. Prediction of probable alzheimer's disease in memory-impaired patients a prospective longitudinal study. *Neurology*, 46(3):661–665, 1996.

[62] YAL Pijnenburg, Y Vd Made, AM Van Cappellen Van Walsum, DL Knol, Ph Scheltens, and CJ Stam. Eeg synchronization likelihood in mild cognitive impairment and alzheimer's disease during a working memory task. *Clinical neurophysiology*, 115(6):1332–1339, 2004.

[63] T Koenig, L Prichep, T Dierks, D Hubl, LO Wahlund, ER John, and V Jelic. Decreased eeg synchronization in alzheimers disease and mild cognitive impairment. *Neurobiology of Aging*, 26(2):165–171, 2005.

[64] CJ Stam, Y Van Der Made, YAL Pijnenburg, and PH Scheltens. Eeg synchronization

in mild cognitive impairment and alzheimer's disease. *Acta Neurologica Scandinavica*, 108(2):90–96, 2003.

[65] Eran Dayan, Nitzan Censor, Ethan R Buch, Marco Sandrini, and Leonardo G Cohen. Noninvasive brain stimulation: from physiology to network dynamics and back. *Nature Neuroscience*, 16(7):838–844, 2013.

[66] Patricio T Huerta and Bruce T Volpe. Transcranial magnetic stimulation, synaptic plasticity and network oscillations. *Journal of Neuroengineering and Rehabilitation*, 6(1):1, 2009.

[67] MA Nitsche and W Paulus. Excitability changes induced in the human motor cortex by weak transcranial direct current stimulation. *The Journal of Physiology*, 527(3):633–639, 2000.

[68] André Russowsky Brunoni and Marie-Anne Vanderhasselt. Working memory improvement with non-invasive brain stimulation of the dorsolateral prefrontal cortex: a systematic review and meta-analysis. *Brain and Cognition*, 86:1–9, 2014.

[69] Kai Heimrath, Pascale Sandmann, Andreas Becke, Notger G Müller, and Tino Zaehle. Behavioral and electrophysiological effects of transcranial direct current stimulation of the parietal cortex in a visuo-spatial working memory task. *Frontiers in Psychiatry*, 3:56, 2012.

[70] Andreas Boehringer, Katja Macher, Juergen Dukart, Arno Villringer, and Burkhard Pleger. Cerebellar transcranial direct current stimulation modulates verbal working memory. *Brain Stimulation*, 6(4):649–653, 2013.

[71] Paulo S Boggio, Roberta Ferrucci, Sergio P Rigonatti, Priscila Covre, Michael Nitsche, Alvaro Pascual-Leone, and Felipe Fregni. Effects of transcranial direct current stimu-

lation on working memory in patients with parkinson's disease. *Journal of the Neurological Sciences*, 249(1):31–38, 2006.

[72] Gerald Oster. Auditory beats in the brain. *Scientific American*, 229(4):94–102, 1973.

[73] Matthew W Spitzer and Malcolm N Semple. Transformation of binaural response properties in the ascending auditory pathway: influence of time-varying interaural phase disparity. *Journal of Neurophysiology*, 80(6):3062–3076, 1998.

[74] Frank E Musiek and Jane A Baran. *The Auditory System: Anatomy, Physiology and Clinical Correlates.* ASHA, 2007.

[75] Douglas C Fitzpatrick, Jason M Roberts, Shigeyuki Kuwada, Duck O Kim, and Blagoje Filipovic. Processing temporal modulations in binaural and monaural auditory stimuli by neurons in the inferior colliculus and auditory cortex. *Journal of the Association for Research in Otolaryngology*, 10(4):579–593, 2009.

[76] Bernhard Ross, Takahiro Miyazaki, Jessica Thompson, Shahab Jamali, and Takako Fujioka. Human cortical responses to slow and fast binaural beats reveal multiple mechanisms of binaural hearing. *Journal of Neurophysiology*, 112(8):1871–1884, 2014.

[77] Rossitza Draganova, Bernhard Ross, Andreas Wollbrink, and Christo Pantev. Cortical steady-state responses to central and peripheral auditory beats. *Cerebral Cortex*, 18(5):1193–1200, 2008.

[78] Dietrich WF Schwarz and P Taylor. Human auditory steady state responses to binaural and monaural beats. *Clinical Neurophysiology*, 116(3):658–668, 2005.

[79] Maria A Pastor, Julio Artieda, Javier Arbizu, Josep M Marti-Climent, Ivan Peñuelas, and Jose C Masdeu. Activation of human cerebral and cerebellar cortex by auditory stimulation at 40 hz. *The Journal of Neuroscience*, 22(23):10501–10506, 2002.

[80] Jon A Frederick, Joel F Lubar, Howard W Rasey, Sheryl A Brim, and Jared Blackburn. Effects of 18.5 hz auditory and visual stimulation on eeg amplitude at the vertex. *Journal of Neurotherapy*, 3(3-4):23–28, 1999.

[81] R Kennerly. Qeeg analysis of binaural beat audio entrainment: A pilot study. *Journal of Neurotherapy*, 8:122–122, 2004.

[82] Shotaro Karino, Masato Yumoto, Kenji Itoh, Akira Uno, Keiko Yamakawa, Sotaro Sekimoto, and Kimitaka Kaga. Neuromagnetic responses to binaural beat in human cerebral cortex. *Journal of Neurophysiology*, 96(4):1927–1938, 2006.

[83] Hillel Pratt, Arnold Starr, Henry J Michalewski, Andrew Dimitrijevic, Naomi Bleich, and Nomi Mittelman. Cortical evoked potentials to an auditory illusion: binaural beats. *Clinical Neurophysiology*, 120(8):1514–1524, 2009.

[84] Xiang Gao, Hongbao Cao, Dong Ming, Hongzhi Qi, Xuemin Wang, Xiaolu Wang, Runge Chen, and Peng Zhou. Analysis of eeg activity in response to binaural beats with different frequencies. *International Journal of Psychophysiology*, 94(3):399–406, 2014.

[85] Ann-Katrin Becher, Marlene Höhne, Nikolai Axmacher, Leila Chaieb, Christian E Elger, and Juergen Fell. Intracranial electroencephalography power and phase synchronization changes during monaural and binaural beat stimulation. *European Journal of Neuroscience*, 41(2):254–263, 2015.

[86] Christos I Ioannou, Ernesto Pereda, Job P Lindsen, and Joydeep Bhattacharya. Electrical brain responses to an auditory illusion and the impact of musical expertise. *PloS ONE*, 10(6):e0129486, 2015.

[87] Richard Cauley Kennerly. Thesis: An empirical investigation into the effect of beta

frequency binaural beat audio signals on four measures of human memory. Master's thesis, West Georgia College, Carrolton, GA., 1994.

[88] James D Lane, Stefan J Kasian, Justine E Owens, and Gail R Marsh. Binaural auditory beats affect vigilance performance and mood. *Physiology & Behavior*, 63(2):249–252, 1998.

[89] A Fernández, F Maestu, P Campo, R Hornero, J Escudero, and J Poch. Impact of auditory stimulation at a frequency of 5 hz in verbal memory. *Actas Espaolas de Psiquiatra*, 36(6):307–313, 2008.

[90] Anke Karabanov, Axel Thielscher, and Hartwig Roman Siebner. Transcranial brain stimulation: closing the loop between brain and stimulation. *Current Opinion in Neurology*, 2016.

[91] Til O Bergmann, Matthias Mlle, Marlit A Schmidt, Christoph Lindner, Lisa Marshall, Jan Born, and Hartwig R Siebner. Eeg-guided transcranial magnetic stimulation reveals rapid shifts in motor cortical excitability during the human sleep slow oscillation. 2012.

[92] Alexander Zhigalov, Alexander Kaplan, and J Matias Palva. Modulation of critical brain dynamics using closed-loop neurofeedback stimulation. *Clinical Neurophysiology*, 2016.

[93] Hong-Viet V Ngo, Thomas Martinetz, Jan Born, and Matthias Mölle. Auditory closed-loop stimulation of the sleep slow oscillation enhances memory. *Neuron*, 78(3):545–553, 2013.

[94] John-Stuart Brittain, Penny Probert-Smith, Tipu Z Aziz, and Peter Brown. Tremor

suppression by rhythmic transcranial current stimulation. *Current Biology*, 23(5):436–440, 2013.

[95] Sittapong Settapat and Michiko Ohkura. An alpha-wave-based binaural beat sound control system using fuzzy logic and autoregressive forecasting model. In *SICE Annual Conference, 2008*, pages 109–114. IEEE, 2008.

[96] JS Damoiseaux, SARB Rombouts, F Barkhof, P Scheltens, CJ Stam, Stephen M Smith, and CF Beckmann. Consistent resting-state networks across healthy subjects. *Proceedings of the National Academy of Sciences*, 103(37):13848–13853, 2006.

[97] Dante Mantini, Mauro Gianni Perrucci, Cosimo Del Gratta, Gian Luca Romani, and Maurizio Corbetta. Electrophysiological signatures of resting state networks in the human brain. *Proceedings of the National Academy of Sciences*, 104(32):13170–13175, 2007.

[98] Lizette Heine, Andrea Soddu, Francisco Gómez, Audrey Vanhaudenhuyse, Luaba Tshibanda, Marie Thonnard, Vanessa Charland-Verville, Murielle Kirsch, Steven Laureys, and Athena Demertzi. Resting state networks and consciousness: alterations of multiple resting state network connectivity in physiological, pharmacological, and pathological consciousness states. *Frontiers in Psychology*, 3, 2012.

[99] Sergul Aydore, Dimitrios Pantazis, and Richard M Leahy. A note on the phase locking value and its properties. *Neuroimage*, 74:231–244, 2013.

[100] Florian Mormann, Klaus Lehnertz, Peter David, and Christian E Elger. Mean phase coherence as a measure for phase synchronization and its application to the eeg of epilepsy patients. *Physica D: Nonlinear Phenomena*, 144(3):358–369, 2000.

[101] DP Schwartz, S Sockeel, M Plgrini-Issac, and H Benali. Data from: Large-scale functional networks identified from resting-state eeg using spatial ica, 2016.

[102] Stéphane Sockeel, Denis Schwartz, Mélanie Pélégrini-Issac, and Habib Benali. Large-scale functional networks identified from resting-state eeg using spatial ica. *PloS one*, 11(1):e0146845, 2016.

[103] Maarten Mennes, Bharat B Biswal, F Xavier Castellanos, and Michael P Milham. Making data sharing work: the fcp/indi experience. *Neuroimage*, 82:683–691, 2013.

[104] Arnaud Delorme and Scott Makeig. Eeglab: an open source toolbox for analysis of single-trial eeg dynamics including independent component analysis. *Journal of Neuroscience Methods*, 134(1):9–21, 2004.

[105] Scott Makeig, Anthony J Bell, Tzyy-Ping Jung, Terrence J Sejnowski, et al. Independent component analysis of electroencephalographic data. *Advances in neural information processing systems*, pages 145–151, 1996.

[106] SI Goncalves, JC De Munck, PJW Pouwels, R Schoonhoven, JPA Kuijer, NM Maurits, JM Hoogduin, EJW Van Someren, RM Heethaar, and FH Lopes Da Silva. Correlating the alpha rhythm to bold using simultaneous eeg/fmri: inter-subject variability. *Neuroimage*, 30(1):203–213, 2006.

[107] Robin I Goldman, John M Stern, Jerome Engel Jr, and Mark S Cohen. Simultaneous eeg and fmri of the alpha rhythm. *Neuroreport*, 13(18):2487, 2002.

[108] Matthias C Meyer, Erik SB van Oort, and Markus Barth. Electrophysiological correlation patterns of resting state networks in single subjects: a combined eeg–fmri study. *Brain topography*, 26(1):98–109, 2013.

[109] William D Penny, Karl J Friston, John T Ashburner, Stefan J Kiebel, and Thomas E Nichols. *Statistical parametric mapping: the analysis of functional brain images*. Academic press, 2011.

[110] Susan Whitfield-Gabrieli and Alfonso Nieto-Castanon. Conn: a functional connectivity toolbox for correlated and anticorrelated brain networks. *Brain connectivity*, 2(3):125–141, 2012.

[111] Xiaoqian J Chai, Alfonso Nieto Castañón, Dost Öngür, and Susan Whitfield-Gabrieli. Anticorrelations in resting state networks without global signal regression. *Neuroimage*, 59(2):1420–1428, 2012.

[112] Ivan W Selesnick. The design of approximate hilbert transform pairs of wavelet bases. *IEEE Transactions on Signal Processing*, 50(5):1144–1152, 2002.

[113] Huanfei Ma, Kazuyuki Aihara, and Luonan Chen. Detecting causality from nonlinear dynamics with short-term time series. *Scientific reports*, 4, 2014.

[114] Lionel Barnett and Anil K Seth. The mvgc multivariate granger causality toolbox: a new approach to granger-causal inference. *Journal of neuroscience methods*, 223:50–68, 2014.

[115] Lionel Barnett, Adam B Barrett, and Anil K Seth. Granger causality and transfer entropy are equivalent for gaussian variables. *Physical review letters*, 103(23):238701, 2009.

[116] Lionel Barnett and Anil K Seth. Detectability of granger causality for subsampled continuous-time neurophysiological processes. *Journal of neuroscience methods*, 275:93–121, 2017.

[117]

[118] Ethan R Deyle, Michael Fogarty, Chih-hao Hsieh, Les Kaufman, Alec D MacCall, Stephan B Munch, Charles T Perretti, Hao Ye, and George Sugihara. Predicting climate effects on pacific sardine. *Proceedings of the National Academy of Sciences*, 110(16):6430–6435, 2013.

[119] Mikail Rubinov and Olaf Sporns. Complex network measures of brain connectivity: uses and interpretations. *Neuroimage*, 52(3):1059–1069, 2010.

[120] Richard W Homan, John Herman, and Phillip Purdy. Cerebral location of international 10–20 system electrode placement. *Electroencephalography and Clinical Neurophysiology*, 66(4):376–382, 1987.

[121] Bo Luan, Peter Sörös, and Ervin Sejdić. A study of brain networks associated with swallowing using graph-theoretical approaches. *PloS ONE*, 8(8):e73577, 2013.

[122] Christine Beauchene. The effect of binaural beats on visuospatial working memory and cortical connectivity., 2016, Available from: DOI: http://doi.org/10.7294/W46Q1V5D.

[123] Patricia S Goldman-Rakic. Regional and cellular fractionation of working memory. *Proceedings of the National Academy of Sciences*, 93(24):13473–13480, 1996.

[124] Yang Jiang, James V Haxby, Alex Martin, Leslie G Ungerleider, and Raja Parasuraman. Complementary neural mechanisms for tracking items in human working memory. *Science*, 287(5453):643–646, 2000.

[125] CHRISTOS Constantinidis and MICHAEL A Steinmetz. Neuronal activity in posterior parietal area 7a during the delay periods of a spatial memory task. *Journal of Neurophysiology*, 76(2):1352–1355, 1996.

[126] Juliane Kmpfe, Peter Sedlmeier, and Frank Renkewitz. The impact of background music on adult listeners: A meta-analysis. *Psychology of Music*, 2010.

[127] Danai Dima, Jigar Jogia, and Sophia Frangou. Dynamic causal modeling of load-dependent modulation of effective connectivity within the verbal working memory network. *Human Brain Mapping*, 35(7):3025–3035, 2014.

[128] Satoru Nakashita, Daisuke N Saito, Takanori Kochiyama, Manabu Honda, Hiroki C Tanabe, and Norihiro Sadato. Tactile–visual integration in the posterior parietal cortex: A functional magnetic resonance imaging study. *Brain Research Bulletin*, 75(5):513–525, 2008.

[129] HR Brown and KJ Friston. The functional anatomy of attention: a dcm study. *Frontiers in Human Neuroscience*, 7(784), 2013.

[130] Philip Nixon, Jenia Lazarova, Iona Hodinott-Hill, Patricia Gough, and Richard Passingham. The inferior frontal gyrus and phonological processing: an investigation using rtms. *Journal of Cognitive Neuroscience*, 16(2):289–300, 2004.

[131] Christine Beauchene, Nicole Abaid, Rosalyn Moran, Rachel A. Diana, and Alexander Leonessa. The effect of binaural beats on visuospatial working memory and cortical connectivity. *PloS ONE*, 11(11):e0166630, 2016.

[132] Christine Beauchene, Nicole Abaid, Rosalyn Moran, Rachel A Diana, and Alexander Leonessa. The effect of binaural beats on verbal working memory and cortical connectivity. *Journal of Neural Engineering*, 14(2):026014, 2017.

[133] Adrian M Owen, Kathryn M McMillan, Angela R Laird, and Ed Bullmore. N-back working memory paradigm: A meta-analysis of normative functional neuroimaging studies. *Human Brain Mapping*, 25(1):46–59, 2005.

[134] Paula Sanz-Leon, Stuart A Knock, Andreas Spiegler, and Viktor K Jirsa. Mathematical

framework for large-scale brain network modeling in the virtual brain. *Neuroimage*, 111:385–430, 2015.

[135] Paula Sanz Leon, Stuart Knock, M. Woodman, Lia Domide, Jochen Mersmann, Anthony McIntosh, and Viktor Jirsa. The virtual brain: a simulator of primate brain network dynamics. *Frontiers in Neuroinformatics*, 7:10, 2013.

[136] Alla Borisyuk, Malcolm N Semple, and John Rinzel. Adaptation and inhibition underlie responses to time-varying interaural phase cues in a model of inferior colliculus neurons. *Journal of Neurophysiology*, 88(4):2134–2146, 2002.

[137] Brian H Scott, Brian J Malone, and Malcolm N Semple. Representation of dynamic interaural phase difference in auditory cortex of awake rhesus macaques. *Journal of Neurophysiology*, 101(4):1781–1799, 2009.

[138] Olivier David and Karl J Friston. A neural mass model for meg/eeg:: coupling and neuronal dynamics. *NeuroImage*, 20(3):1743–1755, 2003.

[139] Kartik B Ariyur and Miroslav Krstic. *Real-time optimization by extremum-seeking control*. John Wiley & Sons, 2003.

[140] Chuong Hoang Nguyen and Alexander Leonessa. Adaptive predictor-based output feedback control for a class of unknown mimo linear systems. *Journal of Nonlinear Science*, pages 1–34, 2017.

[141] Paola Jaramillo Cienfuegos, Adam Shoemaker, Robert W Grange, Nicole Abaid, and Alexander Leonessa. Classical and adaptive control of ex vivo skeletal muscle contractions using functional electrical stimulation (fes). *PloS one*, 12(3):e0172761, 2017.

[142] Yann Renard, Fabien Lotte, Guillaume Gibert, Marco Congedo, Emmanuel Maby, Vincent Delannoy, Olivier Bertrand, and Anatole Lécuyer. Openvibe: An open-source

software platform to design, test, and use brain–computer interfaces in real and virtual environments. *Presence: teleoperators and virtual environments*, 19(1):35–53, 2010.

[143] Alois Schlögl, Claudia Keinrath, Doris Zimmermann, Reinhold Scherer, Robert Leeb, and Gert Pfurtscheller. A fully automated correction method of eog artifacts in eeg recordings. *Clinical neurophysiology*, 118(1):98–104, 2007.

[144] Michael D Fox, Abraham Z Snyder, Justin L Vincent, Maurizio Corbetta, David C Van Essen, and Marcus E Raichle. The human brain is intrinsically organized into dynamic, anticorrelated functional networks. *Proceedings of the National Academy of Sciences of the United States of America*, 102(27):9673–9678, 2005.

[145] Adam P Baker, Matthew J Brookes, Iead A Rezek, Stephen M Smith, Timothy Behrens, Penny J Probert Smith, and Mark Woolrich. Fast transient networks in spontaneous human brain activity. *Elife*, 3, 2014.

[146] Michael D Greicius, Ben Krasnow, Allan L Reiss, and Vinod Menon. Functional connectivity in the resting brain: a network analysis of the default mode hypothesis. *Proceedings of the National Academy of Sciences*, 100(1):253–258, 2003.

[147] Chuong Hoang Nguyen and Alexander Leonessa. Adaptive predictor-based output feedback control for a class of unknown mimo linear systems. *Journal of Nonlinear Science*, 27(4):1257–1290, 2017.

[148] Chuong H Nguyen and Alexander Leonessa. Predictor-based adaptive output feedback control: Application to functional electrical stimulation of a human arm model. *Journal of Dynamic Systems, Measurement, and Control*, 138(11):111014, 2016.

[149] Chuong H Nguyen and Alexander Leonessa. Adaptive predictor-based output feedback

control for a class of unknown mimo systems: Experimental results. In *American Control Conference (ACC), 2015*, pages 3515–3521. IEEE, 2015.

[150] Chuong Hoang Nguyen and Alexander Leonessa. Control motion of a human arm: A simulation study. In *International Conference of Control, Dynamic Systems, and Robotics, Ottawa, Ontario, Canada, May*, pages 15–16, 2014.

Appendices

Appendix A

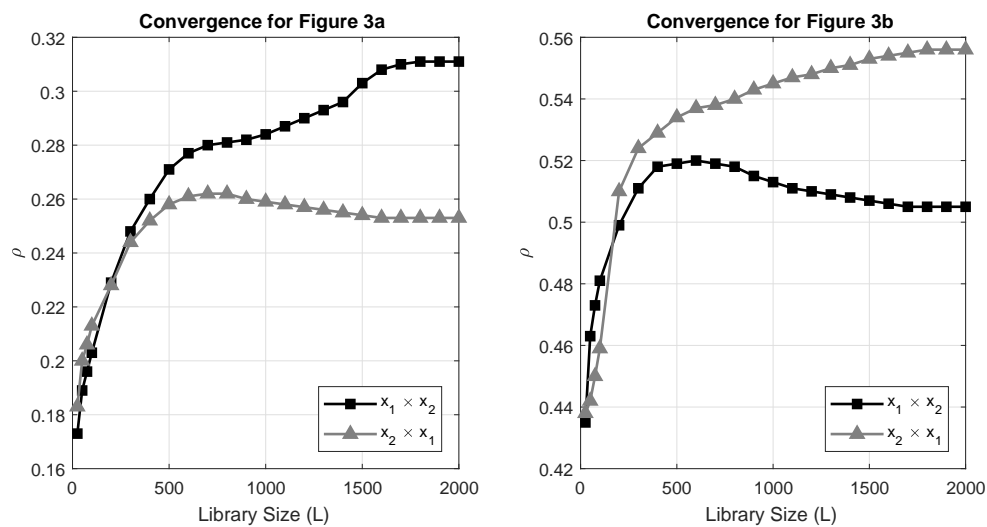# Comparison of Phase Locking Value and Convergent Cross Mapping

Figure A.1: The convergence of the CCM algorithm as the library size increases for the example CCM computation in Figure 2.4a and Figure 2.4b.
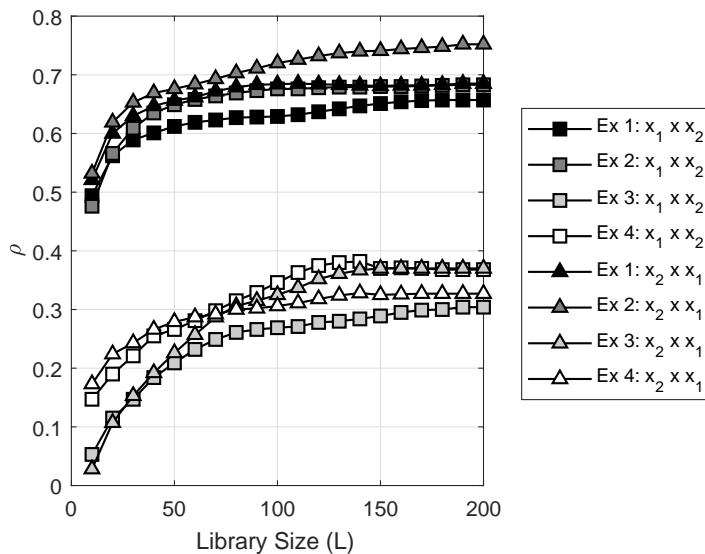
Figure A.2: The convergence of the CCM algorithm as the Library size increases for the EEG data. Four example time series pairs were chosen at random to show the convergence.
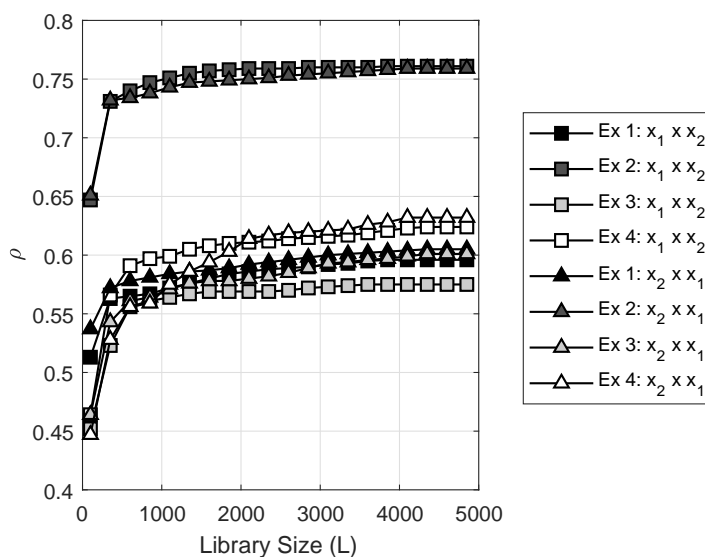

Figure A.3: The convergence of the CCM algorithm as the Library size increases for the fMRI data. Four example time series pairs were chosen at random to show the convergence.

Order	Channel Location	Order	Channel Location
1	Fp2	31	CPz
2	AF8	32	Pz
3	AF4	33	POz
4	F8	34	Oz
5	F6	35	Fp1
6	F4	36	AF7
7	F2	37	AF3
8	FT8	38	F7
9	FC6	39	F5
10	FC4	40	F3
11	FC2	41	F1
12	T8	42	FT7
13	C6	43	FC5
14	C4	44	FC3
15	C2	45	FC1
16	TP8	46	T7
17	CP6	47	C5
18	CP4	48	C3
19	CP2	49	C1
20	P8	50	TP7
21	P6	51	CP5
22	P4	52	CP3
23	P2	53	CP1
24	PO8	54	P7
25	PO4	55	P5
26	O2	56	P3
27	Fpz	57	P1
28	AFz	58	PO7
29	Fz	59	PO3
30	Cz	60	O1

Table A.1: EEG channel order and locations

Order	Location	Order	Location	Order	Location
1	FP r	44	MedFC	49	FP l
2	FOrb r	45	SubCalC	50	FOrb l
3	PaCiG r	46	AC	51	PaCiG l
4	IFG tri r	47	PC	52	IFG tri l
5	IFG oper r	48	Precuneous	53	IFG oper l
6	MidFG r			54	MidFG l
7	SFG r			55	SFG l
8	FO r			56	FO l
9	TP r			57	TP l
10	aPaHC r			58	aPaHC l
11	pPaHC r			59	pPaHC l
12	aTFusC r			60	aTFusC l
13	pTFusC r			61	pTFusC l
14	aITG r			62	aITG l
15	toITG r			63	toITG l
16	pITG r			64	pITG l
17	aMTG r			65	aMTG l
18	toMTG r			66	toMTG l
19	pMTG r			67	pMTG l
20	pSTG r			68	pSTG l
21	aSTG r			69	aSTG l
22	aSMG r			70	aSMG l
23	pSMG r			71	pSMG l
24	TOFusC r			72	TOFusC l
25	LG r			73	LG l
26	AG r			74	AG l
27	HG r			75	HG l
28	PT r			76	PT l
29	PP r			77	PP l
30	IC r			78	IC l
31	PreCG r			79	PreCG l
32	PostCG r			80	PostCG l
33	SMA r			81	SMA L
34	CO r			82	CO l
35	PO r			83	PO l
36	SPL r			84	SPL l
37	Cuneal r			85	Cuneal l
38	SCC r			86	SCC l
39	ICC r			87	ICC l
40	iLOC r			88	iLOC l
41	sLOC r			89	sLOC l
42	OFusG r			90	OFusG l
43	OP r			91	OP l

Table A.2: ROI order and locations

Appendix B

Comparison of Visuospatial and Verbal Working Memory Tasks

Task	CONDITION	CHANNEL	CONDITION × CHANNELS
VS	F(1,3168) = 246.9	F(15,3168) = 95.8	F(15,3168) = 5.5
VB	F(1,3168) = 70.6	F(15,3168) = 153.5	F(15,3168) = 3.8

Table B.1: Results of the two-way ANOVA comparing CHANNEL and CONDITION.

Task	CONDITION	LINK	CONDITION × LINK
VS	F(1,1782) = 831.6	F(8,1782) = 322.6	F(8,1782) = 5.6
VB	F(1,1782) = 112.9	(F(8,1782) = 344.3	F(8,1782) = 8.1

Table B.2: Results of the two-way ANOVA comparing CHANNEL and LINK.

Link	None	15Hz BB	Difference	p-value	t-statistic
F – PO (BL)	0.418 ± 0.010	0.444 ± 0.019	0.027	$< .0001$	12.34
PO – PO (BL)	0.386 ± 0.017	0.424 ± 0.027	0.038	$< .0001$	12.09
CT – PO (L)	0.434 ± 0.020	0.471 ± 0.026	0.038	$< .0001$	11.58
F – PO (R)	0.354 ± 0.024	0.399 ± 0.031	0.045	$< .0001$	11.54
F – CT (R)	0.362 ± 0.024	0.404 ± 0.030	0.042	$< .0001$	10.87
F – F (BL)	0.365 ± 0.013	0.392 ± 0.023	0.027	$< .0001$	10.08
F – CT (L)	0.360 ± 0.024	0.394 ± 0.029	0.034	$< .0001$	8.95
CT – PO (R)	0.429 ± 0.030	0.461 ± 0.030	0.031	$< .0001$	7.40
F – PO (L)	0.374 ± 0.023	0.393 ± 0.029	0.019	$< .0001$	5.12

Table B.3: Results of the visuospatial task regional connections.

Link	None	15Hz BB	Difference	p-value	t-statistic
PO – PO (BL)	0.479 ± 0.019	0.499 ± 0.016	0.020	$< .0001$	8.25
F – PO (BL)	0.500 ± 0.016	0.516 ± 0.016	0.016	$< .0001$	7.16
F – PO (R)	0.477 ± 0.016	0.488 ± 0.014	0.011	$< .0001$	5.37
F – PO (L)	0.501 ± 0.027	0.519 ± 0.024	0.018	$< .0001$	5.01
CT – PO (L)	0.554 ± 0.026	0.564 ± 0.024	0.010	0.005	2.84
F – CT (L)	0.501 ± 0.024	0.510 ± 0.023	0.009	0.005	2.82
F – F (BL)	0.507 ± 0.017	0.514 ± 0.016	0.007	0.006	2.76
CT – PO (R)	0.526 ± 0.019	0.522 ± 0.016	-0.004	0.130	-1.52
F – CT (R)	0.470 ± 0.018	0.471 ± 0.016	0.001	0.777	0.28

Table B.4: Results of the verbal task regional connections.

Appendix C

TVB Controller Testing Environment

Order	Location	Order	Location
1	Fp1	35	CP5
2	Fp2	36	CP6
3	F4	37	CP1
4	F3	38	CP2
5	C3	39	FT9
6	C4	40	FT10
7	P4	41	FC2
8	P3	42	FC1
9	O2	43	AF3
10	O1	44	AF4
11	F8	45	FC6
12	F7	46	FC5
13	T8/T4	47	CPz
14	T7/T3	48	P1
15	P8/T6	49	POz
16	P7/T5	50	P2
17	Pz	51	P6
18	Fz	52	C6
21	AF9	53	P5
22	AF10	54	C1
23	F9	55	C2
24	F10	56	C5
25	CB1	57	F2
26	CB2	58	F6
27	TP7	59	F1
28	TP9	60	AF8
29	TP10	61	F5
30	TP8	62	AF7
31	Oz	63	Fpz
32	Iz	64	FCz
33	PO4	65	Cz
34	PO3		

Table C.1: EEG channel order and locations. For the simulations CB1, CB2, TP10, TP, Iz were discarded.

Appendix D

Closed-Loop Binaural Stimulation Results

D.1 EEG Cap Technical Specifications

Figure D.1: Layout of the 64 EEG channels

Pinning Specifications:

Channel Number	Electrode	Pin numbers active	Pin numbers shield
-	GND	34	68
1	Fp1	33	67
2	Fpz	32	66
3	Fp2	31	65
4	F7	30	64
5	F3	29	63
6	Fz	28	62
7	F4	27	61
8	F8	26	60
9	FC5	25	59
10	FC1	24	58
11	FC2	23	57
12	FC6	22	56
13	M1	21	55
14	T7	20	54
15	C3	19	53
16	Cz	18	52
17	C4	17	51
18	T8	16	50
19	M2	15	49
20	CP5	14	48
21	CP1	13	47
22	CP2	12	46
23	CP6	11	45
24	P7	10	44
25	P3	9	43
26	Pz	8	42
27	P4	7	41
28	P8	6	40
29	POz	5	39
30	O1	4	38
31	O2	3	37
32	EOG	2	36
-	CPz	1	35

Connector 1

Channel Number	Electrode	Pin numbers active	Pin numbers shield
-	-	34	68
33	AF7	33	67
34	AF3	32	66
35	AF4	31	65
36	AF8	30	64
37	F5	29	63
38	F1	28	62
39	F2	27	61
40	F6	26	60
41	FC3	25	59
42	FCz	24	58
43	FC4	23	57
44	C5	22	56
45	C1	21	55
46	C2	20	54
47	C6	19	53
48	CP3	18	52
49	CP4	17	51
50	P5	16	50
51	P1	15	49
52	P2	14	48
53	P6	13	47
54	PO5	12	46
55	PO3	11	45
56	PO4	10	44
57	PO6	9	43
58	FT7	8	42
59	FT8	7	41
60	TP7	6	40
61	TP8	5	39
62	PO7	4	38
63	PO8	3	37
64	Oz	2	36
-	-	1	35

Connector 2
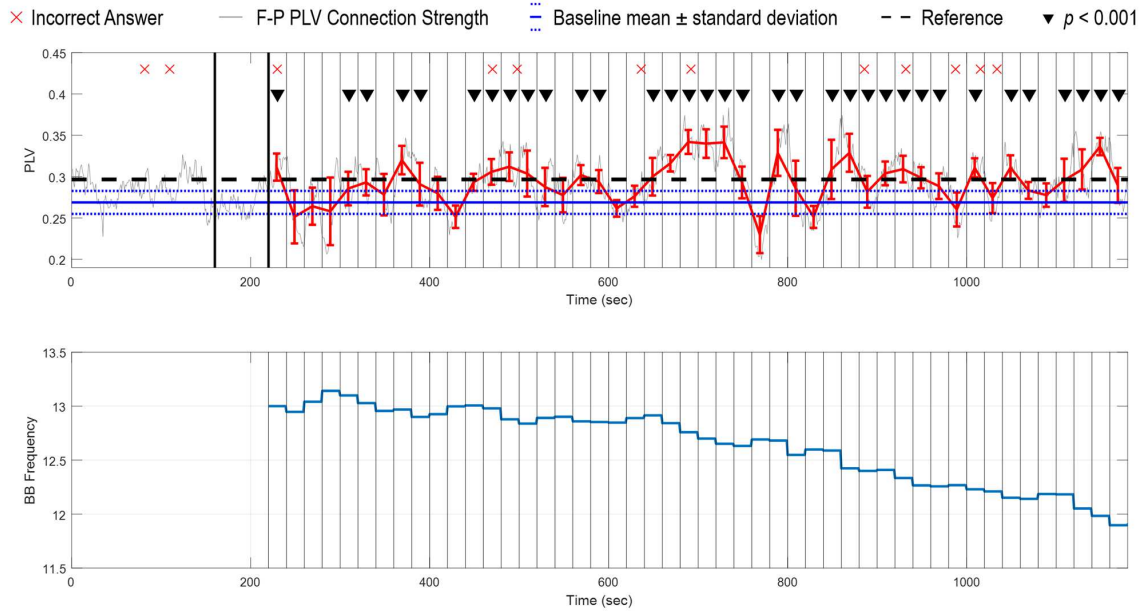
Figure D.2: Order of the EEG channels

D.2 Results
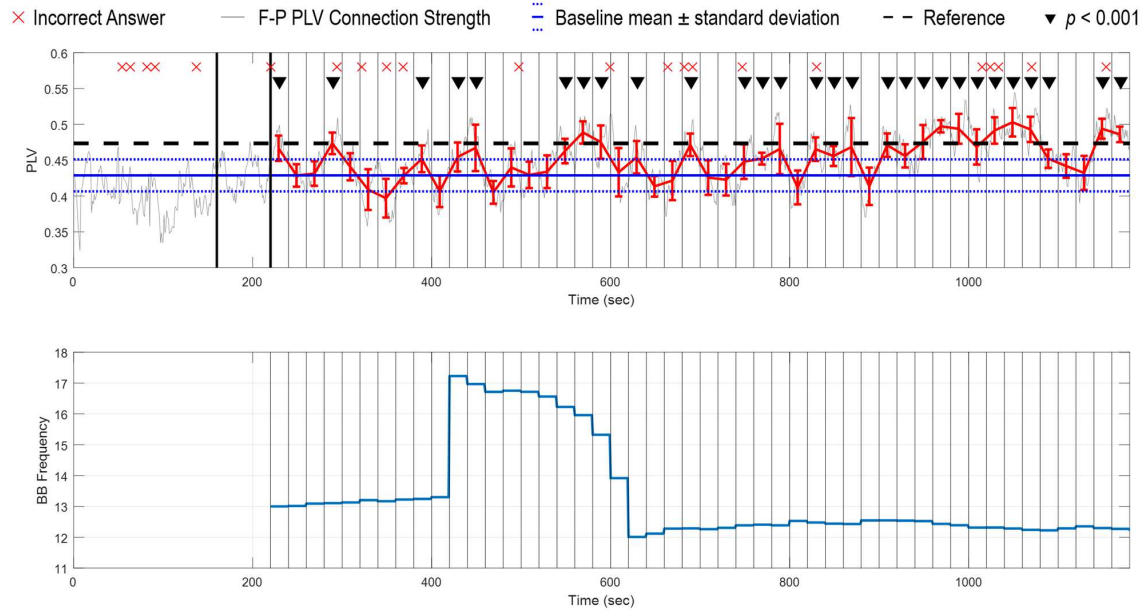
Figure D.3: The frontal-parietal PLV connection strength as a function of time and the corresponding controller output for Participant 3. The mean and one standard deviation of the PLV, for each epoch, is shown by the error bars in red.
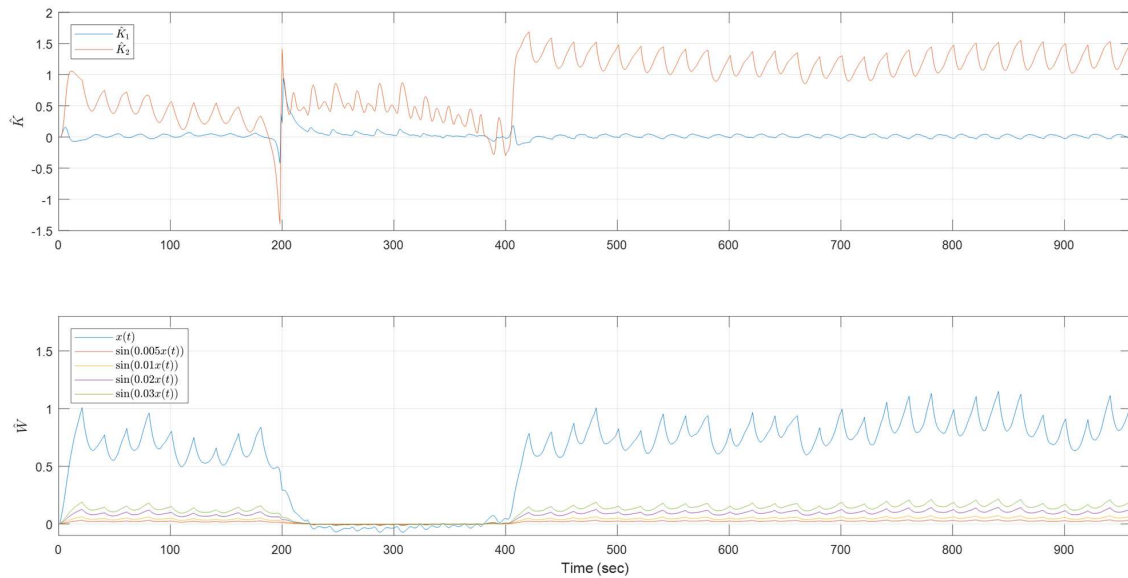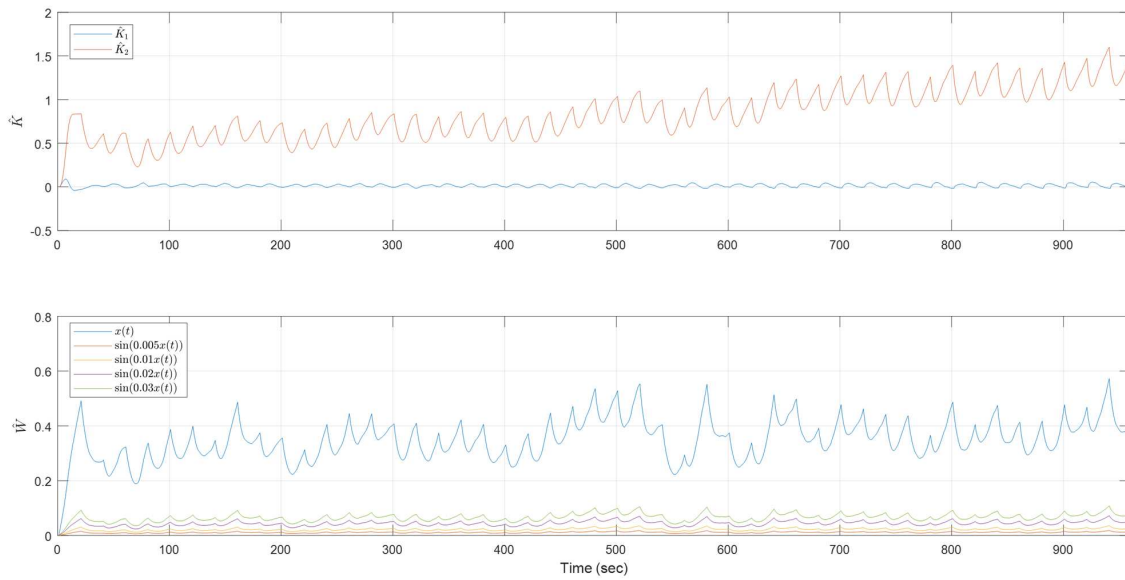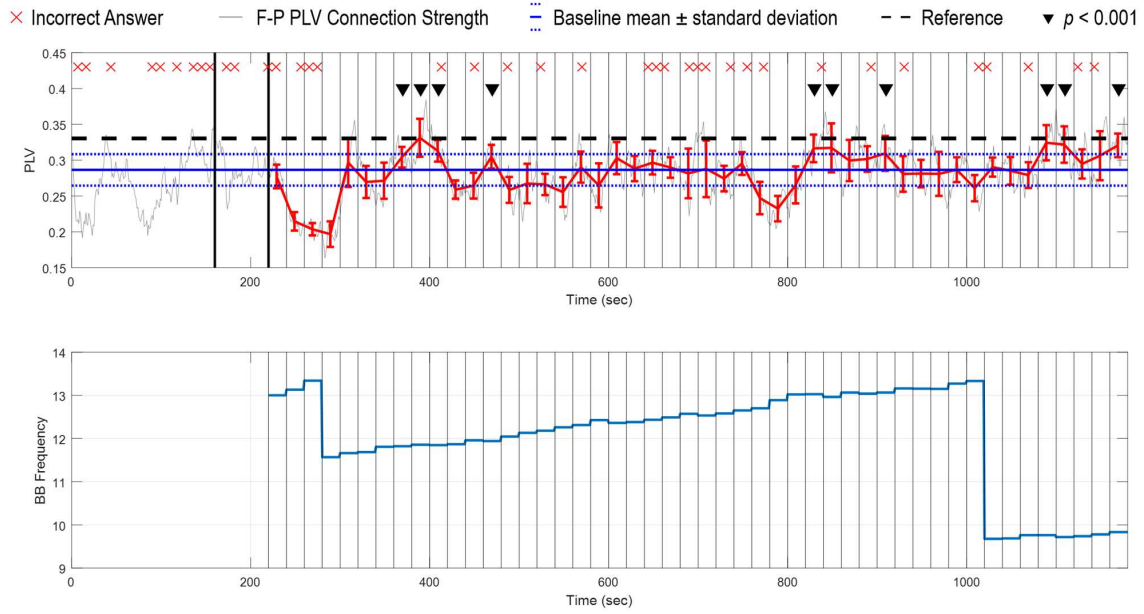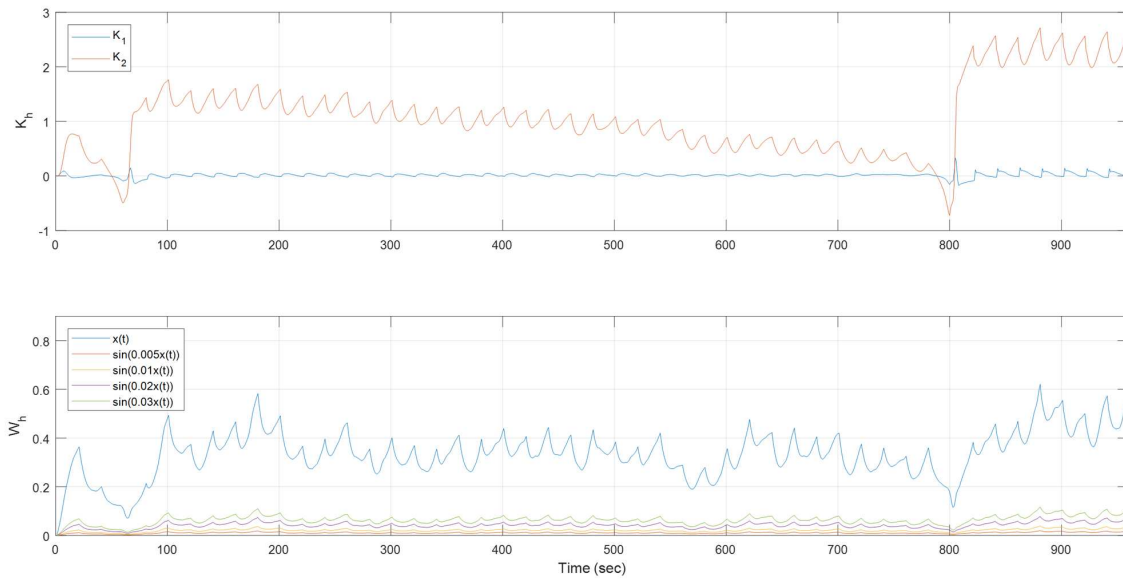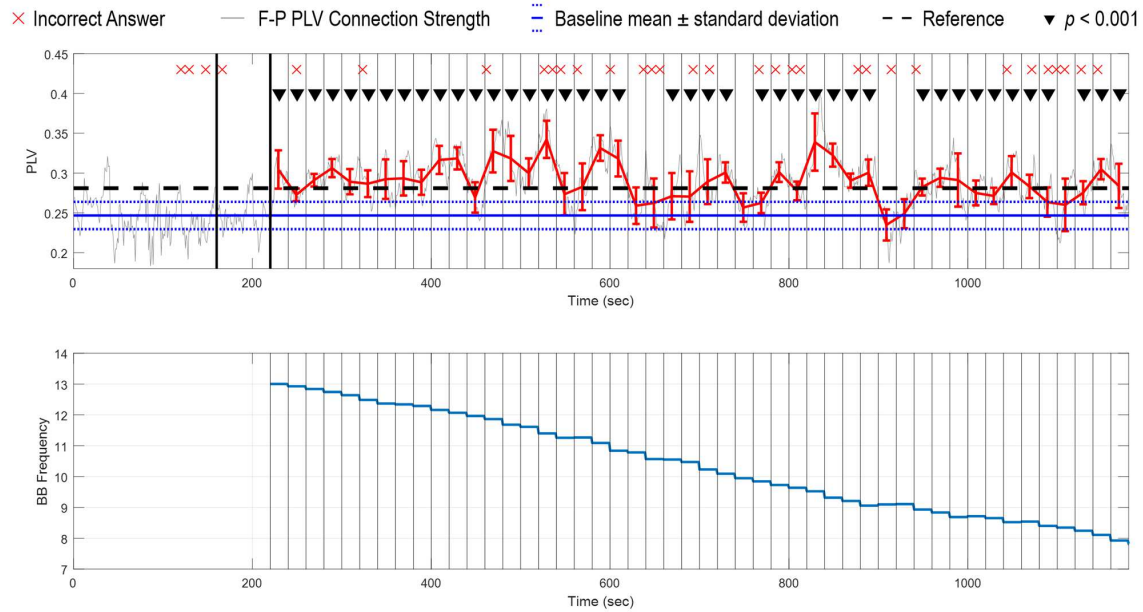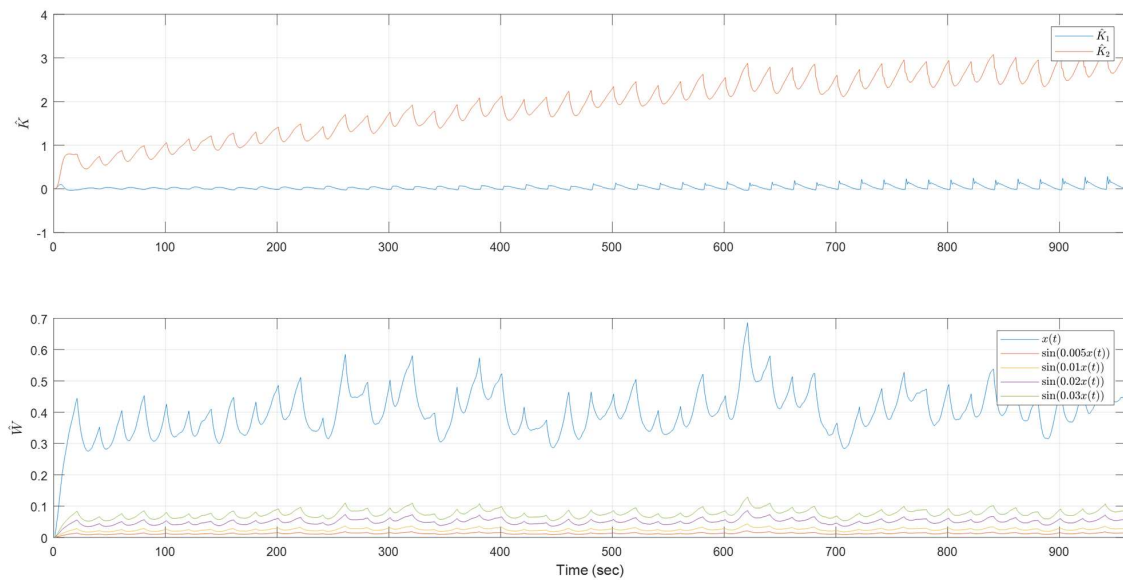

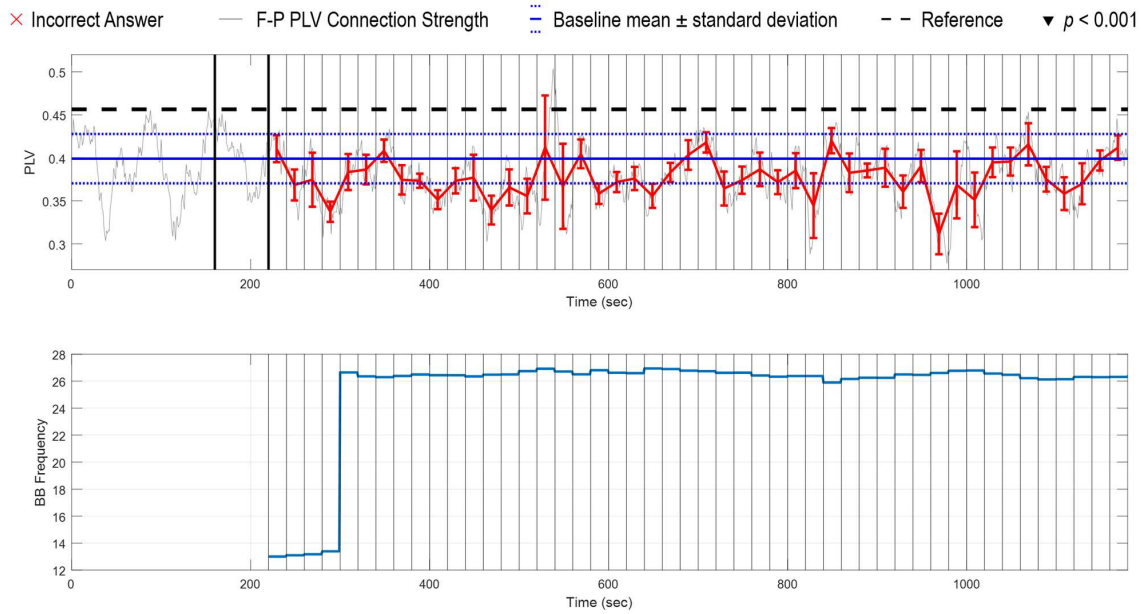Figure D.4: The adaptive laws for Participant 3. 0s indicates the start of the controller.
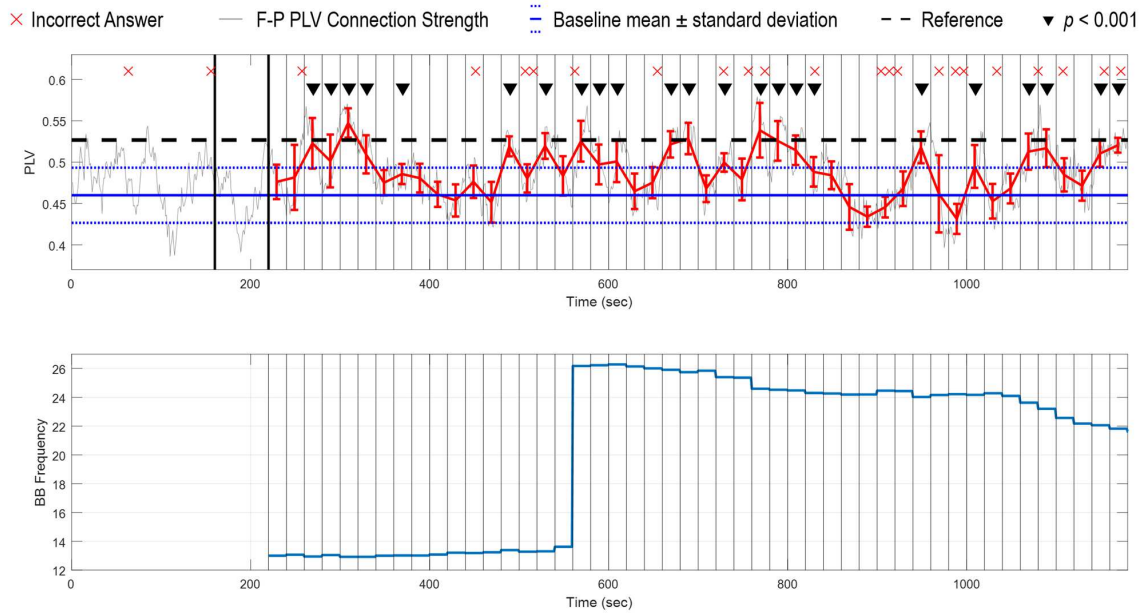
Figure D.5: The frontal-parietal PLV connection strength as a function of time and the corresponding controller output for Participant 4. The mean and one standard deviation of the PLV, for each epoch, is shown by the error bars in red.
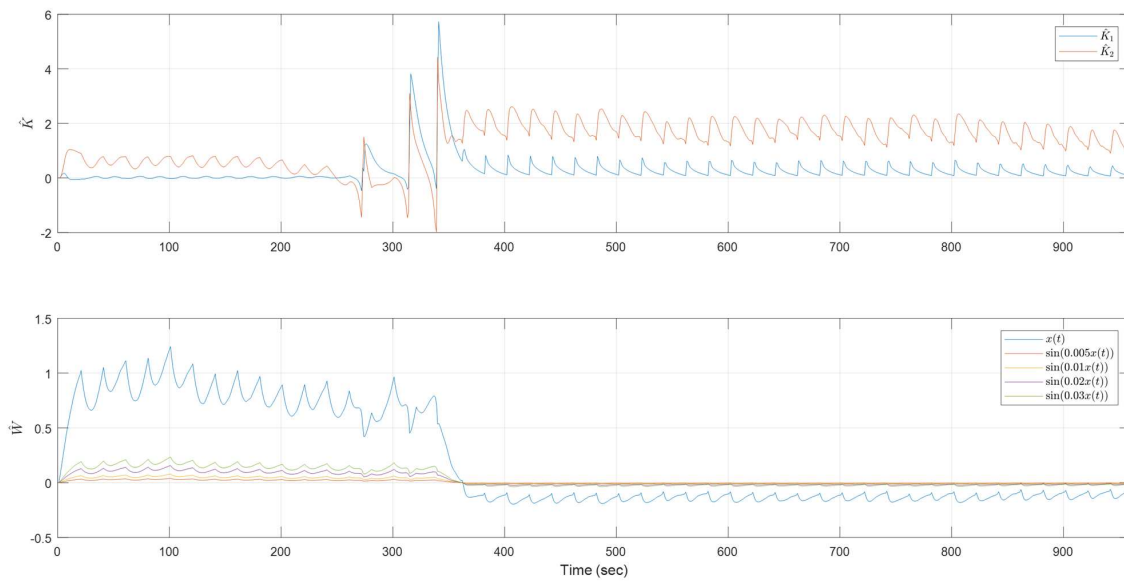
Figure D.6: The adaptive laws for Participant 4. 0s indicates the start of the controller.

Figure D.7: The frontal-parietal PLV connection strength as a function of time and the corresponding controller output for Participant 5. The mean and one standard deviation of the PLV, for each epoch, is shown by the error bars in red.
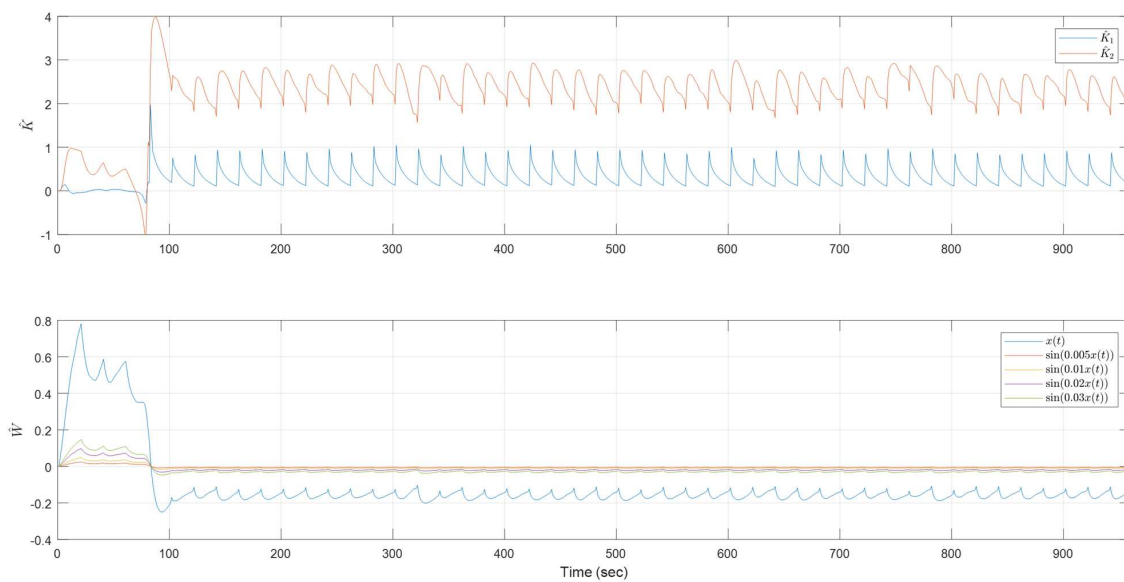

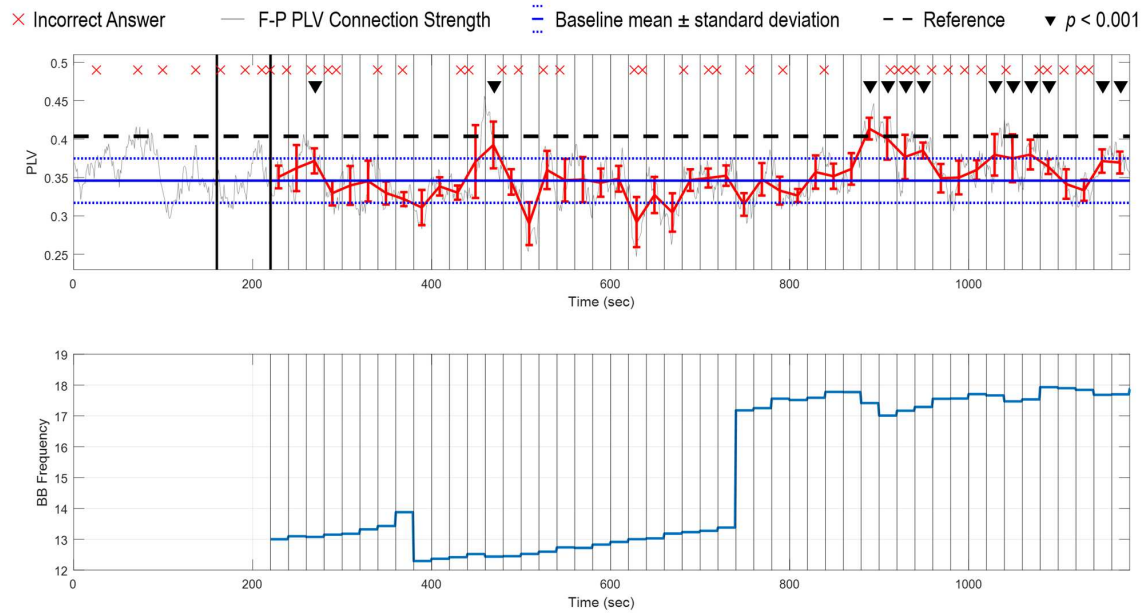Figure D.8: The adaptive laws for Participant 5. 0s indicates the start of the controller.

Figure D.9: The frontal-parietal PLV connection strength as a function of time and the corresponding controller output for Participant 6. The mean and one standard deviation of the PLV, for each epoch, is shown by the error bars in red.

Figure D.10: The adaptive laws for Participant 6. 0s indicates the start of the controller.

Figure D.11: The frontal-parietal PLV connection strength as a function of time and the corresponding controller output for Participant 7. The mean and one standard deviation of the PLV, for each epoch, is shown by the error bars in red.
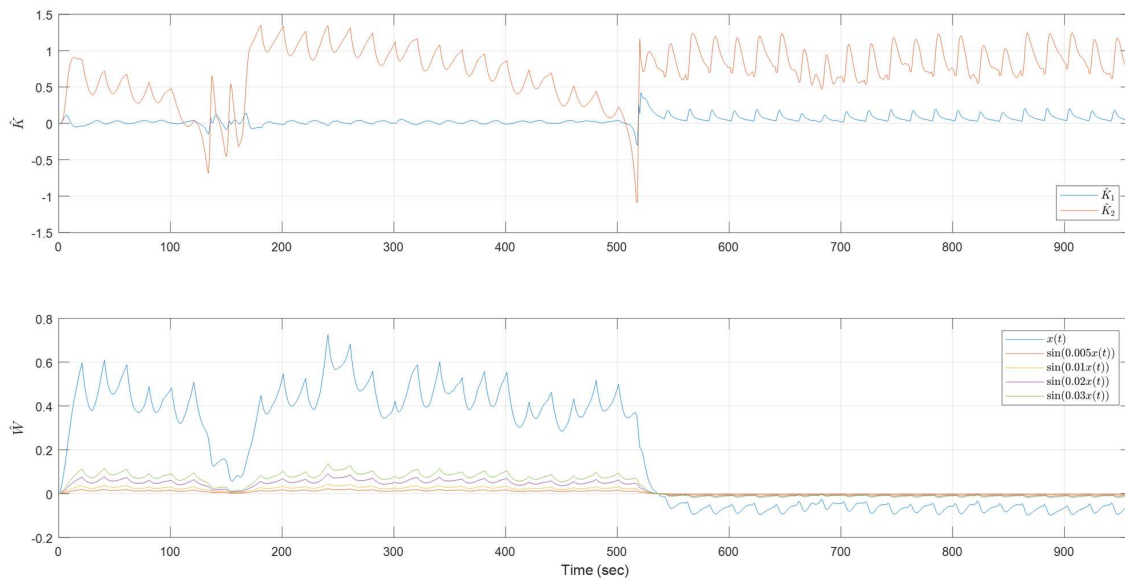

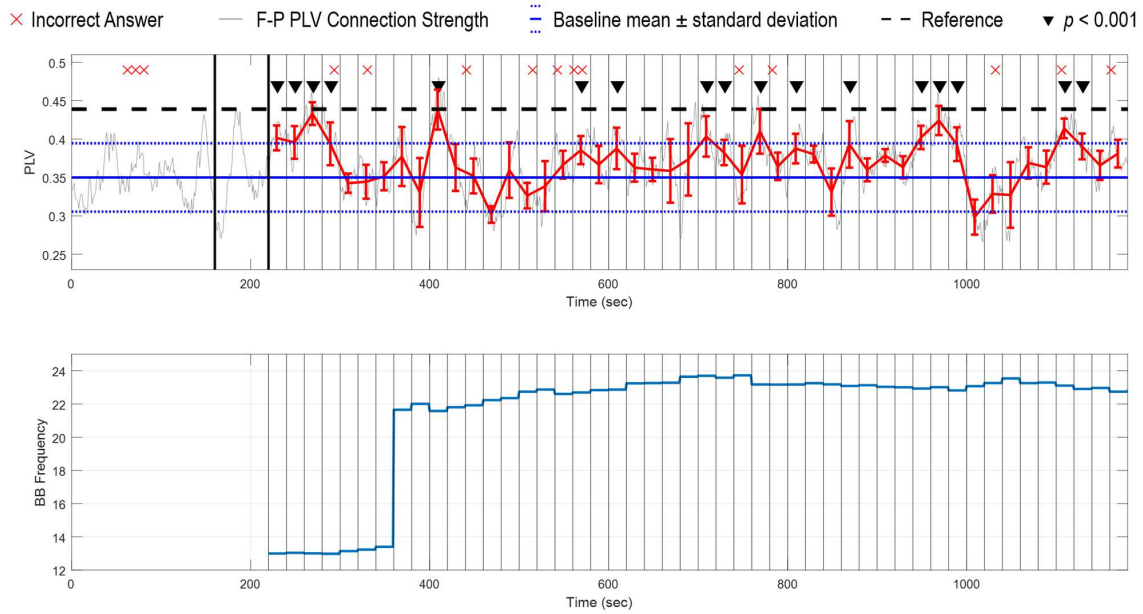Figure D.12: The adaptive laws for Participant 7. 0s indicates the start of the controller.

Figure D.13: The frontal-parietal PLV connection strength as a function of time and the corresponding controller output for Participant 9. The mean and one standard deviation of the PLV, for each epoch, is shown by the error bars in red.
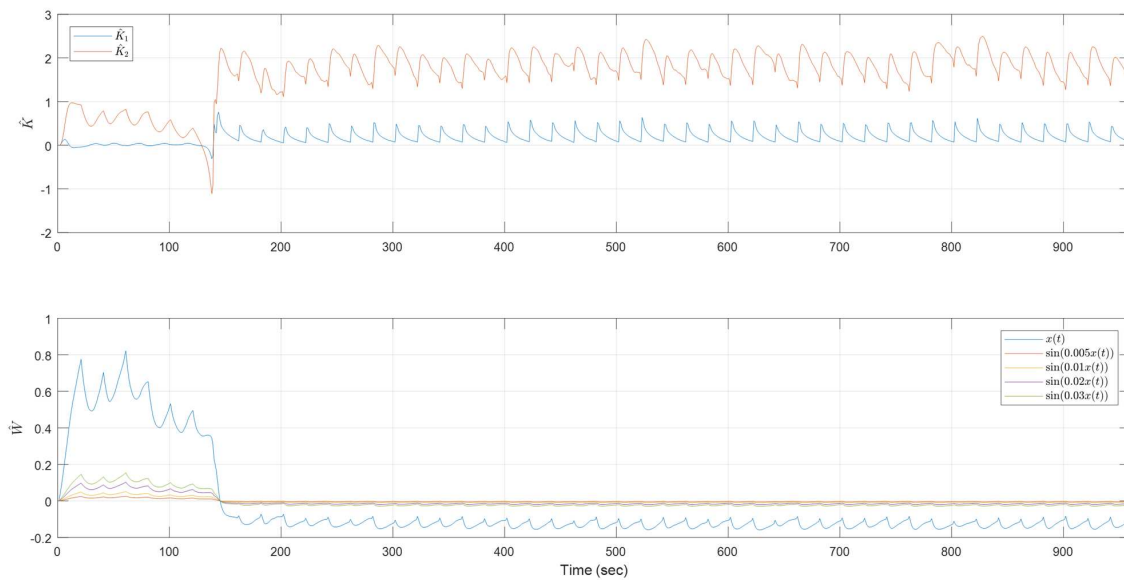

Figure D.14: The adaptive laws for Participant 9. 0s indicates the start of the controller.
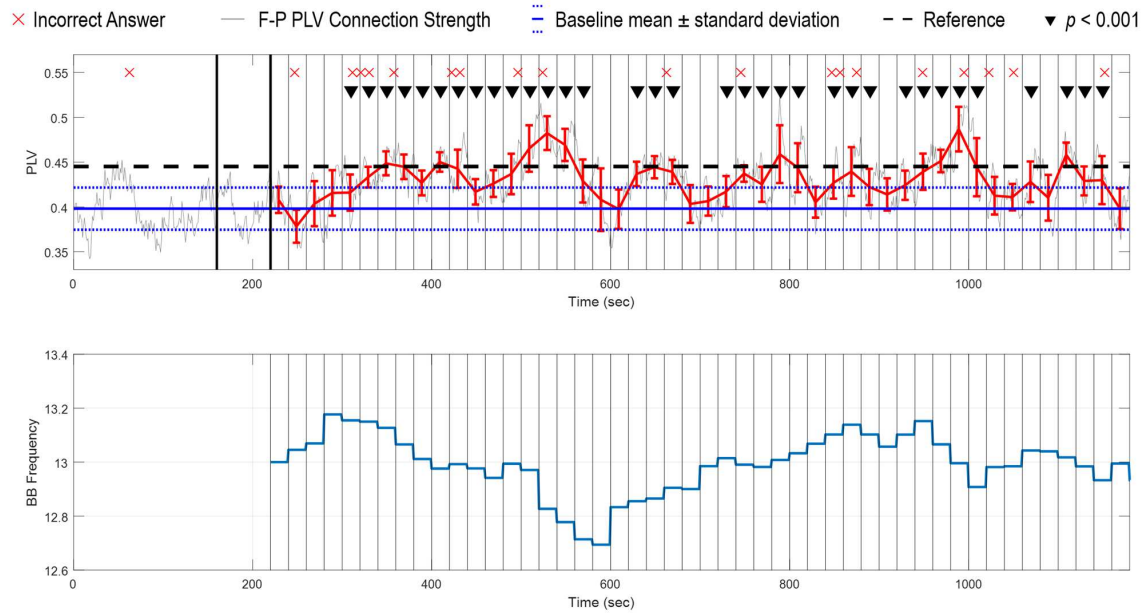
Figure D.15: The frontal-parietal PLV connection strength as a function of time and the corresponding controller output for Participant 10. The mean and one standard deviation of the PLV, for each epoch, is shown by the error bars in red.

Figure D.16: The adaptive laws for Participant 10. 0s indicates the start of the controller.

Figure D.17: The frontal-parietal PLV connection strength as a function of time and the corresponding controller output for Participant 11. The mean and one standard deviation of the PLV, for each epoch, is shown by the error bars in red.
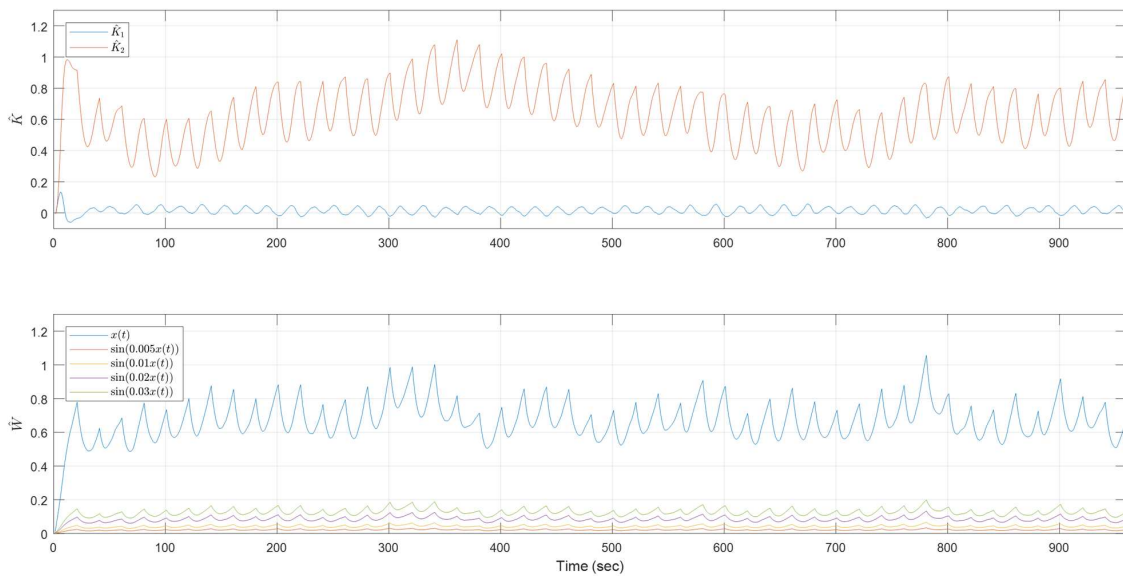

Figure D.18: The adaptive laws for Participant 11. 0s indicates the start of the controller.

Figure D.19: The frontal-parietal PLV connection strength as a function of time and the corresponding controller output for Participant 12. The mean and one standard deviation of the PLV, for each epoch, is shown by the error bars in red.

Figure D.20: The adaptive laws for Participant 12. 0s indicates the start of the controller.
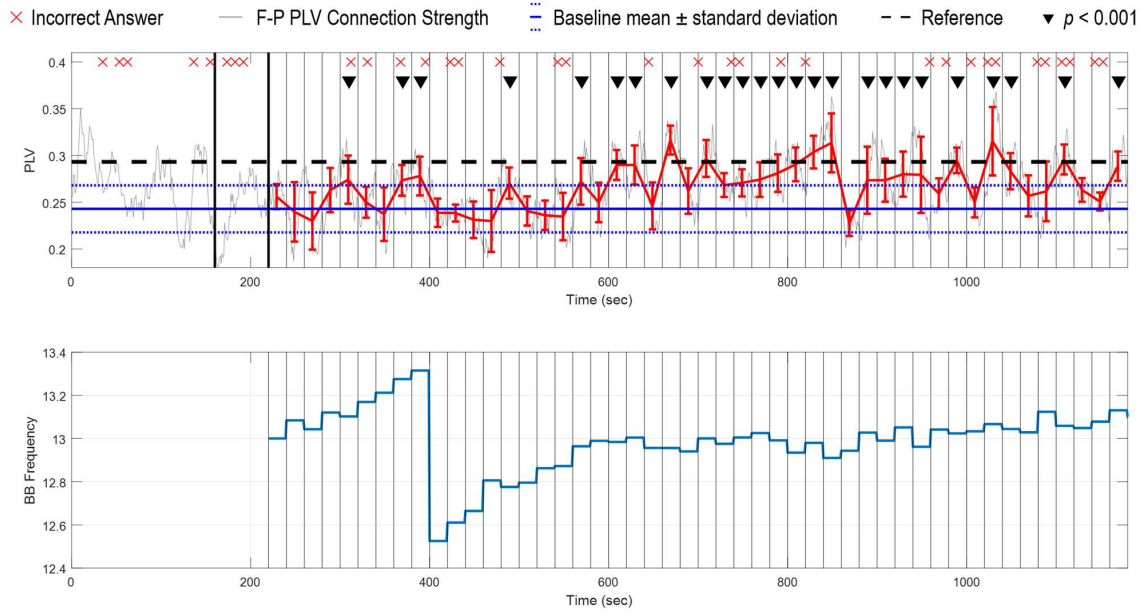
Figure D.21: The frontal-parietal PLV connection strength as a function of time and the corresponding controller output for Participant 13. The mean and one standard deviation of the PLV, for each epoch, is shown by the error bars in red.
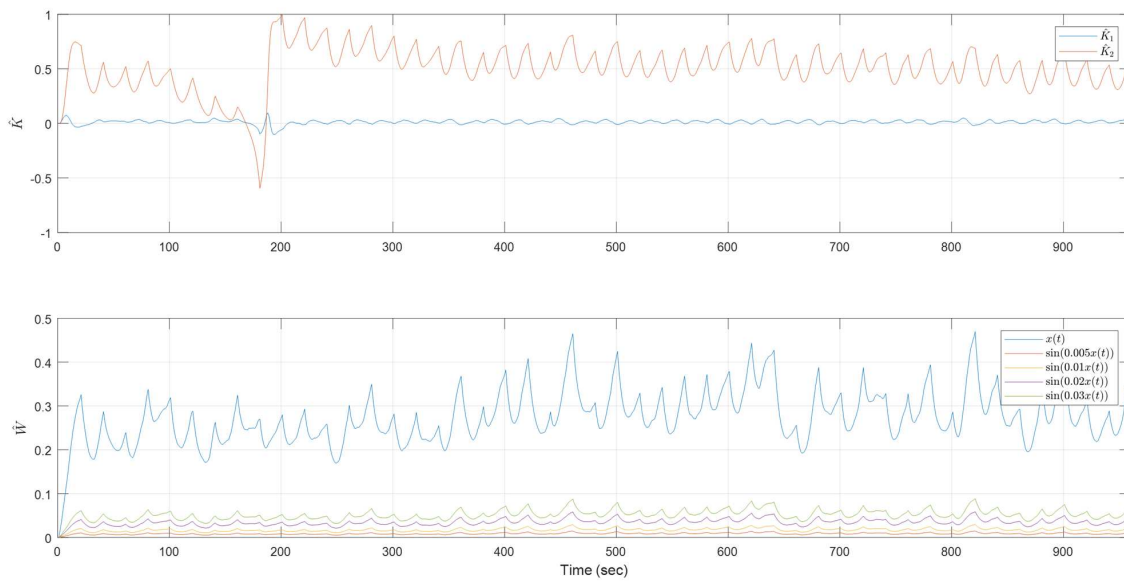

Figure D.22: The adaptive laws for Participant 13. 0s indicates the start of the controller.